Università degli Studi di Padova

DIPARTIMENTO DI INGEGNERIA INDUSTRIALE

Corso di Laurea Magistrale in Ingegneria Elettrica

Tesi di
Laurea Magistrale

Optimization of demodulation rings in professional loudspeakers

Laureando:
Lorenzo Bortot
Matricola 1014762

Relatore:
Prof. Piergiorgio Alotto

Correlatore:
Ing. Mattia Cobianchi

Anno Accademico 2012-2013

To the wind of change

Abstract

A new way to design demodulation rings in loudspeakers is explored, using the finite elements model coupled with stochastic optimization.
The lossy inductance of the motor coil is characterized firstly for small signals, then this process is extended to the large signals, introducing the coil movement. Thus a genetic algorithm, based on the differential evolution theory, is developed and coupled with the finite elements software Comsol:
using the Pareto optimality concept, the minimisation of impedance variation with the coil offset, together with the amount of material used, is found.
The results are shown using the idea of Pareto fronts: this is desirable for any developer, that can choose among a family of solutions. For last the prototypes have been realized and measured, to validate the results got through virtual design.

Keywords

Stochastic optimization, Loudspeakers, Genetic algorithms, Differential evolution, Finite elements method, Comsol

Contents

List of Figures

List of Tables

Chapter 1

The loudspeakers

1.1 History and Background

The history of modern loudspeakers can be considered starting (and in some way ending)in 1925: this was the year when Rice and Kellogg developed the moving coil cone loudspeaker, showing it to the world in a very well known work [22]:
what Rice and Kellogg developed is still the essence of the modern moving coil loudspeaker,as can be seen from Fig. 1.1 and 1.2.

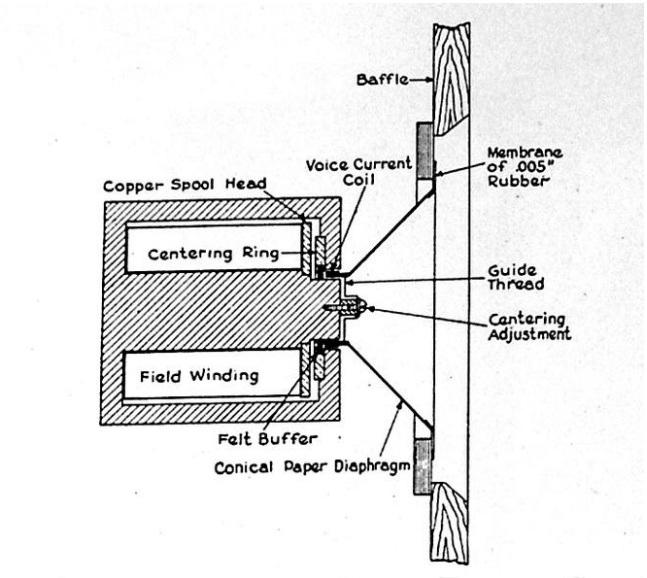

Figure 1.1: the original design proposed by Rice and Kellogg

Although Sir Oliver Lodge had patented the concept in 1898 (following on from earlier work by Ernst Werner Siemens in the 1870s, made at the Siemens company in Germany), it was not until Rice and Kellogg that practical devices began to evolve:
indeed Sir Oliver had had no means of electrical amplification - the thermionic

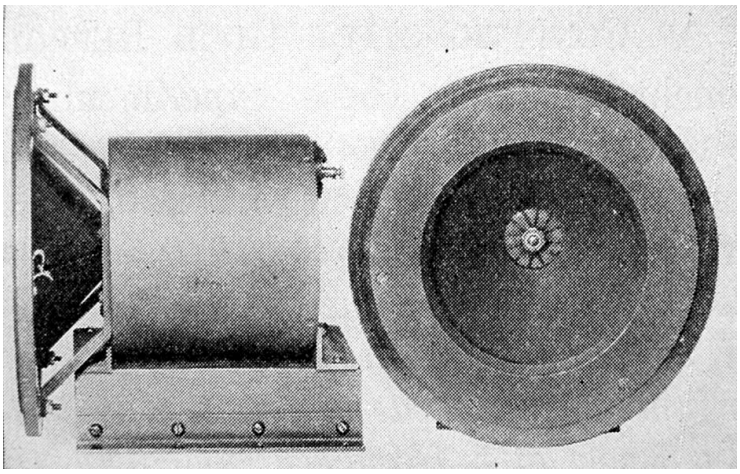

Figure 1.2: the original prototype

valve (or vacuum tube) had still not been invented, and the transistor was not to follow for 50 years.
Although Rice and Kellogg lacked the benefit of modern materials and technology, they had the basic principles very well within their understanding, but their goals at the time were quite less demanding than those of current design. Such responses were not required because they did not even have signal sources of such a wide bandwidth or dynamic range. It was not until the 1940s that microphones could capture the full frequency range, and the 1950s before it could be delivered commercially to the public via the microgroove, vinyl record.

The six inch, rubber surround device of Rice and Kellogg used a powerful electro-magnet (not a permanent magnet), and as it could *speak* to a whole room full of people, as opposed to just one person at a time via an earpiece, it became known as a loud speaker. The inventors were employed by the General Electric Company, in the USA, and they began by building a mains-driven power amplifier which could supply the power of *one watt* (a negligible power if compared with current power amplifiers but a huge power for those times).
The result became the *Radiola Model 104*, which with its built in power amplifier was sold for a really expensive price, 250 US dollars.
Gilbert Briggs, the founder of *Wharfedale loudspeakers*, wrote in his book of 1955[ref]: 'It is fairly easy to make a moving-coil loudspeaker to cover 80 to 8,000 cycles [Hz] without serious loss, but to extend the range to 30 cycles in the bass and 15,000 cycles in the extreme top presents quite a few problems. Inefficiency in the bass is due mainly to low radiation resistance, whilst the mass of the vibrating system reduces efficiency in the extreme top'.
The problem in the bass was, and still is, that with the cone moving so relatively slowly, the air in contact with it simply keeps moving out of the way, and then returning back when the cone direction reverses, so only only relatively weak pressure waves are being propagated and with very low efficiency.
The only way to efficiently couple the air to a cone at low frequencies is to either make the cone very big, so that the air cannot get out of the way so easily, or

to constrain the air in a gradually flaring horn, mounted directly in front of the diaphragm. Unfortunately, both of these methods can have highly detrimental effects on the high frequency response of the loudspeakers:

- for a loudspeaker cone to vibrate at 20 kHz it must change direction forty thousand times a second. If the cone has the mass of a big diaphragm needed for the low frequencies, its momentum would be too great to respond to so many rapid accelerations and decelerations without enormous electrical input power, hence the loss of efficiency alluded to by Briggs;

- Large surfaces are also problematical in terms of the directivity of the high frequency response, since the size of the cone is comparable with the wavelength of sound. Since not all the membrane points lay at the same distance from the listener, there will be a lot of interference effects which will result in a polar diagram with an increasing number of secondary lobes as the frequency increases.

We can now begin to see how things get more complicated once we begin to extend the frequency range from 20 Hz to 20 kHz, since the requirements for effective radiation become conflicting at the opposing frequency extremes.
The wavelength of a 20 Hz tone in air is about 17 m, whereas the wavelength at 20 kHz is only 1.7 cm, a ratio of 10^3 to 1, and for high quality audio applications we want our loudspeakers to produce all the frequencies in between at a uniform level.
We would also like for the devices to radiate the same waveforms, differing only in amplitude (but not shape) over a power range of at least 10^9 to 1 and with no more than one part in a hundred of spurious signals (non-linear distortion). Indeed, for a single drive unit, it still cannot be achieved at any realistic SPL (sound pressure level) if the full frequency range is required.

Although the original moving-coil, cone loudspeaker of Rice and Kellogg was the first true loudspeaker of a type that we know today, it was, itself, a development of ideas already applied in telephone earpieces design.
The moving coil direct radiator, along with amplifiers as great as 15 W output,which was then huge,soon opened a door to room filling sound levels, and, within only a couple of years, talking pictures at the cinema.
The need to fill larger and larger theaters with sound led to horn designs, and the need for a larger bandwidth led to the separation of the drive units into frequency ranges where they could operate more efficiently:
this operation is called *Cross-overing* and the Fig. 1.3 shows a principle scheme. Even if this topic is extremely interesting, it is simply too wide to give a brief overview, thus the interested reader is referenced to [ref].

From this separation of the frequency range started a never ending refinement and specialization involving magnet materials, diaphragm materials and radiators shape and concepts, with the same and one goal of converting electrical signals into sound waves.

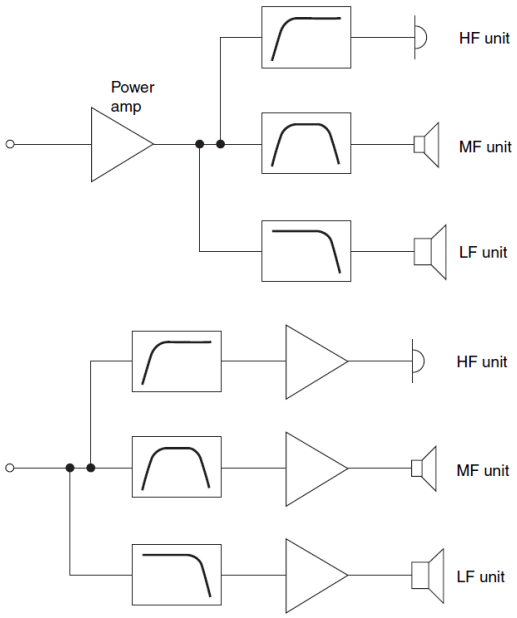

Figure 1.3: On top, Crossover network with high level filters. On bottom, crossover network with low level filters

1.2 Electromagnetic loudspeakers working principles

For the purpose of our work, we won't make any discrimination among diaphragm-loudspeakers,dome-loudspeakers and compression drivers:
the physics related to the acoustic wave propagation is fairly different, but on the electromagnetic side they follow the same construction design and the same principles. Moreover we will focus especially on the electromagnetic features related to the transducer mechanism.

In spite of the huge variety of sizes, shapes, materials of constructions and performances, all the moving coil cone loudspeakers follow the same concept, shown in Fig. 1.5 which is very similar to the one proposed by Rice and Kellogg.

They all need a source to generate a magneto-static field: at the beginnings it was provided by a *field coil*, supplied with a DC current high enough to generate the required flux density field in the air gap; the *voice coil* was fed by the output signal from the amplifier, and the Lorentz force generated by the interaction of the current and the field provided the driving force for the cone to produce enough sound pressure level.
When the developing of magnets with high energy density took place, the field coil was eliminated:
Early permanent magnets were often made from iron and chromium. Aluminum, nickel and cobalt were variously used in the early 1930s, alloyed with iron in different combinations, material usually known as *AlNiCo*.

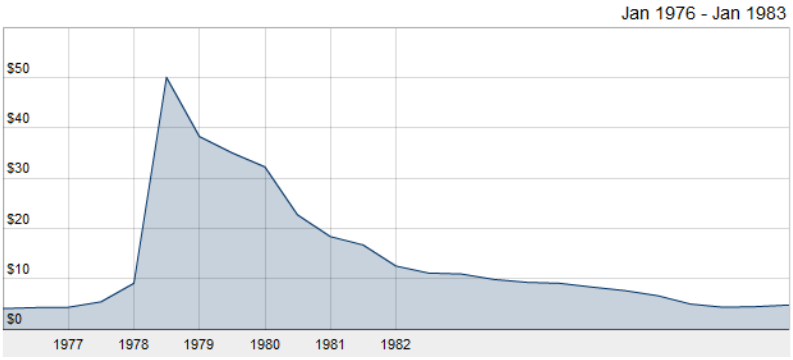

Figure 1.4: shock in the price of cobalt in 70's

In the 1970s, the civil war in the Congo (then Zaire) created a big hole in the production of cobalt, whose price rose astronomically in a very short period of time:
this led to the use of ferrite materials, known as ceramic magnets. More recently, *rare earth* magnets, principally made from neodymium and samarium based alloys, such as neodymium with iron and boron, or samarium and cobalt, have led to very light weight magnets, and opened a door to new magnet shapes and magnetic field designs.

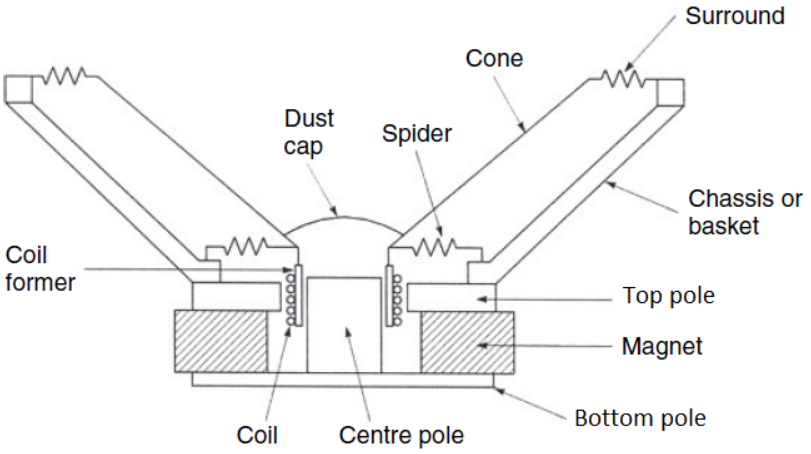

Figure 1.5: the main components of a modern moving coil loudspeaker

The Fig. 1.6 show the typical design employing ferrite or neodymium ring magnets, whilst the Fig 1.7 illustrates the main components and the electric equivalent network of the magnetic circuit.

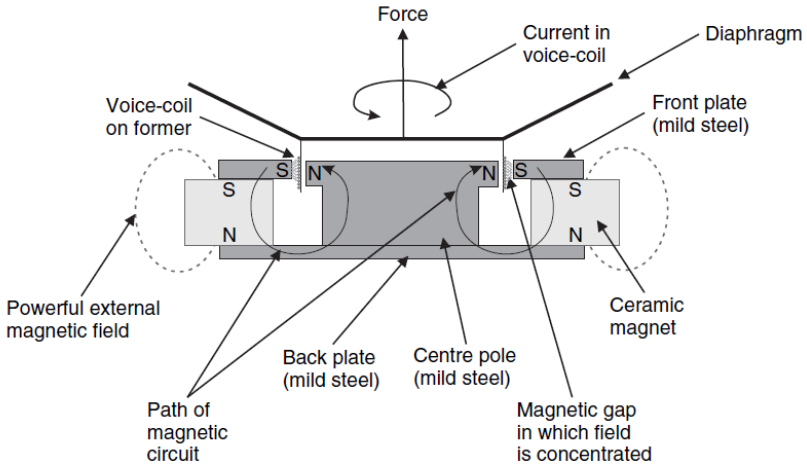

Figure 1.6: ceramic ring magnet topology

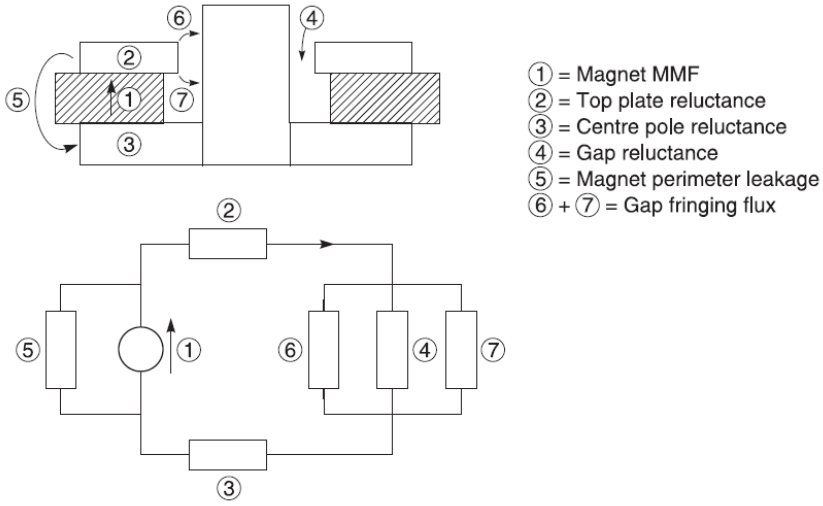

Figure 1.7: components and equivalent circuit

The Fig. 1.8 shows an alternative design with a central magnet (usually neodymium or alnico),where the volume is strongly reduced respect to the previous configuration.

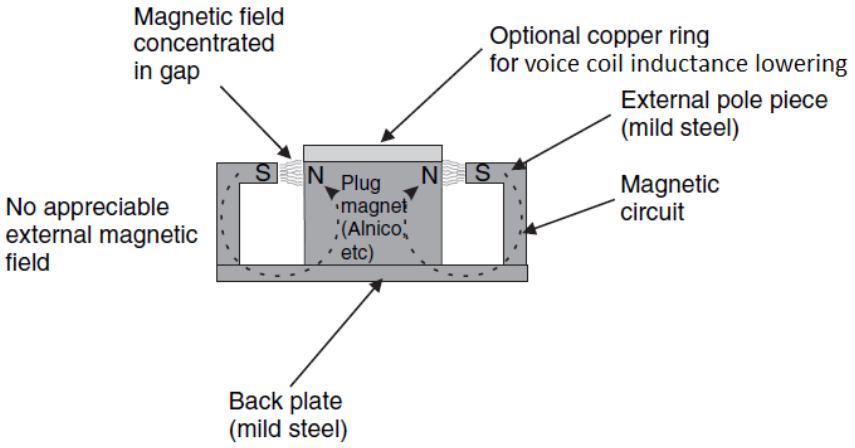

Figure 1.8: central disc magnet topology

The magnetic circuits are designed to concentrate the magnetic field in a circular gap: in this gap is inserted the voice coil, which receives the electrical drive current from the power amplifier. This current produces its own, alternating magnetic field, whose phase and amplitude depend on the drive signal. This AC field interacts with the static field in the circular gap, and creates a force which either causes the voice coil to move into or out of the gap. Of course, a mean is required to maintain the coil centered radially in the gap with the chance to move only axially, and this is achieved by the use of centering device, or inner suspension,called spider due to the shape of early models.

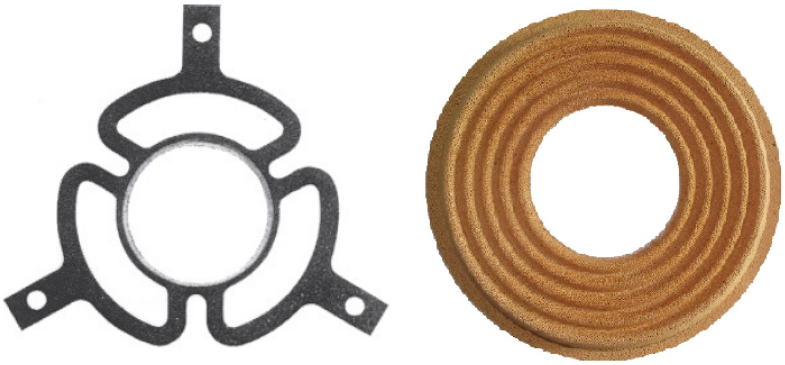

Figure 1.9: comparison between old (left) and modern (right) spider design

A chassis, also known as frame or basket, supports the whole assembly and enables it to be mounted on a front baffle. The cone is connected rigidly to the former upon which the voice coil is wound, and is also connected more or less at

the same point to the inner suspension. At the chassis' outer edge the cone is attached via a flexible outer suspension, or surround, which may take the form of half-rolls, multiple corrugations, or pleats.
A dust cap is then normally placed in the apex of the cone in order to prevent the ingress of dust and any abrasive dirt, and may also be used as an air pump to cool the voice coil when the cone assembly moves in and out.

Chapter 2

Geometry and materials

2.1 Introduction

Before starting to work on the new prototype,we agreed about performing an analysis of two different loudspeakers, designed to work in two different frequency ranges. This choice had been made according to the following purposes:

- to let me make experience with Comsol software and the electro-mechanical equivalent models commonly used for small and large signals;
- to validate the finite element models with already available real devices easily accessible for all the measurements needed;
- to understand the ranges of reliability of the Klippel Distortion Analyzer, that was used to take the measurements, in particular its behavior at extremely low frequencies and signals, where noise contribution is an issue.

The devices chosen were:

- a midrange speaker, called SV 165, already on the market [32];
- a sub-woofer, called $DS30.3$,already on the market [31];
- the prototype sub-woofer,that was yet to be developed, called $SSF-082$.

All the following quotes are expressed in mm.

2.2 Dimensions

$DS30.3$ Woofer

The device is not characterized by a completely axial symmetric geometry: indeed there are two cuts on the aluminum former, this to reduce the circulation of the induced Eddy currents,so rigorously we should consider the whole three dimensional model.
We proceed anyway with axial symmetric modeling: the quality of results and the limitations of this approach will be discussed in the further chapters.

Figure 2.1: the woofer loudspeaker

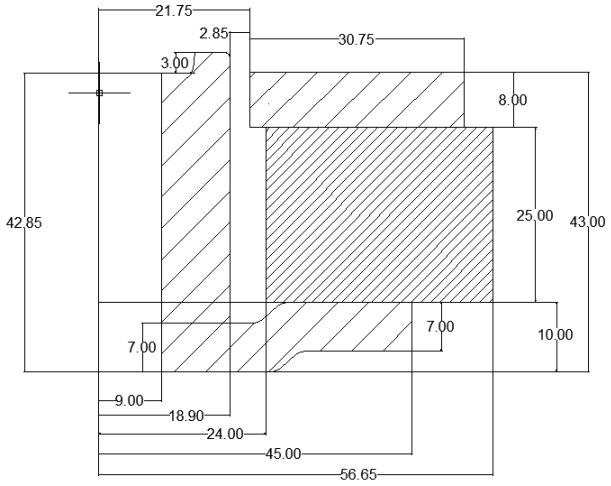

Figure 2.2: magnet assembly section

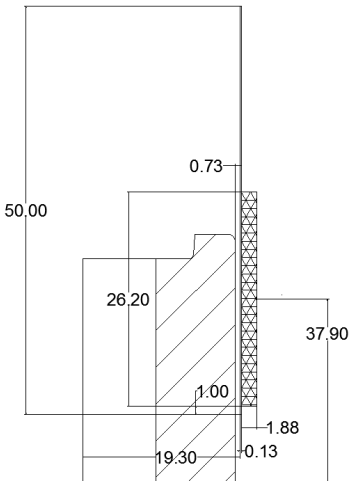

Figure 2.3: voice coil detail

SV 165 **midrange**

This device is characterized by a full axial symmetry: so we will expect more accurate results from a $2d$ analysis. The geometry of this device is characterized by the presence of three different areas colored in blue (see Fig. 2.4):
these represent the maximum space reserved for the demodulation rings.

Figure 2.4: the midrange loudspeaker

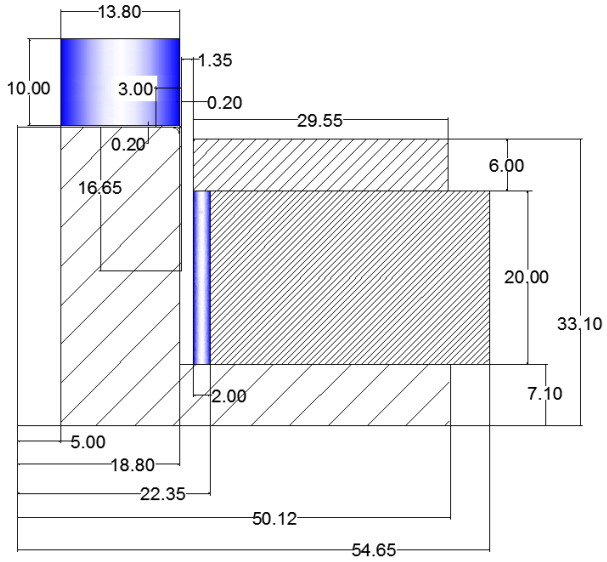

Figure 2.5: magnet assembly section

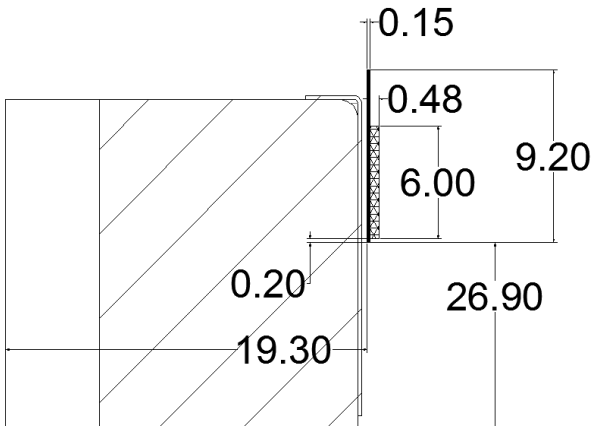

Figure 2.6: voice coil detail

$SSF - 082$ **prototype woofer**

The geometry of this device is characterized by the presence of three different areas colored in blue (see Fig. 2.7):
these represent the maximum space reserved for the demodulation rings. Since the device is thought to allow the installation up to three rings that are expensive in terms of material cost, this product will be sold in the high-end market.
Rings number, position and size are all parameters which have to be optimized and which will be discussed in the next chapter.

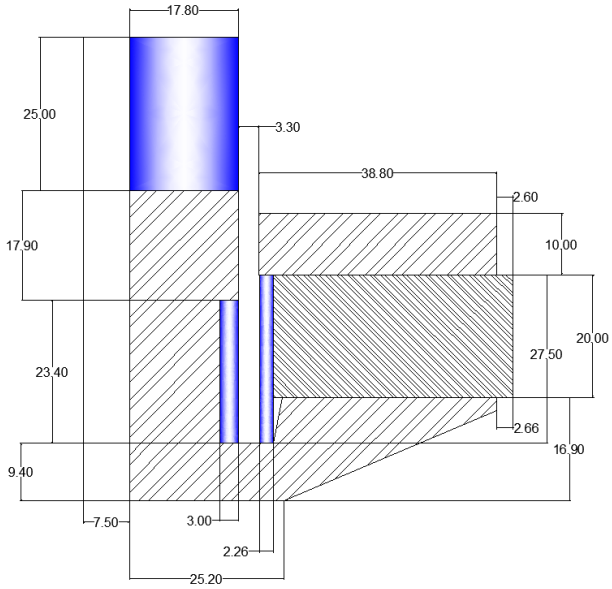

Figure 2.7: body half section

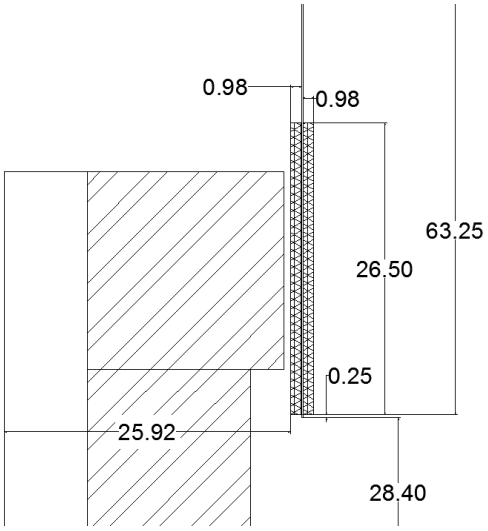

Figure 2.8: voice coil detail

2.3 Materials and details of modeling

Magnet

The magnet is an Y30 grade ferrite of ring shape. Its magnetic characteristic and the BH energy function are shown in the figure 2.9.

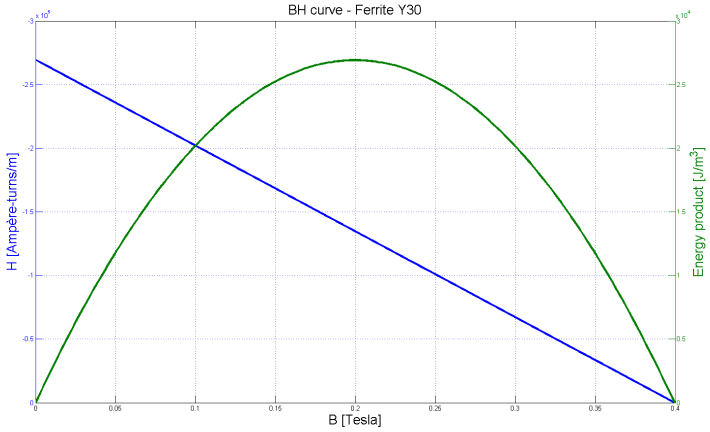

Figure 2.9: magnet characteristic and BH product

Concerning the relative permeability, the magnet exhibits an isotropic behavior: then the matrix of coefficients related to the relative permeability can be characterized just by a constant scalar value. The main features of the magnet are remarked in the Tab. 2.2

Property	Value	Units
Coercitive Field	$2.69453 * 10^5$	$[H]$
Relative Permeability	1.18	$[-]$
Residual Induction	$3.9955 * 10^{-1}$	$[T]$
Conductivity	0	$[S/m]$
Maximum energy product	$2,71 * 10^4$	$[J/m^3]$

Table 2.1: Main features of the magnet

Soft iron materials

The magnetic circuits of all the three devices are made with the same material,a quite common low carbon steel. To implement it in Comsol, we created a new material, then we characterized it with its magnetization curve and conductivity. Note that no hysteresis phenomena were considered in the model, this because:

- the losses related to the hysteretic cycle are neglectable with respect to the induced Eddy currents;

- the distortion related to local hysteretic cycles is neglectable with respect to the other non linearities that characterize the behavior of the device (like for example the dependence of the force factor with the position);

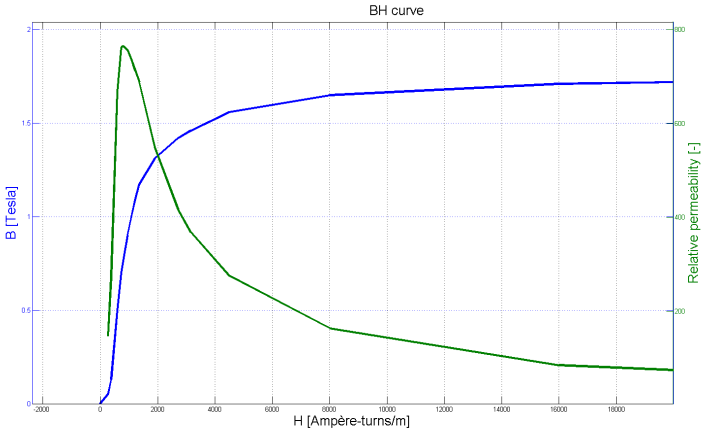

Figure 2.10: magnetic characteristic

Property	Value	Units
Conductivity	$5.8 * 10^6$	$[S/m]$
Maximum relative permeability	$7.64 * 10^2$	$[-]$

Table 2.2: Main features of the ferromagnetic material

The magnetic characteristic was linearized in the first part:
this was done to speed up the convergence of the numerical solver. Furthermore this approximation is valid since a ferromagnetic circuit is expected to work from the knee to the saturation plateau, to well exploit the ferromagnetic properties. The continuous blue line represents the interpolation based on measured point values, the red dashed one shows the curve used in Comsol.

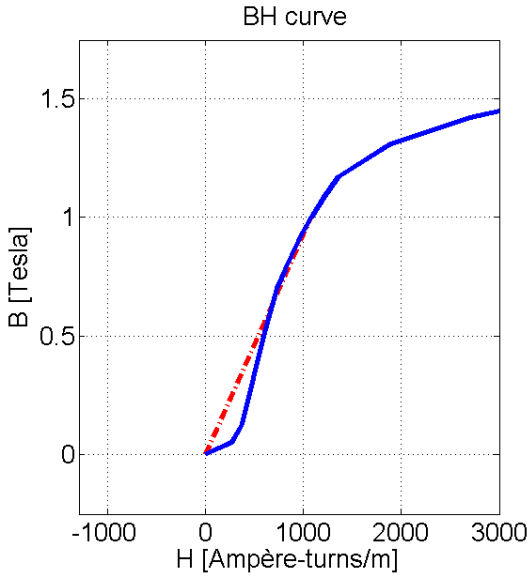

Figure 2.11: linearization of the first points of magnetic characteristic

Figure 2.12: Overview of the $SV165$ magnetic circuit. From upper left going clockwise there are the top pole, the magnet and the central pole

Voice coil and former

Each coil has its own specifications, which are summarized in the Tab. 2.3and 2.4. The physical properties related to the wire come from(rif),whilst the details about the formers are taken from (rif). With the acronym *CCA* we refer to the well known Copper-Clad-Aluminum technology, used in realizing wires.

Coil properties	SV 165	$DS30.3$	$SSF-082$
Wire material	CCA	CCA	CCA
Wire inner diam. [mm]	0.26	0.43	0.45
Wire outer diam [mm]	0.294	0.47	0.49
Wire resistivity [Ohm/m]	0.482	0.187	0.160
Specific weight [kg/km]	0.221	0.593	0.652
Turns	48	220	213
Number of layers	2	4	4

Table 2.3: Voice coils specifications

Former properties	SV 165	$DS30.3$	$SSF-082$
Material	$Kapton$	$Aluminum$	$GlassFiber$
Resistivity [Ohm·m]	10^8	$2.650*10^{-7}$	10^6
Dielectric relative constant [-]	3.5	1	6.2

Table 2.4: Main features of the formers

Demodulation rings

The woofer $DS30.3$ does not have any kind of demodulation ring:
his former is made by aluminum but, as previously discussed, it is cut along the zeta coordinate, in order to strongly reduce the magnitude of Eddy currents.
The midrange SV 165 shows a copper cap covering the central pole, whilst the woofer $SSF-082$ that is the target of the optimization,could have a maximum of three rings made by aluminum.
To consider the fact that the material used is not ideal, but like every kind of real material it is affected by the presence of impurities, we needed to give an estimation of the conductivity:
we took the ideal conductivities of copper and aluminum,then we have reduced them by 8%.

Rings properties	SV 165	$DS30.3$	$SSF-082$
Material	$Copper$	[–]	$Aluminum$
Conductivity [S/m]	$5.211*10^7$	[–]	$3.472*10^6$

Table 2.5: Main features of the demodulation rings

Chapter 3

Magneto static analysis

3.1 introduction

The magneto-static analysis is the first step that a designer usually deals with in the development of a new motor, since from this study worthy information could be extracted about the ferromagnetic circuit and the flux density, that is the first mechanism of transduction, in this case of electrical energy in mechanical energy. In particular the main goals of the analysis are:

- the evaluation of the saturation of the magnetic circuit, to understand if the ferromagnetic material is well exploited;
- the evaluation of the working point of the magnet, and the verification about the robustness of that point against demagnetization;
- the evaluation of the flux density profile in the air gap, (magnitude, shape, symmetry) and the possibility to enhance the shape to get a better profile or an higher flux density;
- the evaluation of the static force factor acting on the voice coil;
- the global evaluation of the motor AC performances taking into account the induced currents in iron and demodulation ring/copper cap, linearizing the equations around a stable working point for small signal analysis.

On one hand, the magneto-static analysis is a very flexible and powerful tool since it has a computational cost that is very low for today computers:
then through the use of commercial software like Autocad, the design of the model becomes very fast, the solution of the finite element problem can be obtained in a very short time; moreover it's easy to make changes in the geometry of the device to get the desired behavior and features, avoiding to waste time in the *cut'n try* prototype procedure.

On the other hand, the only use of the magneto-static analysis does not allow the quantification of the distortions that show up in the dynamic behavior of the device, in particular it neglects:

- the flux modulation produced by the voice coil self induced flux;

- the flux modulation produced by the eddy's currents in the conductive parts of the device, especially the demodulation rings and the pole piece;
- the variation of the coil self inductance with the position (due to the different quantity of linked ferromagnetic material);
- the variation of the coil self inductance as a function of the current flowing in the coil (due to the different saturation levels that will be generated in the ferromagnetic circuit).

For the characterization of the materials and the permanent magnets, reference is made to the previous section about geometry and materials. In the following pages two studies are showed, one about a midrange loudspeaker ($SV165$) and the other about a subwoofer loudspeaker ($DS30.3$).

3.2 formulation of the static field problem

The starting point of any electromagnetic field problem is the well known set of Maxwell equations

$$\begin{cases} \nabla \times \bar{E} = -\frac{\partial \bar{B}}{\partial t} \quad Faraday\ Law \\ \nabla \cdot \bar{B} = 0 \quad Gauss\ magnetic\ Law \\ \nabla \cdot \bar{D} = \delta \quad Gauss\ electric\ Law \\ \nabla \times \bar{H} = \bar{J} + \frac{\partial \bar{D}}{\partial t} \quad Ampère\ Maxwell\ Law \end{cases} \tag{3.1}$$

They are accompanied by the constitutive laws, assuming materials that are homogeneous, linear and isotropic

$$\begin{cases} \bar{D} = \epsilon \bar{E} \\ \bar{B} = \nu^{-1} \bar{H} \\ \bar{J} = \sigma \bar{E} \end{cases} \tag{3.2}$$

In a magneto-static problem all the derivative terms vanish from the Maxwell equations set:
since the $\bar{B}$ field is solenoidal, and the problem domain is simply surface connected (it is a plane without holes), we can introduce a vector potential field $\bar{A}$ which is related to $\bar{B}$ according to the equation

$$\nabla \times \bar{A} = \bar{B} \tag{3.3}$$

coupling it with the Ampère-Maxwell law and the magnetic constitutive law, we can get the equation that gives the solution of the field problem

$$\nabla \times \nu \nabla \times \bar{A} = \bar{J} \tag{3.4}$$

Due to the geometry of the device, it's easy to find a symmetry axis that allow to transform the three dimensional problem in a two dimensional one:

thanks to that symmetry, the flux density field can be written in cylindrical coordinates (r, z, θ) like $\bar{B}(B_r, B_z, 0)$.
According to the relation by which in a two dimensional system the rotor of a quantity is orthogonal to the same quantity, the vector potential has just one component, $\bar{A}(0, 0, A_\theta(r, z))$.
Applying two times the rotor operator, defined in cylindrical coordinates as

$$\begin{bmatrix} \frac{1}{r}\bar{i} & \bar{j} & \frac{1}{r}\bar{k} \\ \partial r & \partial\theta & \partial z \\ A_r & rA_\theta & A_z \end{bmatrix} \tag{3.5}$$

we can derive from the equation 3.5 the following one

$$\left\{ \frac{\partial}{\partial r}\left(\frac{\nu}{r}\frac{\partial\left(rA_\theta\right)}{\partial r} \right) + \frac{\partial}{\partial z}\left(\nu\frac{\partial rA_\theta}{\partial z} \right) \right\} \cdot \bar{u_\theta} = J_\theta \cdot \bar{u_\theta}.$$

Defining

$$\nu/r = \nu', rA_\theta = \Phi$$

and introducing a new differential operator

$$\nabla_{cil} = \left(\frac{\partial}{\partial r}, \frac{\partial}{\partial z} \right)$$

we can finally get the classical scalar formulation for the electromagnetic two dimensional problems

$$\nabla_{cil} \cdot \nu' \nabla_{cil}\left(\Phi\right) = J_\theta. \tag{3.6}$$

The reason because we use the Φ symbol is not casual, indeed

$$\Phi = \int_\Sigma \bar{B} \cdot d\bar{\Sigma} \quad = \int_\Sigma \nabla \times \bar{A} \cdot d\bar{\Sigma}$$

using Stokes theorem

$$\int_\Gamma \bar{A} \cdot d\bar{\Gamma} \quad \rightarrow \quad \bar{A} = A_\theta(r, z) \quad \rightarrow \quad \Phi = A_\theta \int_\Gamma d\bar{\Gamma} = 2\pi \cdot rA_\theta$$

then at last we can see that the quantity rA_θ is just the flux linked with a circumference of radius r, less than a 2π constant.

3.2.1 characterizing factors

Bl factor

The electrodynamic coupling factor, also called Bl-product or force factor $Bl(x)$, is defined by the integral of the magnetic flux density B over voice coil length l, and translates current into force.
In traditional modeling this parameter is assumed to be constant: the force factor $Bl(0)$ at the rest position corresponds with the Bl-product used in linear modeling. We considered in our computation only the B_r component of the field, since it is the only one that generates a force whose direction lays on the

z axis.
The other field components just give rise to radial and tangential deformation forces: since we consider the voice coil as a rigid body, we can neglect them. a single point, in a coil with one Ampere of current flowing through, feels a force equal to

$$d\bar{F}_z = i(t) \cdot (d\bar{l} \times \bar{B} \cdot \bar{\theta})$$
$$\frac{d\bar{F}_z(r,z)}{i(t)} = 2\pi \cdot r \cdot \bar{B}_r(r,z)$$

Extending the equation to the whole coil domain, we get the formula that was applied directly in the finite element post processing phase:

$$Bl(x) = \frac{\int_{\Sigma_{coil}} \frac{d\bar{F}_z}{i(t)} \cdot d\Sigma}{\int_{\Sigma_{coil}} d\Sigma} = \frac{2\pi \cdot r_{mean} \int_{\Sigma_{coil}} \bar{B}_r(r,z) \cdot d\Sigma}{\int_{\Sigma_{coil}} d\Sigma} \tag{3.7}$$

β factor

The second most important factor is called β and it represents the figure of merit for the motor force, regardless the nominal voice coil impedance.
It represents a ratio expressed in $[N/W]$ and it is defined as

$$\beta(x) = \frac{(Bl)^2}{R_{Dc\ coil}}$$

$$\beta(x) = \frac{{B_{mean}}^2 \cdot (2\pi \cdot N \cdot r_{mean})^2}{R_{Dc\ coil}}$$

$$\beta(x) = \frac{{B_{mean}}^2 \cdot (2\pi \cdot N \cdot r_{mean})^2 \cdot \Sigma_{wire}}{N \cdot 2\pi \cdot \rho \cdot r_{mean}}$$

$$\beta(x) = \frac{B_{mean}^2}{\rho} \cdot Vol_{coil} \tag{3.8}$$

For a given voice coil wire, copper or aluminum, β depends only on the square of the flux density and the volume of conductor in the magnetic gap.

3.3 Implementation in Comsol

The analysis of the device can be divided in five fundamental steps:

1. construction of the geometry;
2. assignment of the materials to the sub domains of the geometry;
3. discretization of the domain through the use of the finite elements;
4. imposition of the boundary conditions and setting of the parameters and their ranges of variation;
5. solving and post processing of results.

Every step is managed with specific tools provided by the software.

3.3.1 Geometry

The first thing to do is to create a box that encloses all the geometry and delimits the area where the solver will compute the solution field. Since the loudspeakers usually don't have external components that act like a Faraday cage, the magnetic field comes out the device and distributes itself outside.

By the way, it is obviously necessary to limit the computational area, then it is needed to set a domain that is finite, but large enough in order to avoid artefacts inside the region of interest:
the domain size has been parameterized and progressively increased up to the point that the solution in the region of interest doesn't change considerably. Since the fields are largely guided to follow the minimum reluctance path inside the magnet assembly, we saw that to get a good solution it was enough to set a semi-circumference domain with a radius that is equal to the double of the biggest linear dimension of the device.

The geometry could be drawn directly inside the finite element software, using the internal CAD tool: this is the easiest and fastest way if and only if the geometry is not very complicated. It is a very good idea to parametrize all the dimensions and link them together, in order to easily change the geometry lately. The other way is to design the device using specialized CAD software and then import the geometry in Comsol.

At first approximation some details are neglected on purpose,like holes, fillets and small chamfers:
they don't influence the flux density average value in the air gap or the leakage flux, but they can be considered in a second step to refine the flux density distribution over excursion. Moreover it is worth to eliminate all the elements that have no influence on the magneto-static solution, in particular the components made of non magnetic materials, like the voice coil, the former and the demodulation rings.

For example during the implementation of the *SV*.165 *midrange* geometry, we neglected the copper cap to save some mesh elements, since copper is a material that behave like air if it is pervaded by a magneto-static flux density field. The reason we did that is to keep the number of the finite elements as low as possible, and shorten the time needed to obtain the solution.

3.3.2 Materials

The various regions must match the materials they represent. Air, as well as any non-magnetic material found in the device (copper cap and aluminium demodulation rings) behaves with the same characteristics of the vacuum. The permanent magnet is defined by material type (Neodymium, Ferrite etc) and magnetization direction. Obviously, the type can be chosen among those already present in the database, or one can create their own materials, specifying remanence and coercive field for a linear magnet,or the whole family of points for a non-linear magnet.

The best way to define the ferromagnetic materials it the one that considers the introduction point by point of the whole $B = f(H)$ characteristic. It is a good idea to linearize the first part of characteristic (known also as

air gap characteristic),mostly for two reasons:

- if the device is well designed, it will never work in that part of the characteristic;
- the solver, at the beginning, draws a tangent to the curve in the zero point of the characteristic, and then move to the intersection point, then the small curl will make the solver run far away from the actual working point, requiring more iteration to get the solution.

3.3.3 Mesh

When the geometry is complete, it must be divided into finite elements. Mesh sizes and distribution can be parameterized. The software has an efficient automatic algorithm for the mesh generation with triangular elements (Lagrange second order) or rectangular ones.
In magneto static computations, triangular elements are the best option, customized in each region for what concerns:

- the minimum and the maximum size of the elements;
- the element growth rate over a transition domain (for example the air between the device and the boundaries);
- the number of elements over a line or a curve,in order to generate a finer mesh where needed;

After the assignment of mesh sizes we can begin the process of automatic discretization and check if that the mesh obtained is satisfactory. The important thing to keep always in mind is that the mesh has to be dense where the electromagnetic fields show steeper gradients,otherwise the solution will be approximative and it will lack in resolution.
It the effort to lower the number of elements,we decided to use a kind of hybrid mesh,(see figure 3.1) with both element shapes: where the geometry was regular it was introduced the square cross linking (bottom plate and its hole, magnet, top plate, voice coil). The target of our effort was to keep the number of elements, for every geometry, below 15000:
indeed the purpose of this thesis is to demonstrate the feasibility of an automatic optimization in a industrial R & D dept. where a fast and approximate result is preferable over a more accurate but slower result.
The air gap is the region of interest, since since here the flux density converts the coil current in driving force. It's critical to have a good resolution in this area,(see figure 3.2) to avoid numerical errors that can arise if the number of elements is too low: indeed most of the magneto-motive force drop takes place here. Note the lines added to bound the regions with finer mesh. For both the DS30 and SSF082 similar considerations regarding the mesh constructions can be applied, thus we have shown here only SV165 mesh details.

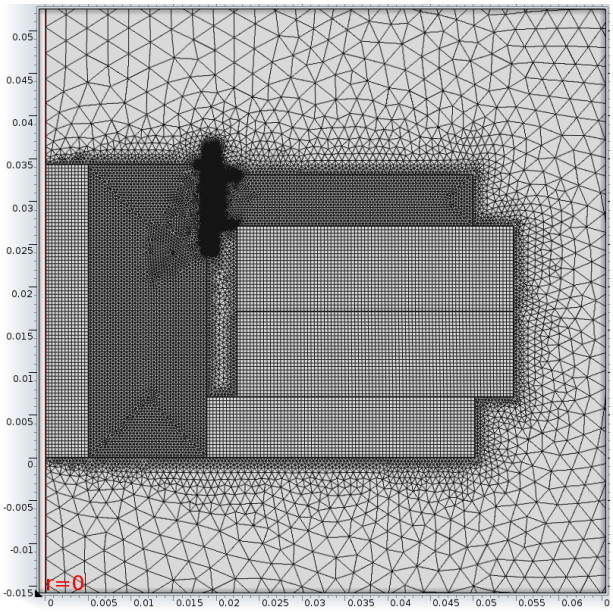

Figure 3.1: a whole view over the adopted mesh

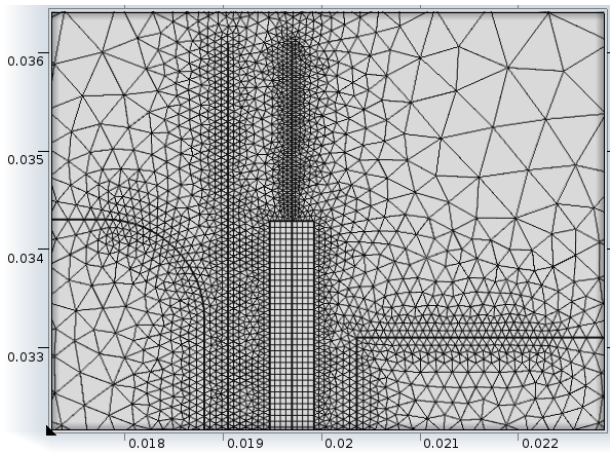

Figure 3.2: a detail of the mesh in the air gap

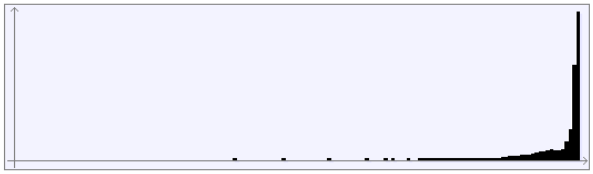

Figure 3.3: COMSOL mesh quality istogram, SV 165

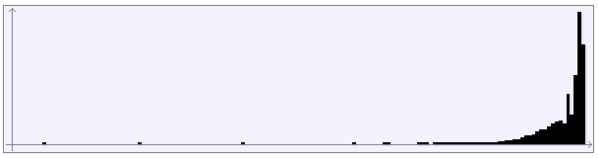

Figure 3.4: COMSOL mesh quality istogram, $DS30.3$

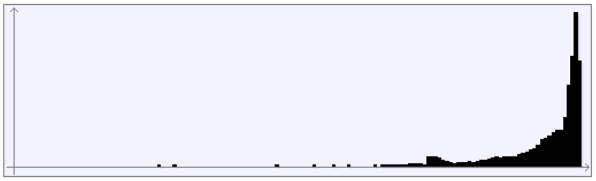

Figure 3.5: COMSOL mesh quality istogram, $SSF - 082$

3.3.4 Boundary conditions and parameters setting

On the points that belong to to symmetry axial (i.e. points with $r = 0$ coordinate) it was imposed a boundary condition of symmetry, in agreement with the geometry of the problem. On the semi-circumference that delimits the outer domain it was imposed a Dirichlet condition, that means $\bar{A} = 0$ over that boundary: this creates an equipotential line that runs all over the frontier and forces the $\bar{B}$ field lines to be bounded inside the domain. This is not physically correct, since the fields should extend to the infinite: by the way, since most of the flux density is located inside the magnetic circuit, we saw that this approximation has a negligible influence on the solution in the region of interest
The parameters can be set to vary one at a time (mono-parametric analysis) or all together in all possible combinations (multi-parametric analysis). The geometrical parameters are created during the construction of the geometry, while by default setting all the physical properties of the materials can be parameterized. To assign a set of values for a parameter, it is possible to assign:

- a list of values;
- an interval and the number of values inside of it;
- an interval and the step of increase of the parameter.

For both magneto static and AC analysis, the position of the voice coil was parametrized, this to allow the introduction of a vertical offset: it's then possible to compute the Bl $[N/A]$ factor over the whole voice coil excursion, equal to $\pm 1,2\ mm$.

3.3.5 solving and post processing

Once the solution has converged, the most interesting results that can be easily extracted through the proper post processing tools are four:

1. the flux density distribution in the motor;
2. the magnetic field distribution in air;

3. the relative permeability distribution in the magnetic circuit;

4. the flux density distribution in the air gap, along the voice coil excursion.

Everyone of these results play a very important role during the design and the analysis of the device.

flux density

With this result one can obtain an initial assessment of the value of B in the air gap and therefore of the *energy* that the motor provides to the air gap, while by evaluating the average B in the magnet one can calculate the working point of the permanent magnet and judge then $efficiency$ of the motor. Indeed, in motors designed with a minimum magnet volume as the target, the working point of the permanent magnet must be positioned in the point of maximum energy of the BH curve, while for motors intended to have minimum distortion and maximum stability versus demagnetization, the working point will be positioned higher, near the ordinate Br corresponding to the residual induction, to make the working point less sensitive to variations induced by the alternating flow produced by the moving coil and to temperature variation (loudspeakers are indeed employed at both temperature extremes, below zero temperature in cold countries in outdoor application as well as over 50C temperatures in cars left during summer in the parking lot)

magnetic field in air

The distribution of magnetic field around the device is a useful information to assess its electromagnetic compatibility, according to national standards.

relative permeability in the magnetic circuit

With this result, one can evaluate qualitatively the order of magnitude of the resistivity that the iron is opposing to the flowing of the flux density field. It is easy to detect which parts are in saturation, and decide if it is the case or not to add or subtract iron, with the purpose of optimizing the behaviour or the cost and weight of the motor.

flux density distribution over the voice coil

One needs for first to create a line (which will constitute the abscissa axis) along which to extract the normal B. The desired profile of normal B along voice coil excursion is always symmetrical but with a plateau that depend largely on the frequency range, power handling, and distortion of the device.
Then a parameter (from materials or geometry) can be associated to the curves and their selected values of interest (for example the mean value). In this way one can obtain a family of curves in which it is possible to compare the best performances of various geometric configurations and materials.

It is also possible to select the domain associated to the voice coil and compute the mean value of B over the coil for every position:
knowing the wire length, it is easy to get the value of the Bl parameter for every position of the coil.

3.4 Main results

3.4.1 Magnetic circuit

In a practical magnet not all of the available flux passes through the air gap because the air in the gap does not differ from the air elsewhere around the magnet and the flux is happy to take a shorter route home via a leakage path. As there are no practical magnetic equivalents of insulators, the art of magnetic circuit design is to choose a configuration in which the pole pieces guide the flux where it would tend to go naturally. Designs which force the flux in unnatural directions are doomed to have high leakage, needing a larger magnet and possibly also maybe some screening in sensitive environments. This is the case of the configuration that use a central pole piece to gather all the radial flux density (configuration that is common to all the three devices under study):
lines are forced to pack together going toward the centre, and then the result is a non neglictible leakage flux, as one can see in Fig. 3.6, 3.7 and 3.8.

Looking at theBH curve, we can assume that the knee is located around the point $BH(1,71;16000)$: then the iron could be considered saturated if it shows a relative permeability that is lower than

$$\mu_{rel} \quad _{min} = \frac{B_{knee}}{\mu_0 \cdot H_{knee}} = \frac{1,71}{4\pi \cdot 10^{-7} \cdot 16 \cdot 10^3} \cong 85 \quad [-]$$

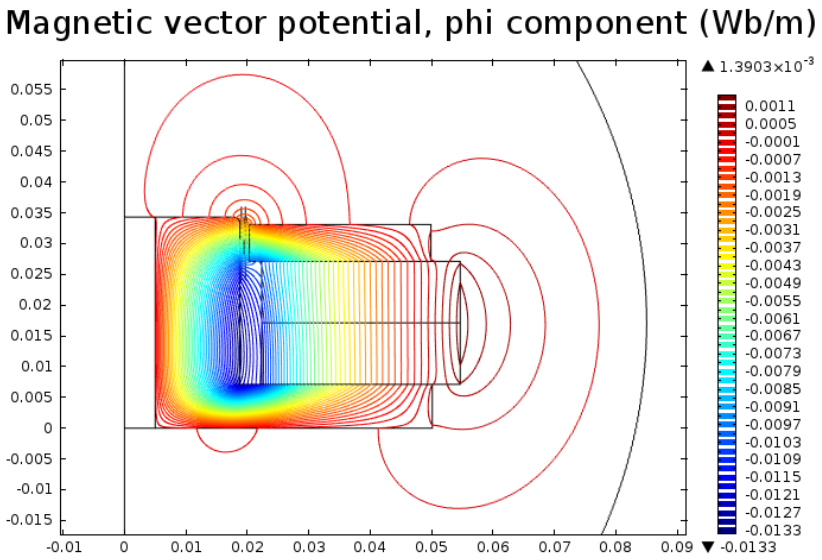

Figure 3.6: behaviour of the flux lines,SV 165

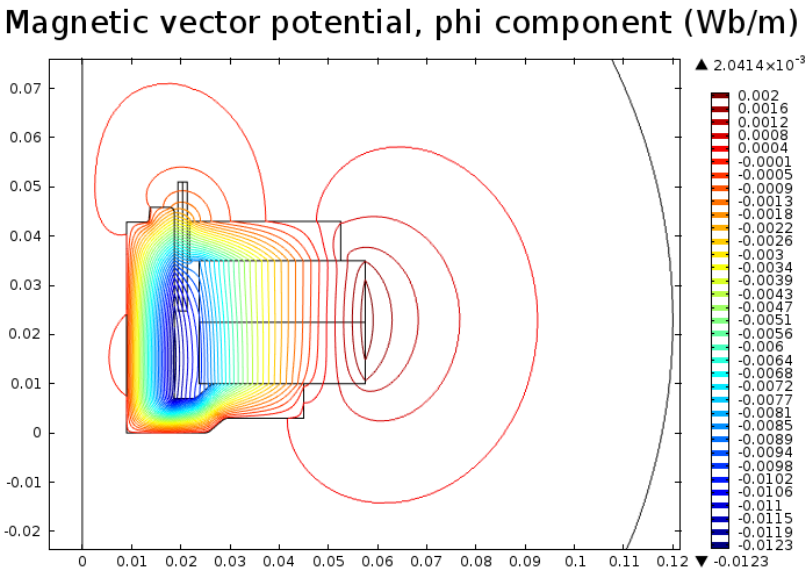

Figure 3.7: behaviour of the flux lines,$DS30.3$

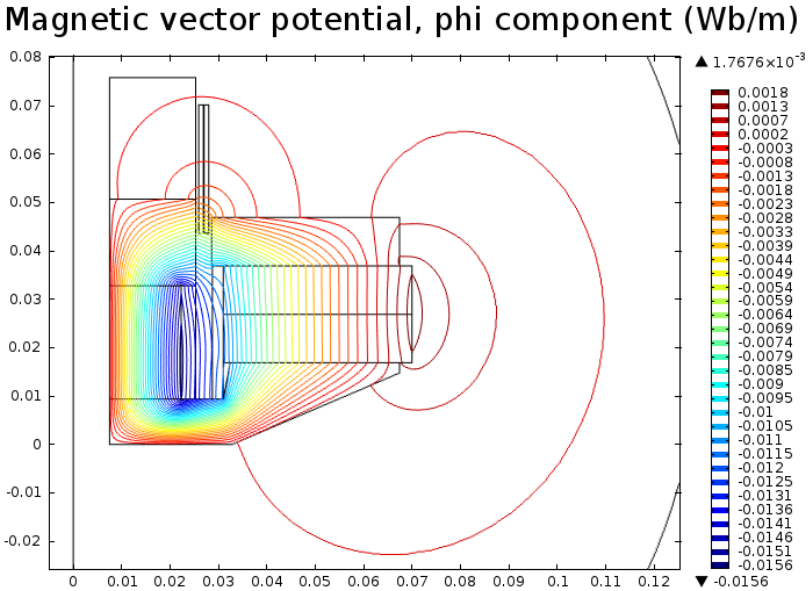

Figure 3.8: behaviour of the flux lines,$SSF - 082$

In the figures 3.9and 3.10 it is possible to see the situation of the magnetic circuit of the SV 165: the elbow between the central pole and the the outer part of the bottom plate show a significant saturation, there is indeed a bottleneck for the flux since the thickness is not enough (probably it's due to other design considerations like weight or total depth of the speaker).

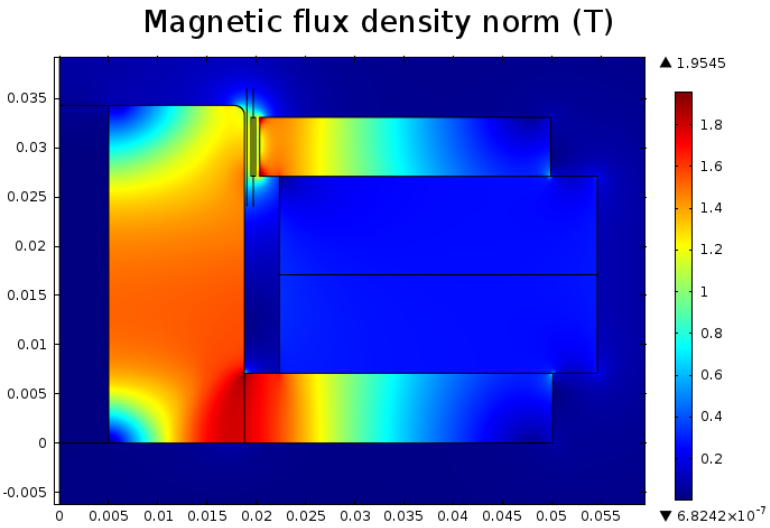

Figure 3.9: flux density magnitude, SV 165

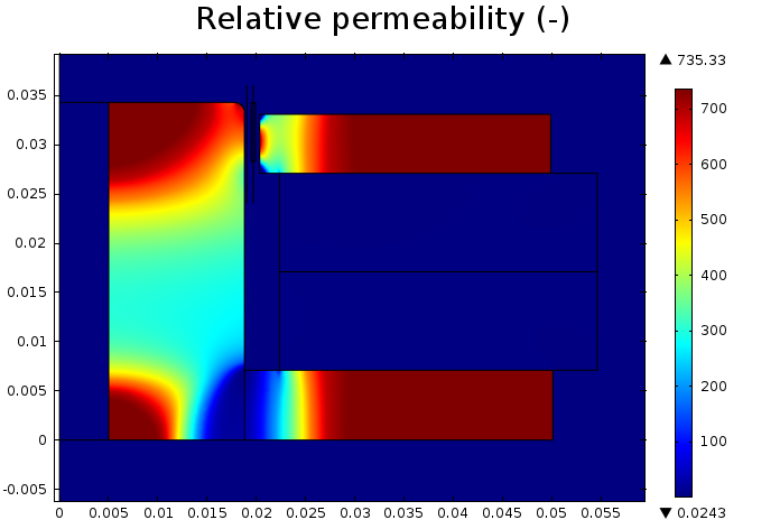

Figure 3.10: relative permeability of the magnetic circuit, SV 165

In the figures 3.11and 3.12 it is possible to see the situation of the magnetic circuit of the $DS30.3$; Almost all the central pole is working near the saturation, the magnetic circuit is very well exploited.

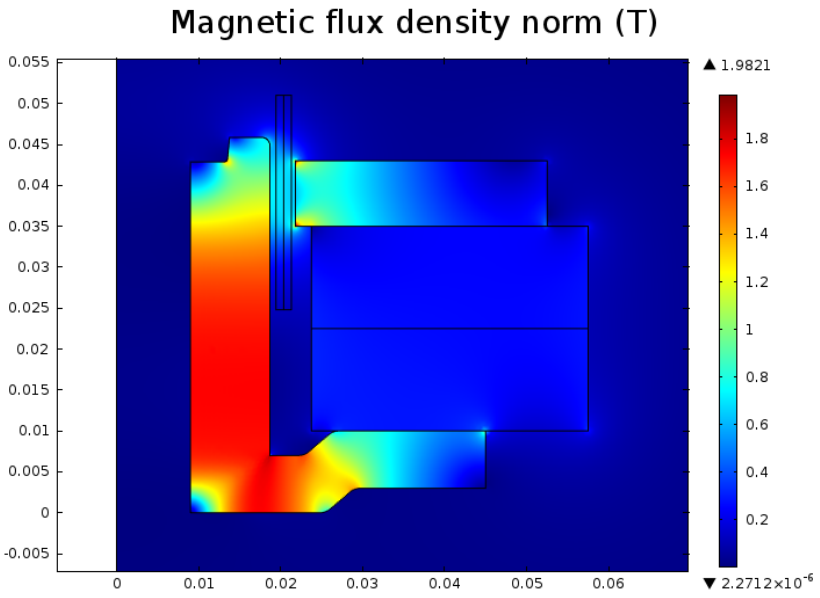

Figure 3.11: flux density magnitude, $DS30.3$

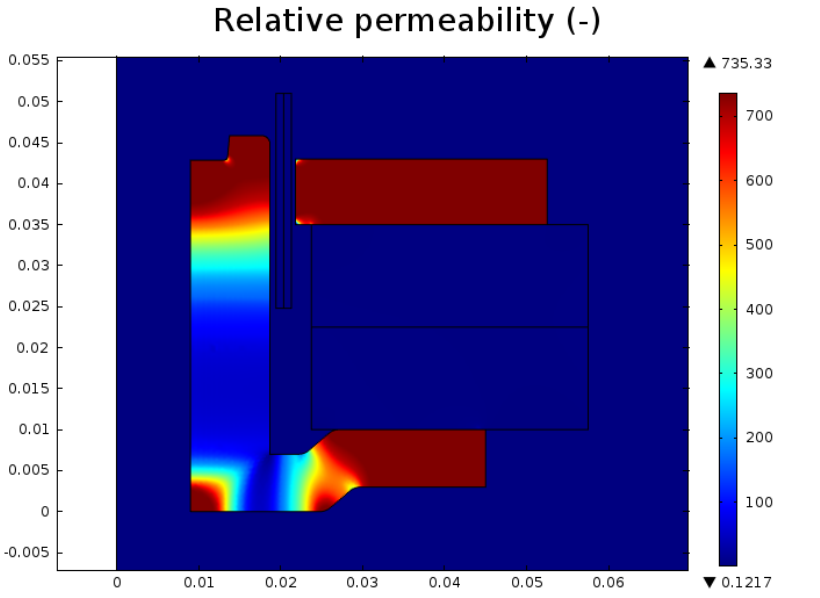

Figure 3.12: relative permeability of the magnetic circuit, $DS30.3$

In the figures 3.13and 3.14 it is possible to see the situation of the magnetic circuit of the $SSF-082$; There is just a small part in saturation between the outer part of the bottom plate and the central pole.

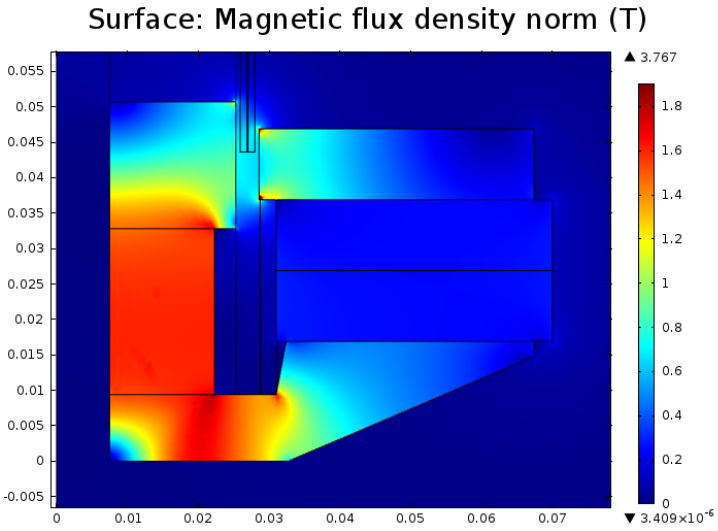

Figure 3.13: flux density magnitude, $SSF-082$

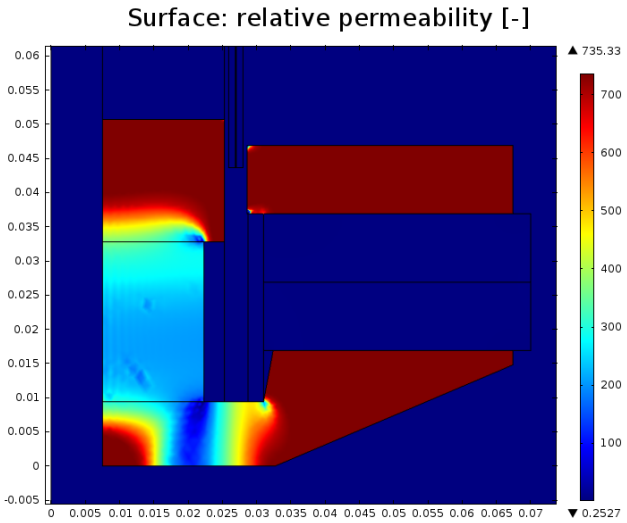

Figure 3.14: relative permeability of the magnetic circuit, $SSF-082$

Due to the shape of the magnetic circuit, there is a strong magnetic field that surrounds all the device: indeed the lines run down also on a path which even if in air has an high cross section, thus a not negligible permeance.

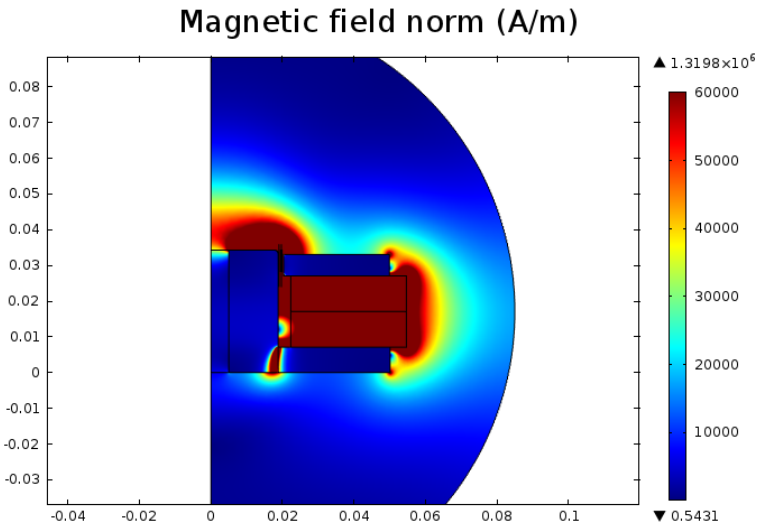

Figure 3.15: magnetic field magnitude, SV 165

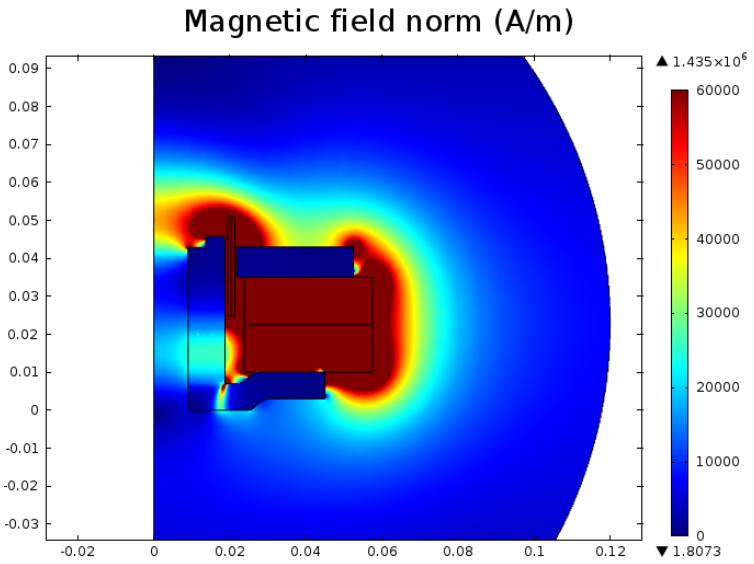

Figure 3.16: magnetic field magnitude, $DS30.3$

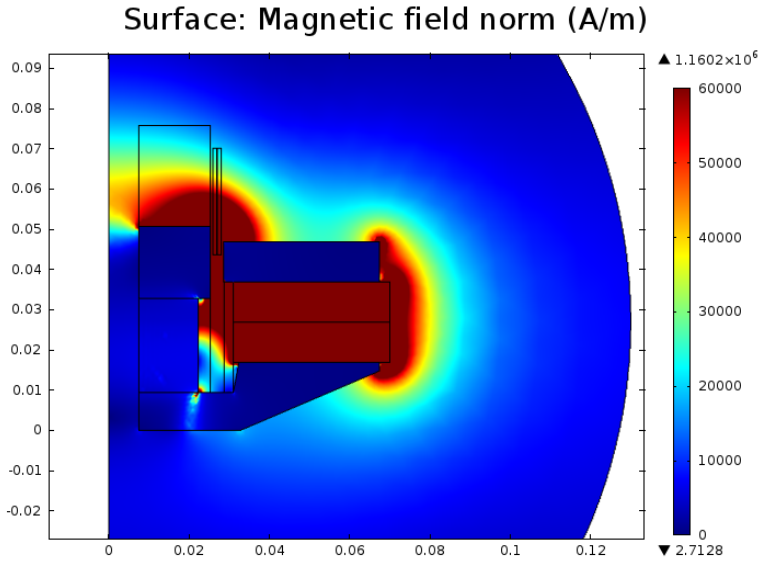

Figure 3.17: magnetic field magnitude, $SSF - 082$

3.4.2 Air gap

The Fig. 3.18, 3.19, 3.20 show the main feature of the transducer: indeed the Bl factor is the element that couples the electrical and the mechanical part of the device,and at the same time it is the main source of non linearities in the output signal, due to the strong dependence on coil position $Bl(x)$.

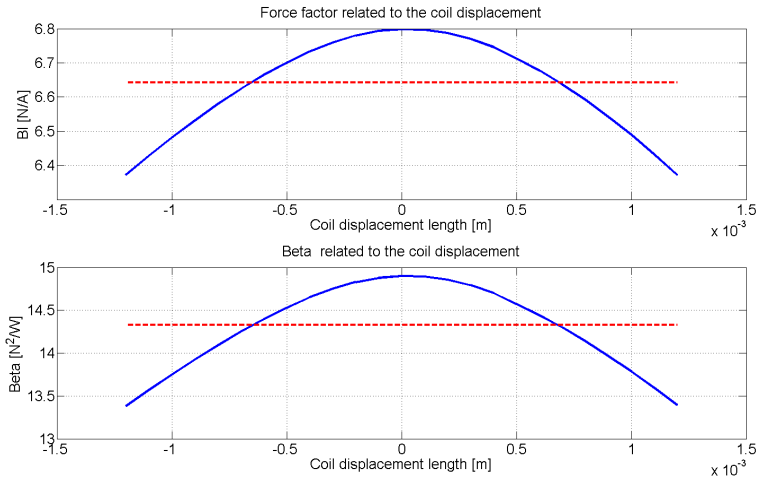

Figure 3.18: force factor related to the coil displacement, SV 165

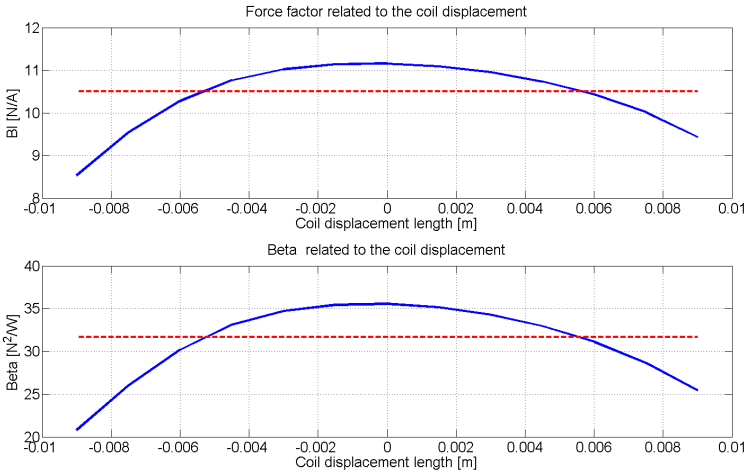

Figure 3.19: force factor related to the coil displacement,$DS30.3$

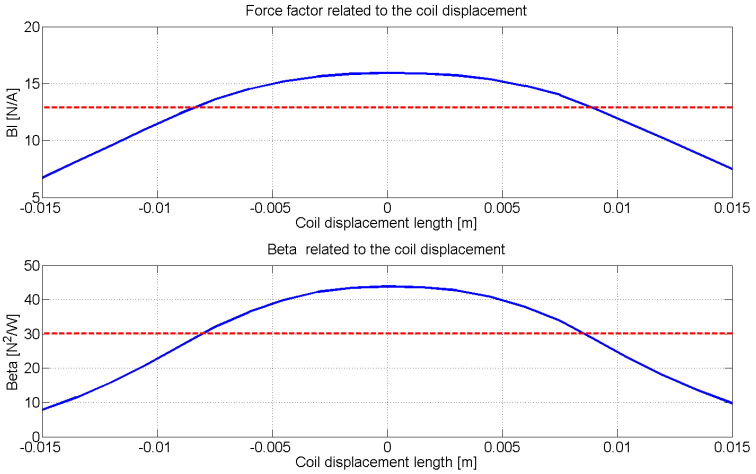

Figure 3.20: force factor related to the coil displacement, $SSF - 082$

A useful quantity to plot is the flux density profile in the air gap along the voice coil excursion. There can be two different targets: an almost constant profile to minimize distortion, given the suspensions allow for such a great excursion, or a symmetrical and "narrower" profile to get the highest possible small signal SPL sacrificing the distortion figures.
The Fig. 3.21, 3.22, 3.23 show these profiles, with the associated mean value.

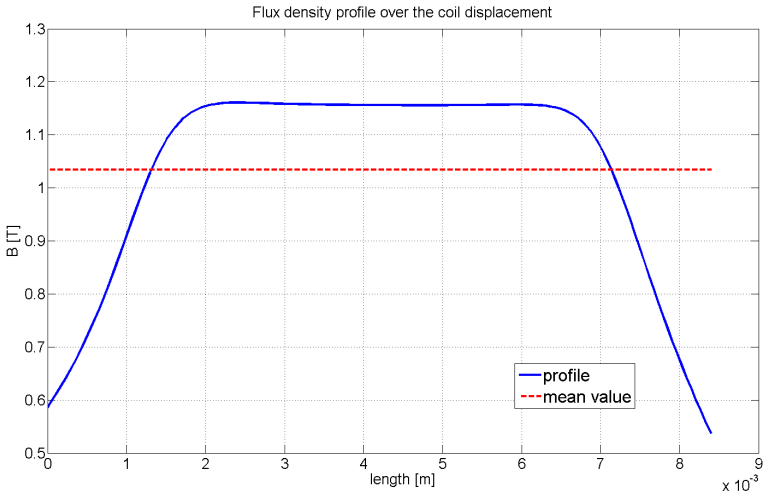

Figure 3.21: Flux density in air gap of the SV 165

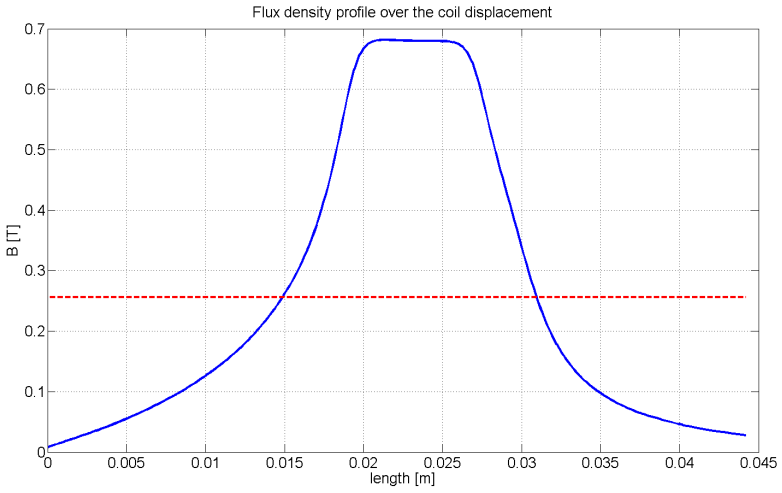

Figure 3.22: Flux density in air gap of the $DS30.3$

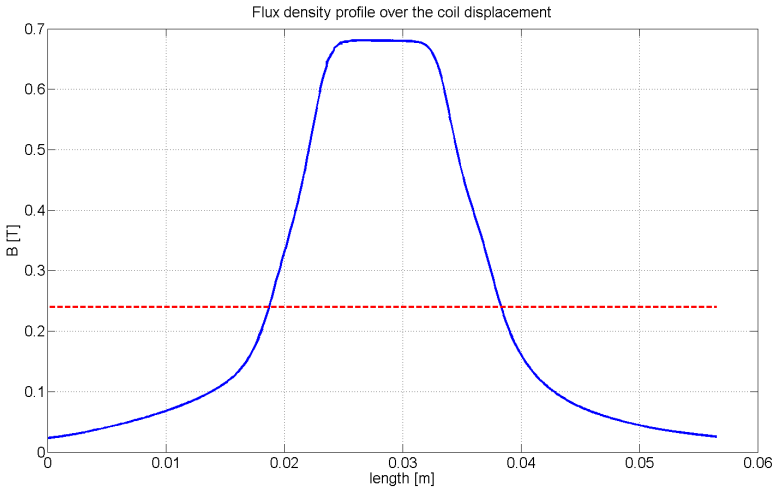

Figure 3.23: Flux density in air gap of the $SSF-082$

3.4.3 Magnet

The following elaborations were processed through Matlab software: the data sets came from Comsol simulation, then they were elaborated through some algorithms to get more information, especially the mean values. We used the trapezoidal integration technique:

$$B_{zmean} = \frac{\int_a^b B_z(r)\cdot dr}{(b-a)} \cong \frac{(r_b - r_a)}{n}\cdot\frac{1}{2}\cdot\frac{[f(r_a)+2\cdot\sum_{i=1}^{n-1} f(r_i)+f(r_b)]}{(r_b-r_a)}$$

where $(r_a,\ r_b)$ represent the extremes of the integration domain.

Each magnet was divided in two parts by an horizontal radial line. The axial -or z - component of the flux density was evaluated along this line. The array of values was then exported in Matlab to compute the magnet working point.Then the array was eleborated in Matlab environment. The results are the working point coordinates B,H as follows (see Fig. 4.19, 3.26, 3.28):

$$B_{SV\ 165} = 0.2714\ [T] \quad H_{SV\ 165} = \frac{(B_{magnet}-B_{res})}{\mu_{rel}\cdot\mu_0} = -86450\ [A/m]$$

$$B_{DS30.3} = 0.2681\ [T] \quad H_{DS30.3} = \frac{(B_{magnet}-B_{res})}{\mu_{rel}\cdot\mu_0} = -88652\ [A/m]$$

$$B_{SSF-082} = 0.2540\ [T] \quad H_{SSF-082} = \frac{(B_{magnet}-B_{res})}{\mu_{rel}\cdot\mu_0} = -98150\ [A/m]$$

to determine the $efficiency$ of the magnets, we drawn on the same plane:

- the characteristic of the magnet;
- an horizontal line passing through the value at the average B in the magnet;
- the $B \cdot H$ characteristic.

From Fig. 3.25, 3.27, 3.29 we can see that all the working points are above the maximum of the energy product function. This choice is made to strengthen the working point versus low temperature demagnetization and make it less susceptible to the perturbation introduced by the variable field generated by the coil: the flux modulation will drop and also the associated distortion.

3.4.4 Field profiles and working point of the magnets

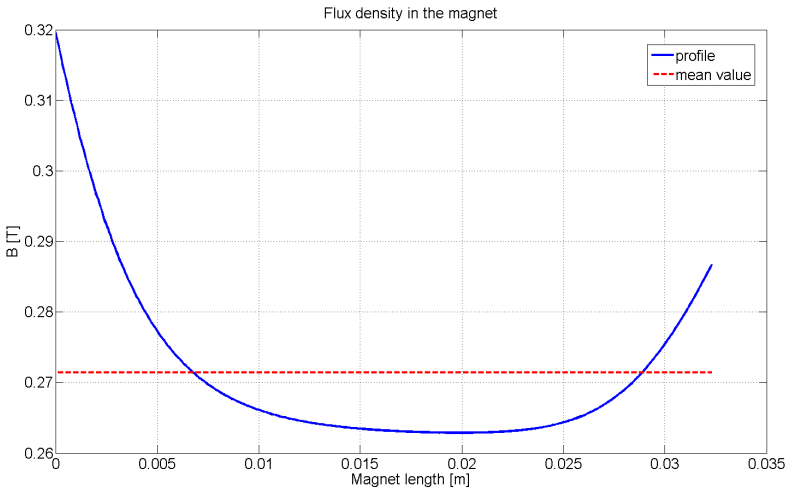

Figure 3.24: flux density profile in the magnet, *SV* 165

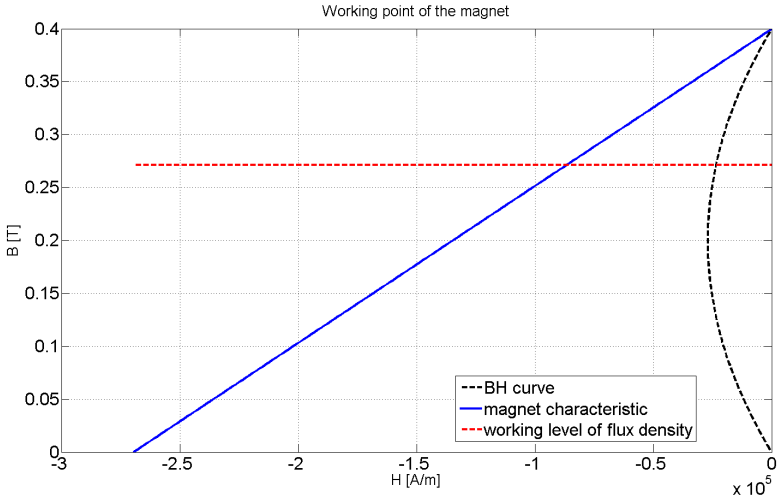

Figure 3.25: working point of the magnet, SV 165

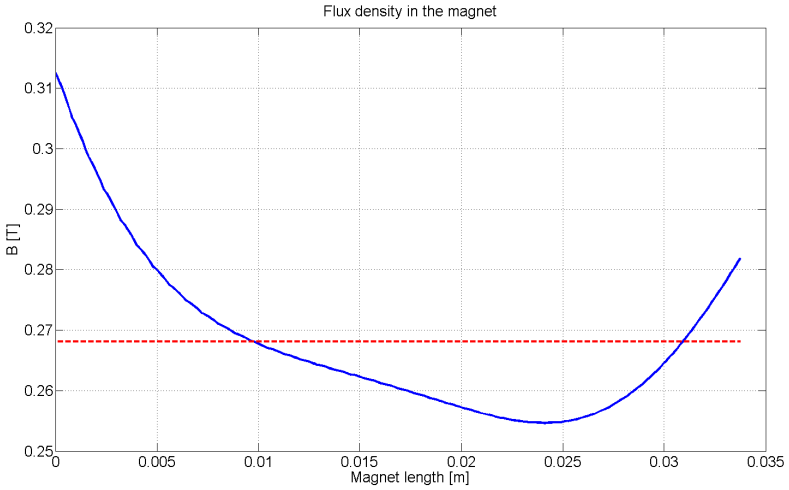

Figure 3.26: flux density profile in the magnet, $DS30.3$

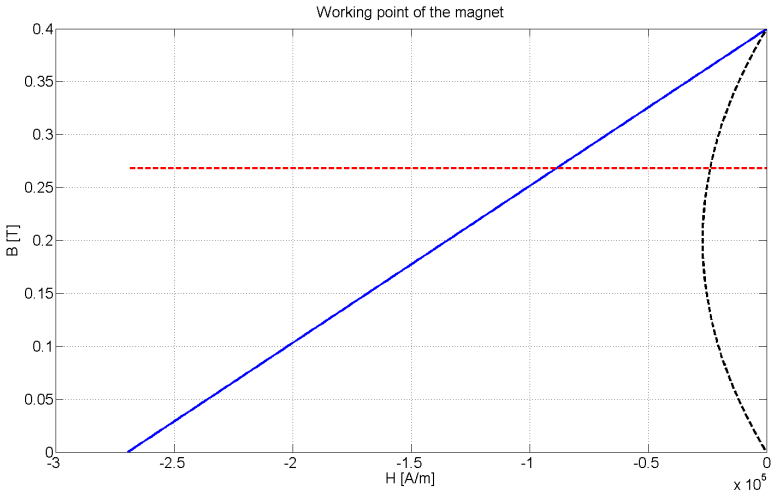

Figure 3.27: working point of the magnet, $DS30.3$

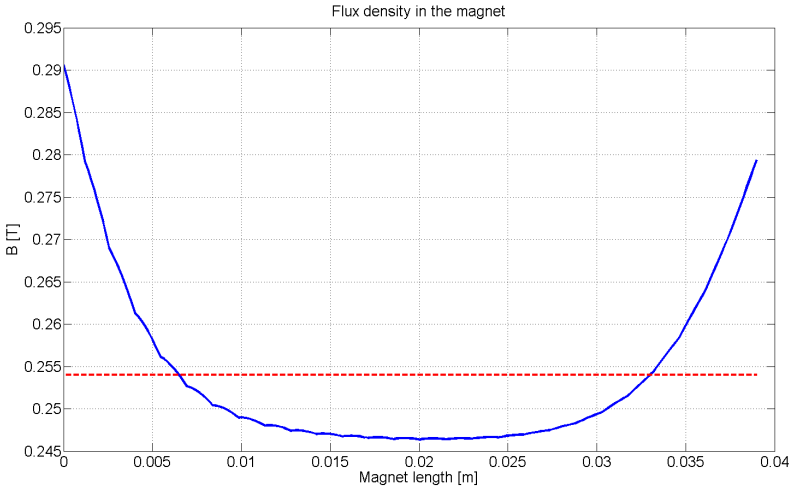

Figure 3.28: flux density profile in the magnet, $SSF - 082$

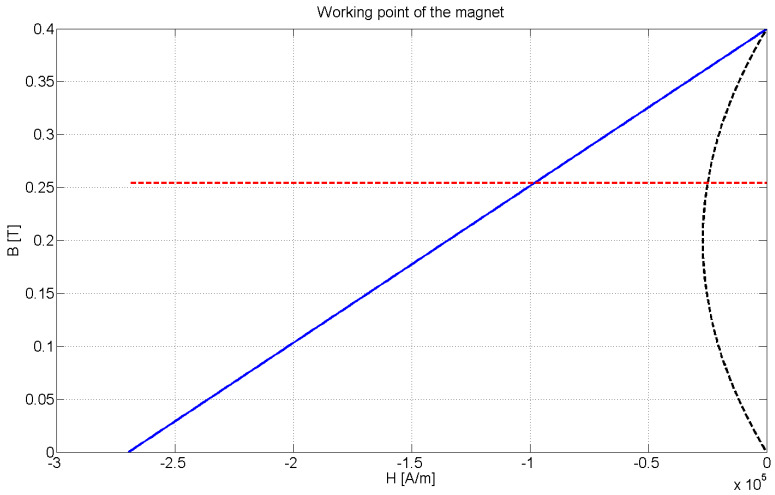

Figure 3.29: working point of the magnet, $SSF - 082$

3.4.5 Exploitation of the magnet

$$\eta_{SV\ 165} = 1 - \frac{(0.2714 \cdot 2\pi \cdot 49.6 \cdot 32.3 - 1.035 \cdot 2\pi \cdot 19.6 \cdot 9)}{0.2714 \cdot 2\pi \cdot 49.6 \cdot 32.3} \cdot 100 = 42.11\%$$

$$\eta_{DS30.3} = 1 - \frac{(0.2681 \cdot 2\pi \cdot 40.3 \cdot 32.3 - 0.2559 \cdot 2\pi \cdot 20.3 \cdot 44.2)}{0.2681 \cdot 2\pi \cdot 40.3 \cdot 32.3} \cdot 100 = 65.27\%$$

$$\eta_{SSF-082} = 1 - \frac{(0.2540 \cdot 2\pi \cdot 39.1 \cdot 50.4 - 0.2397 \cdot 2\pi \cdot 26.9 \cdot 56.9)}{0.2540 \cdot 2\pi \cdot 39.1 \cdot 50.4} \cdot 100 = 73.38\%$$

Another index can be obtained if we consider not all the coil offset, but just the extension of the coil at the rest position

$$\eta_{SV\ 165} = 1 - \frac{(0.2714 \cdot 2\pi \cdot 49.6 \cdot 32.3 - 1.1437 \cdot 2\pi \cdot 19.6 \cdot 6)}{0.2714 \cdot 2\pi \cdot 49.6 \cdot 32.3} \cdot 100 = 30.93\%$$

$$\eta_{DS30.3} = 1 - \frac{(0.2681 \cdot 2\pi \cdot 40.3 \cdot 32.3 - 0.3957 \cdot 2\pi \cdot 20.3 \cdot 26.2)}{0.2681 \cdot 2\pi \cdot 40.3 \cdot 32.3} \cdot 100 = 60.31\%$$

$$\eta_{SSF-082} = 1 - \frac{(0.2540 \cdot 2\pi \cdot 39.1 \cdot 50.4 - 0.4419 \cdot 2\pi \cdot 26.9 \cdot 26.5)}{0.2540 \cdot 2\pi \cdot 39.1 \cdot 50.4} \cdot 100 = 62.93\%$$

Chapter 4

Small signals analysis

4.1 introduction

The attribute *Thiele/Small* about a kind of analysis commonly refers to a set of electromechanical parameters that define the specified low frequency performance of a loudspeaker driver. Many of the parameters are strictly defined only at the resonance frequency, but the approach is generally applicable in the frequency range where the diaphragm motion is largely pistonic, i.e. when the entire cone moves in and out as a unit without cone breakup.
The figure 4.1 shows an example how the cone breakup modes can influence and modify the input impedance profile of the device.

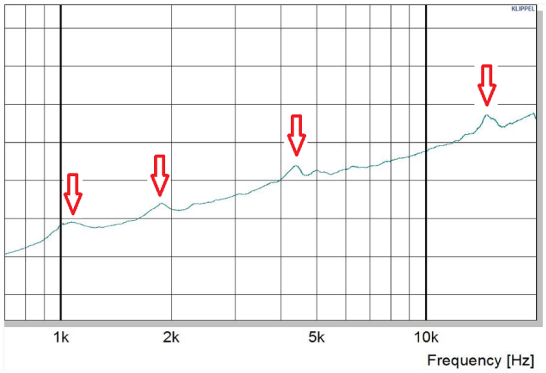

Figure 4.1: influence of cone breakup modes on the input impedance

Our analysis is extended to all the audio frequency spectrum: to reduce at the minimum the influence of the cone breakup modes, we used in the measures some very small voltage input signals.
Our input voltage standards were chosen to be $0.03 - 0.015 - 0.01[V]$:
this ultimately reduces by far the motion of the cone, and then the influence of the break-up modes in the input impedance seen at the loudspeaker terminals.

4.2 The hybrid equivalent circuit

The well-known Thiele equivalent circuit for a dynamic loudspeaker is shown in figure 4.2. Here the admittance analogy is used. This has the advantage that the electrical side of the system is *coupled* to the mechanical side through an ideal transformer with a turn's ratio of $Bl : 1$, where Bl is the force factor of the loudspeaker motor. The input of the system is voltage and the output is the cone velocity u. These are the physical parameters of a loudspeaker driver, as measured at small signal levels, used in the equivalent electrical circuit models. Starting from right to left we find:

- M_{ms} is the mass of the diaphragm and coil, including the acoustic load (air mass), in $[kg]$;
- C_{ms} is the compliance of the driver's suspension, in $[N/m]$ (the reciprocal of its stiffness);
- R_{ms} is the mechanical resistance of the driver's suspension, and it represent the dissipative effects that take place due to the frictions. This parameter is expressed in $[Ns/m]$;
- Bl is the coupling factor, representing the product of flux density field strength in the voice coil gap and the length of wire in the magnetic field, expressed in $[T \cdot m]$;
- L_e is the voice coil inductance, usually expressed in $[mH]$ and function of the frequency; R_e is the DC resistance of the voice coil, measured in $[\Omega]$.

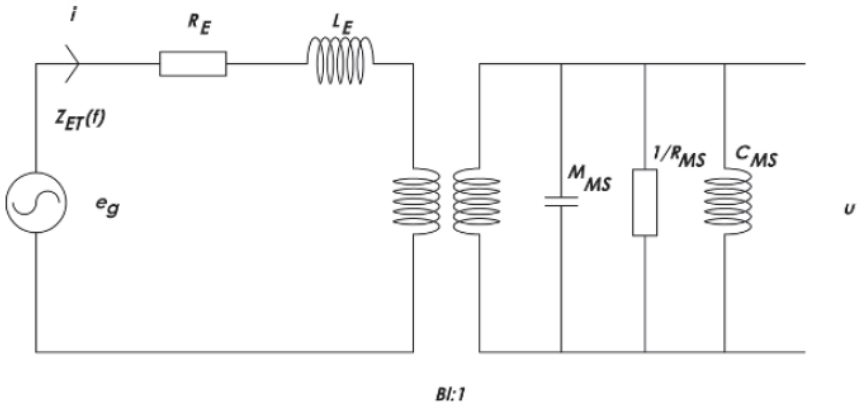

Figure 4.2: traditional equivalent circuit diagram for loudspeaker using admittance analogy

4.3 The electric equivalent circuit

4.3.1 construction

The transformer coupling in figure 4.2 makes it simple to convert the circuit representing the mechanical part (moving assembly) to the primary (electrical) part. The conversion is based on the following equivalences:

$$[V] \Leftrightarrow [m/s] \qquad and \qquad [A] \Leftrightarrow [N]$$

Ideal transformer

On the left side one can find the back EMF generated by the coil motion: this voltage drop is equal to $V = Blv$ volts. Since in the model the fictitious turns ratio is equal to $N = Bl/1$, on the right side we will find a velocity that is equal to $V/N = v$.
Moreover, we will find to the mechanical side a force F that is related to the current flowing inside the coil by the relation $F = (Bl) \cdot I$.

Mass

the law that rules a mass motion is the well known Newton second law:

$$F = M_{ms} \cdot \frac{dv}{dt} \qquad (Bl) \cdot I = M_{ms} \frac{1}{Bl} \frac{dV}{dt}$$

$$I = \left(\frac{M_{ms}}{(Bl)^2} \right) \frac{dV}{dt} \qquad C_{es} = \frac{M_{ms}}{(Bl)^2} \quad [C] \tag{4.1}$$

In conclusion, from the equation 4.1, we can see that the mass behaves like a capacitor in its equivalent representation on the electrical side.

Spring

Since we are dealing with a small signals analysis, we neglect the creep effect that will be discussed in the further chapter(!!). Introducing Hook's law we get

$$F = K_{ms} \cdot x \qquad (Bl) \cdot I = K_{ms} \cdot \int_0^t v \cdot dt \qquad (Bl) \cdot I = K_{ms} \cdot \int_0^t \frac{V}{Bl} \cdot dt$$

if we derive the last expression left and right and introducing the spring compliance $C_{ms} = 1/K_{ms}$ we get

$$V = \left(C_{ms} \cdot (Bl)^2 \right) \frac{dI}{dt} \qquad L_{es} = C_{ms} \cdot (Bl)^2 \tag{4.2}$$

In conclusion, from the equation 4.2, we can see that the spring behaves like an inductor in its equivalent representation on the electrical side.

Damper

The lumped parameter that represents the damping effect in the motion of the motor coil takes care to account all the dissipation effects that are generated almost totally by the friction with the air. Then we neglect the hysteretical effects inside the materials that don't behave like pure elastic and linear materials. The friction is proportional to the velocity of the body, then

$$F = R_{ms} \cdot v \qquad Bl \cdot I = R_{ms} \cdot \frac{V}{Bl}$$

$$V = \left(\frac{(Bl)^2}{R_{ms}} \right) \qquad R_{es} = \frac{(Bl)^2}{R_{ms}} \tag{4.3}$$

In conclusion, from the equation 4.3, we can see that the damper behaves like a admittance in its equivalent representation on the electrical side.

Final model

All the past observations and equivalences yield to the circuit shown in Fig 4.3. The electrical impedance of a loudspeaker $Z_{ET}(f)$ can be considered to consist of two parts, as shown by the dashed boxes in Fig. 4.3.
The components shown in the first box represent the *blocked impedance* Z_e, which for small signals is independent of the motion of the loudspeaker cone: this property can be considered valid since small signals generate a small coil displacement around a rest point, then in first approximation we can consider the problem as linear and introduce lumped parameters.
The components shown in the second box include the motional impedance Z_{EM}. Motional impedance occurs when the voice coil moves through the magnetic field of the motor. This in turn sets up an electromotive force (EMF or voltage) equal to Blv, where v is the cone velocity.
The resulting current will oppose the motion of the voice coil.

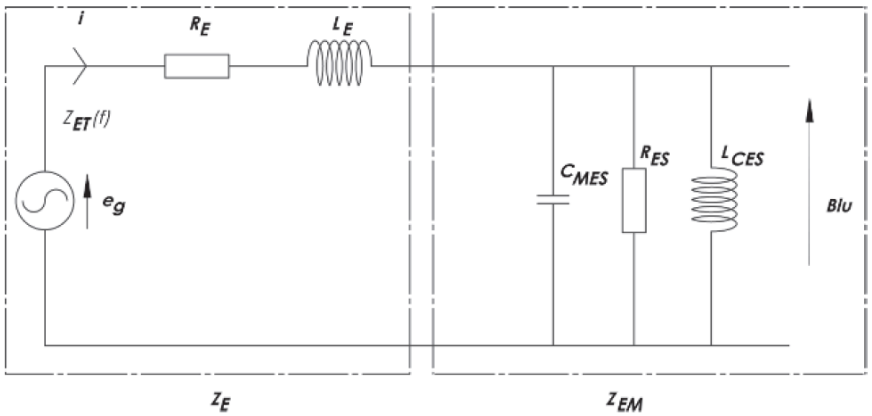

Figure 4.3: Equivalent circuit diagram of Fig. 4.2 for loudspeaker converted to electrical side.

4.4 Differences between measured and modeled impedance

The shape of the loudspeaker impedance curve $Z_{ET}(f)$ is well known:

- at very low frequencies it starts very close to R_E;
- going up in frequency, we can find a peak at f_{res}, due to the mechanical parallel resonance, determined by the electrical equivalents to M_{MS} and C_{MS}, that is, C_{ES} and L_{ES};
- above resonance frequency there is a minimum at f_{min} (mainly due to the series resonance between L_E and C_{ES});
- above the previous minimum the impedance magnitude, according to the model, should rise proportionally with asymptotically to the value of $+90°$.

Introducing the Laplacian variable s the transfer function of the model shown in Fig. 4.3 can be written as

$$Z_{em}(s) = \frac{R_{em}L_{em} \cdot s}{R_{em}L_{em}C_{em} \cdot s^2 + L_{em} \cdot s + R_{em}} \tag{4.4}$$

$$Z_e(s) = R_e + L_e \cdot s \tag{4.5}$$

$$Z_{input} = Z_{em}(s) + Z_e(s) \tag{4.6}$$

and then drawn in $Simulink - Matlab$ to analyze the dynamic stability

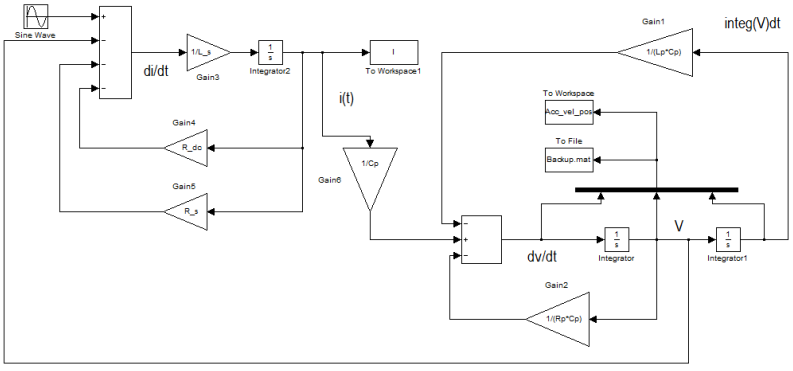

Figure 4.4: Simulink scheme of the dynamic impedance

To verify the model, we considered the loudspeaker *SV.*165 *midrange* and made a measurement with the Klippel Distortion Analyzer, to get the mechanical parameters for filling the Z_{EM} impedance and see the shape of the $Z_{input}(f)$. After that we performed a finite element simulation at $1kHz$ to get the value of inductance L_E; the parameter R_E, accordingly with the model,was interpreted as the DC resistance of the wire and was computed by hand (see cap. geometry

and materials).
In the Fig. 4.5 and 4.6 where one can see the function $Z_{input}(f)$ given by the model and by the measures.

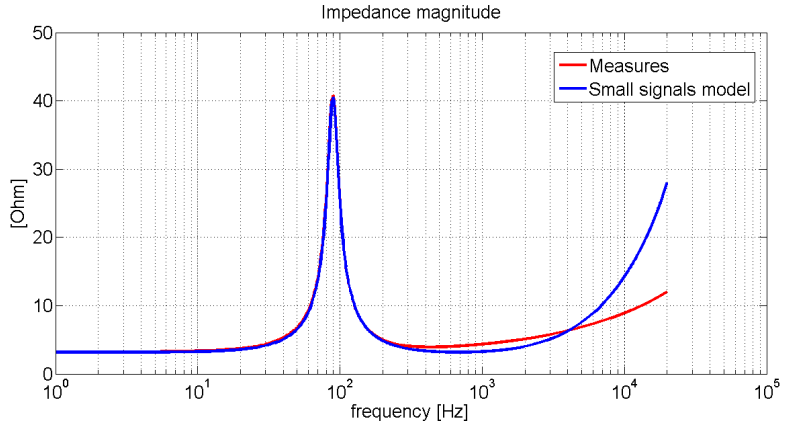

Figure 4.5: Magnitude of the $Z_{input}(f)$ seen at the coil terminals

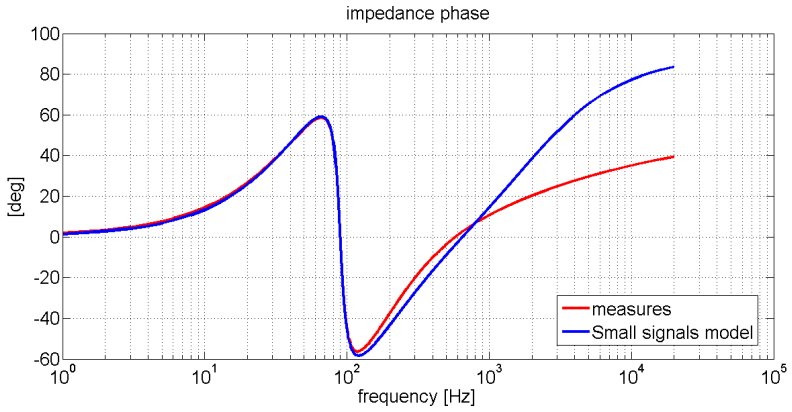

Figure 4.6: Phase of the $Z_{input}(f)$ seen at the coil terminals

Comparison between the impedance curve predicted by the simple equivalent circuit and the actual measured impedance reveals some differences:

- first, at f_{min} the impedance magnitude should be very close to R_E, and the phase angle should be zero;as we can see, this does not happen.

- Secondly, the measured slope of the impedance curve at high frequencies is approximatively closer to $3dB/decade$ rather than the $6dB/decade$ we would expect if the only inductive element in the circuit were a conventional inductor.

4.5 Eddy currents effect and approximated models

Vanderkooy [27] explained the $3dB$ slope of the impedance curve as the result of eddy currents in the iron core of the speaker's pole piece and as the result of the $skineffect$.
As the skin depth decreases with the square root of frequency, the electrical conductivity of the iron in the pole piece is gradually reduced:
a new component is needed, it is called *Semi-inductance* or *Lossy inductance*, and it is measured in *semi-Henry* $[sH]$. The electrical part of the equivalent scheme,i.e. Z_E, has to be changed: now it is composed by the DC resistance and the lossy inductance $Z_L(j\omega)$ that is shown like a general lumped parameter

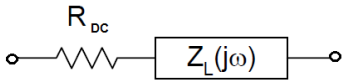

Figure 4.7: general representation of the Z_E

To describe the frequency dependence of $Z_{input}(f)$, several models with a minimal number of free parameters were introduced. These models move from the hypothesis that the R_{dc} resistance has been previously subtracted from the total electric impedance, this with the purpose to focus only on the lossy inductance behaviour.

WRIGHT model

Wright [30] proposed a model using separate weighted power functions in ω for both the real and imaginary part of impedance.

$$Z_L(j\omega) = K_{rm} \cdot \omega^{Erm} + j \cdot \left(K_{xm} \cdot \omega^{Exm}\right)$$

This model uses four free parameters and normally gives a better fit than the other models with less parameters.

LEACH model

M. Leach [15] proposed a weighted power function of the complex frequency as an approximation for Z_L

$$Z_L(j\omega) = K_{rm} \cdot (j\omega)^n$$

Although using only two free parameters this function can sometimes give a very good fit over a wide frequency range.

$LR-2$ (shunted inductor) Model

This model [12]uses three components, in a series/parallel configuration:

- the inductance $L_e(x)$ represents the frequency independent part of the voice coil inductance;

- the parallel of $L_2(x)$ and $R_2(x)$ that together try to reproduce the combined effect of the inductance of the coil and the presence of Eddy currents in the conductive regions of the device.

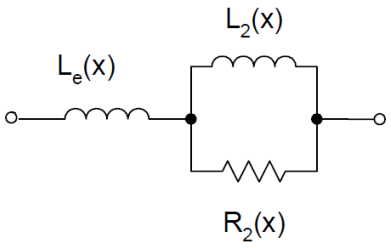

Figure 4.8: equivalent electrical circuit

Although this model uses three free parameters it often provides a worse fit to measured Z_L than the LEACH model. On the other hand its parameters are independent from frequency.

Effective inductance Model

$$Z_L(j\omega) = L_{eff}(f)j\omega + R_{eff}(f)$$

M. Leach also proposed [12] normalizing the imaginary part of the electrical impedance $Z_L(j\omega)$ to the frequency $j\omega$ and introducing an effective inductance $L_{eff}(f)$ which varies with frequency. The real part of $Z_L(j\omega)$ may be considered as a frequency depending resistance $R_{eff}(f)$ describing the losses due to eddy currents as shown in Fig. **??**.

Figure 4.9: representation of the electrical impedance

Though the number of parameters is very high, two parameters for each frequency point, both parameters are easy to interpret and convenient for graphical representation.

Criticism

All these previous models can produce a good fit of the data sets that usually come out from the Klippel Distortion Analyzer:
by the way they are quite useless for the synthesis process, indeed they are used over measures of existing devices. In a certain meaning, the lumped parameters models are forced to be correct: if there is a systematic error in the measures, the equivalent parameters will fit as well the error, without the possibility to see it.
Moreover they are weakly related to the physics of the problem:

even if they move from physical considerations, their expressions try to be as simple as possible, with the fewest degrees of freedom, introducing then a strong approximation.
These are the reasons why we consider the finite elements analysis as a *must* in the process of a design of a new device and especially in its optimization. Just in the end of the work, we will

Our target

It was shown that there is a big problem in modeling the blocked coil impedance, especially if one wants to create an equivalent lumped parameters model.
Since our target is the optimization of the demodulation rings, and having seen that they affect just the blocked coil impedance, in the next part of the work we will focus just on the modeling of the lossy inductance, neglecting the mechanical part of the impedance.

4.6 validation of the measurement equipment

4.6.1 the idea

To verify the quality and reliability of the instrument, we decided to set up a very simple experiment. This was done with the purpose to understand the wired phenomena that sowed up during the measure of the lossy inductance under the mechanical resonance frequency.

The idea was to use the instrument over a very trivial problem, to measure the inductance of a simple copper coil in air: since the materials and the laws that rule the physics are linear and the geometry is simple, this problem can be also verified easily through an analytical model.

Off course this assumption about linearity is true until the skin depth starts to show its influence: by the way, as it can be seen in figure 4.10, we can neglect this effect and consider the problem as linear, at least for the audio frequencies, where the skin depth is considerably greater than the radius of the copper wire of which the coil is made.

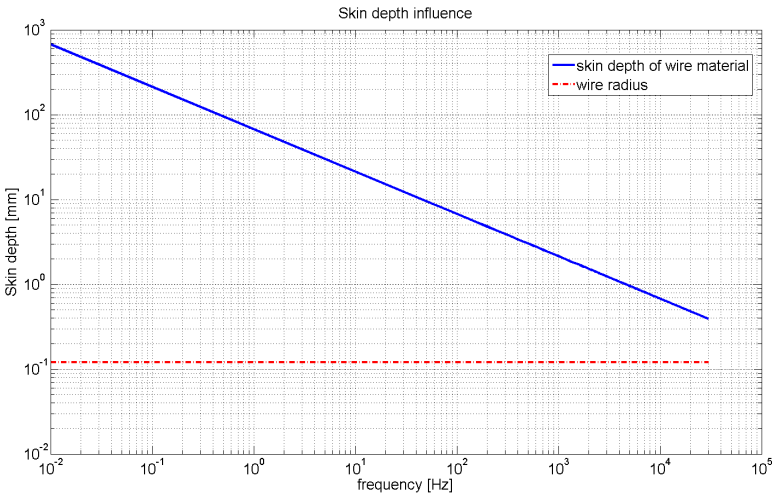

Figure 4.10: Skin depth influence

Then we disassembled the *SV*.165 loudspeaker, extracting the coil, the former and the cone from the magnetic circuit, as one can see in figure 4.11 and after that we hanged the piece in air, we linked the terminals of the cone to the Klippel Distortion Analyzer, and we launched a set of measures.

4.6.2 the simulation

We prepared the simulation, considering a rectangle that approximates the coil, in which we imposed a constant current density and the electrical conductivity equal to zero. Since we work with am equivalent single turn that has an height greater of the skin depth at high frequencies, we need to be careful avoid the thickening of the current density on the extremes of the coil. The figure 4.12 shows what happens at $10KHz$ if just a single turn domain is imposed: the

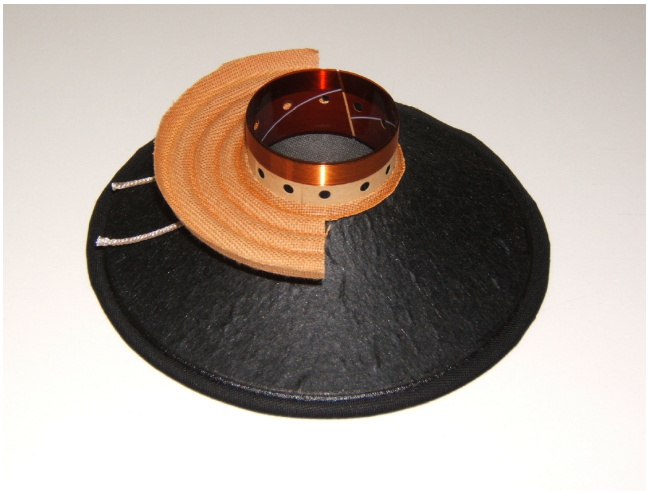

Figure 4.11: the coil after being removed from the magnetic circuit

physics of the problem is violated, since the conductors are strained and actually there is no skin effect at all.

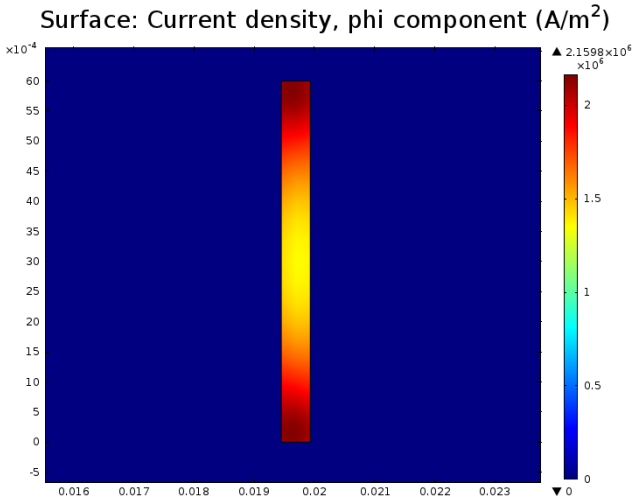

Figure 4.12: skin depth effect at 10 kHz

Then we considered a $\sigma_{coil} = 0$, in that way the equivalent turn does not skin and the simulation is nearer to the actual behavior of the device. Assuming that the measures are fast enough we can assume that the coil is working at room temperature: for the dc resistance we refer to the same calculated in the section that deals with the materials.

To set up a good mesh, we introduced a fictitious box around the coil and the coil core, to allow a softener transition from the interesting zone to the surroundings.

I greatly deepened the mesh on the coil domain since I used the solution over

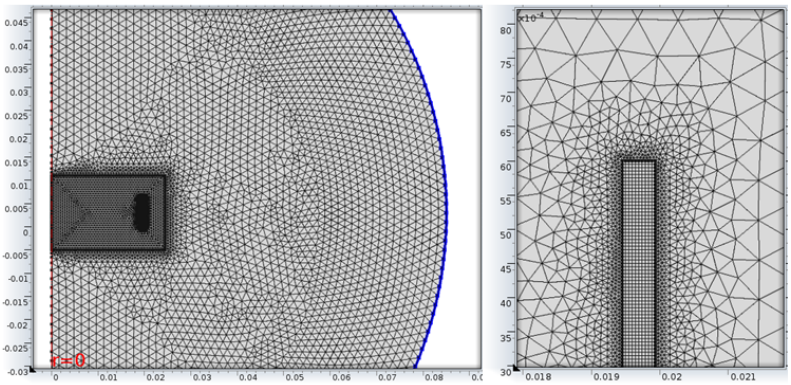

Figure 4.13: snapshots about mesh details

Figure 4.14: element quality histogram

that points to compute the linkage flux with the coil, and then the inductance. Assuming to work with a sinusoidal input signal, we have

$$L_{coil} = \frac{N \cdot \dot{\Phi}}{\dot{I}} = \frac{2\pi \cdot N \cdot \frac{1}{\Sigma_{coil}} \int_{\Sigma_{coil}} r\dot{A}_{\phi}(r,z)\ d\Sigma}{\dot{I}} \tag{4.7}$$

In this situation, the electric equivalent model is very simple

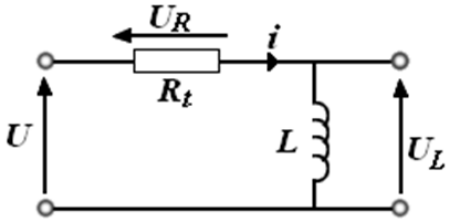

Figure 4.15: equivalent electric network

and also the equation that rules the circuit is trivial

$$\dot{U} = R_{dc}\dot{I} + j\omega L_{coil}\dot{I}$$

Looking from the terminals, we should see at very low frequencies almost a pure resistance that coincides with the DC coil resistance; growing the frequency, the impedance should change its behavior, since the weight of the inductive

part grows more and more. For high frequency, the impedance should rise proportionally to the frequency, and the phase should asymptotically approach the value of $\pi/2$ There is a very good matching between the finite elements model and the measures.

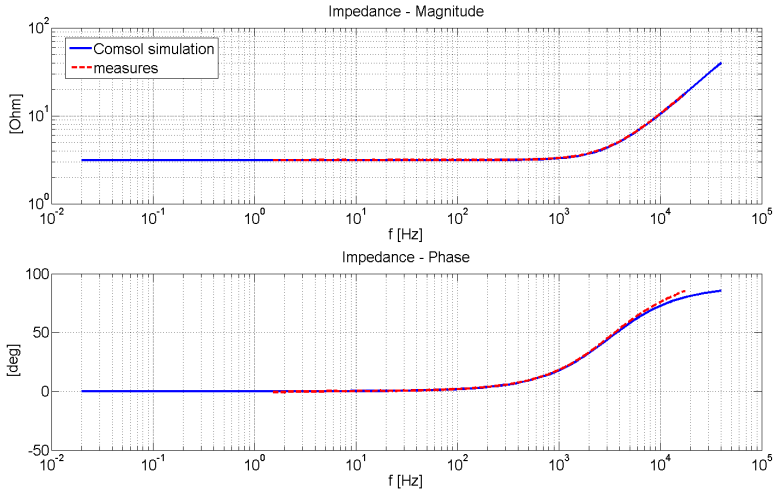

Figure 4.16: impedance of the coil

The result of simulation, concerning the lossy inductance, should be a pure imaginary impedance, with a constant inductance, an impedance growing linearly with the frequency and a phase constantly equal to $\pi/2$.

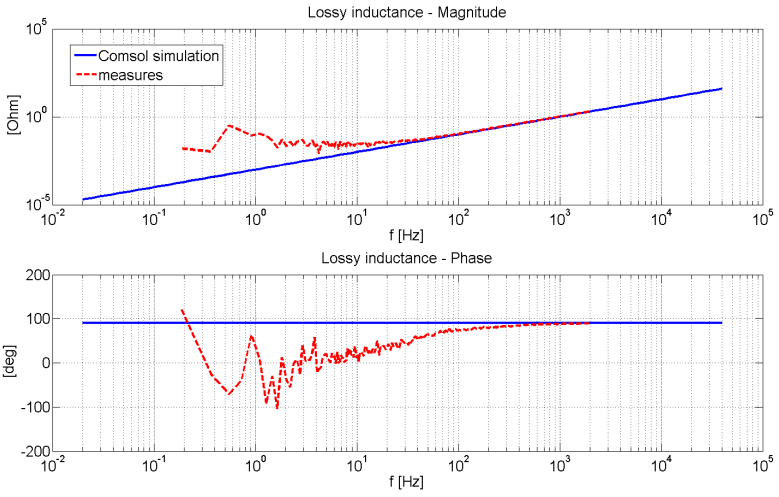

Figure 4.17: lossy inductance of the coil

As it is easy to see, there is a big problem in the measures, since they start to diverge around the threshold of 100 Hz and for the frequencies under this value, there is no more any physical mean.

4.6.3 The analytical formulation

Concerning the evaluation of the inductance, the problem has also an analytical solution. We could use the the expression taken from the classic theory, where all the flux lines are straight and parallel inside the solenoid and link the whole solenoid.

$$L_{coil} = \frac{\mu \cdot N^2 \cdot \Sigma_{coil}}{h_{coil}} = 0.61132 \ [mH]$$

By the way,as we can see from the Fig. 4.18, it is not our situation, since the solenoid has an aspect ratio too low. The color scale represents the intensity of the flux density field, whilst the lines represent the $equi - A_\theta$ concerning the vector potential field. As already discussed, the equipotential lines of the potential magnetic vector are tangential to the lines of the flux density field.

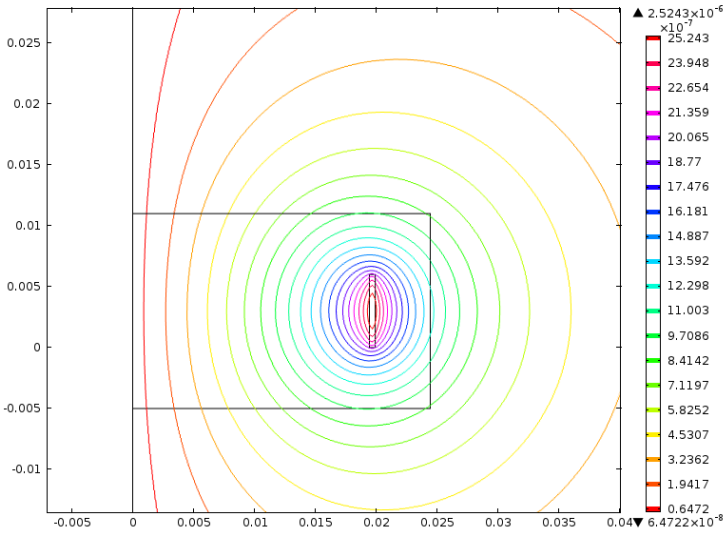

Figure 4.18: flux density lines at 5 kHz

The distribution of the magnitude of flux density inside the coil can be see setting a (r, θ) cut plane located at half the height of the coil.

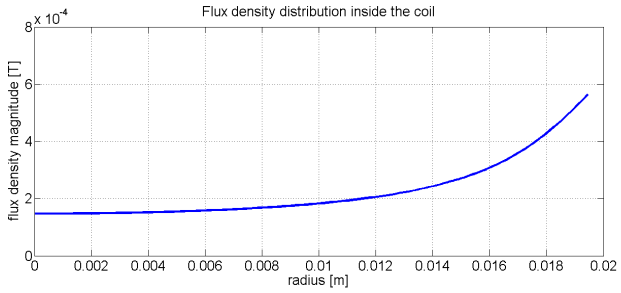

Figure 4.19: distribution of the flux density magnitude

Then we need to use a more accurate formula: in literature there are a lot of studies and approaches (theoretical, semi empirical, totally empirical), we chose to use a semi empirical one taken from "ARRL Handbook, 66th Ed. American Radio Relay League (1989)"', developed on purpose for the short air core solenoids

$$L_{coil} = \frac{r_{mean\ coil} \cdot N^2}{9 \cdot r_{mean\ coil} + 10 \cdot h_{coil}} = 0.156876\ [mH]$$

The relative difference is equal to

$$\epsilon_{\%} = \frac{1.59182 - 1.56876}{1.56876} = 1.47\ \%$$

then we can consider the finite element model accurate enough for the purpose. In conclusion we can see that the finite elements model is correct, indeed it fits the forecast about the shape of curves, and gives a good estimation of the inductance value. On the other hand, we enlightened a problem relative to the measurement apparatus.

4.6.4 Measures with the new amplifier

The previous results pushed us to change the amplifier model on the measuring instrument, shifting from a low budget Behringer to a Crown amp with linear power supply stage.

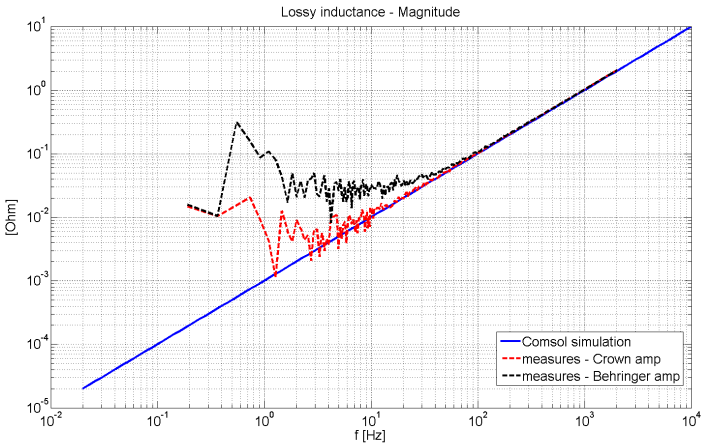

Figure 4.20: comparison between measures and simulations

As you can see, now there is an excellent agreement up to very low frequencies, until around 10 Hz: since the lowest frequency that a mean human hear can feel is conventionally 16 Hz, any discrepancy below this threshold is meaningless since these data don't help the design of a good loudspeaker.

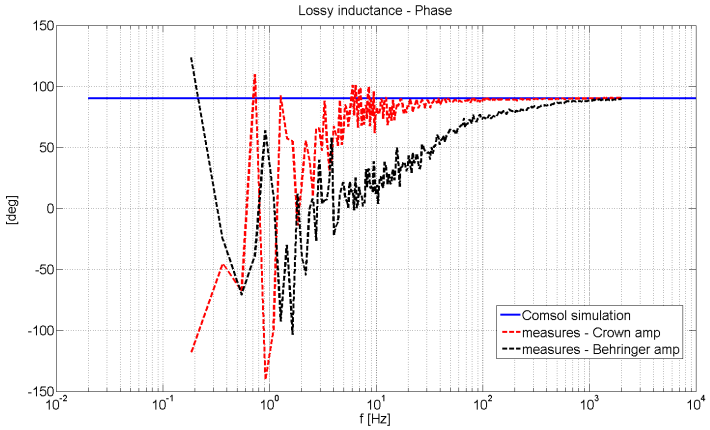

Figure 4.21: comparison between measures and simulations

4.7 Main results form FEM simulation

In the following section, we will show how a proper design through finite elements method can predict the behaviour of the blocked coil lossy inductance, with an excellent agreement with the measures that come out from the Klippel Distortion Analyzer. There are some considerations we need to explain before, to better understand the results:

- we found the lossy inductance for both two devices, the $SV.165\ midrange$ and the $DS30.3\ woofer$; this was made with the purpose to show that the method is valid regardless of the type of device;
- the blocked coil inductance was calculated for the rest position of the coil;
- the blocked coil was calculated over a wide range of frequencies, $2[Hz] - 20[kHz]$,regardless of the fact that the woofer was thought to work in the range of $28[Hz] - 300[Hz]$ and the midrange between $100[Hz] - 10[kHz]$; this with the purpose to extend and strengthen the validation of the method over a wider range of the frequency spectrum.
- the coil conductivity in the FE model was arranged to be equal to zero,like in the free air simulations(as discussed in the previous section), to avoid the influence of the DC resistance and the skin effect.
- only the measure sets made by the Crown amplifier, since with the experiment of the coil in free air we have already shown that the ones made with the Behringer amplifier are not reliable.

$SV.165midrange$

The result of simulation, compared with the measures, is shown in the Fig. 4.22 and 4.23:
the difference between the two pictures lays on the fact that the frequency intervals of the measures are different.

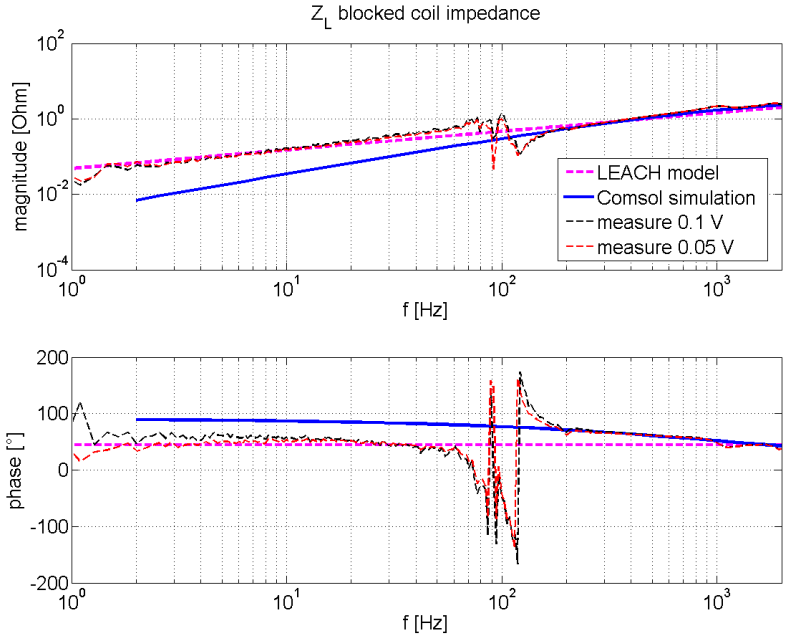

Figure 4.22: comparison of the results, measures up to $2kHz$

As one can see, the correspondence between the FE model and the measures is very good just over the mechanical resonance frequency of the device. To find an answer to this behavior, we wrote directly to the creator of the Klippel Analyzer, Mr. Wolfgang Klippel:
He explained us that the lossy inductance provided by the instrument is based on COMPLETE modeling of the mechanical, electrical and (acoustical) behavior of the driver using lumped parameters. Then the lossy inductance is actually the residual electrical impedance which cannot be explained by the other electrical and mechanical transducer parameters:
thus all deficiencies of the model, measurement errors and noise take place in this curve.
At the mechanical resonance the total impedance is very high due to the back EMF (maybe 100 times higher than the magnitude of the lossy impedance) and then is vain to try to extract a precise value that is just the 1% of a measure and filled by uncertainty:
then the data below the resonance have not to be used.

It is worth to note that the interpolation through the lumped parameters models (LEACH in this case) will fit any kind of systematic error, as one can see from the previous figures. If we bound ourselves to observe just the data fitting over $100Hz$, we can see that the FE model can predict the impedance with an exceptional agreement with the measures.

By the way, it exists a way to measure the exact value of the impedance related to the lossy inductance: it is necessary to block the motor coil in the

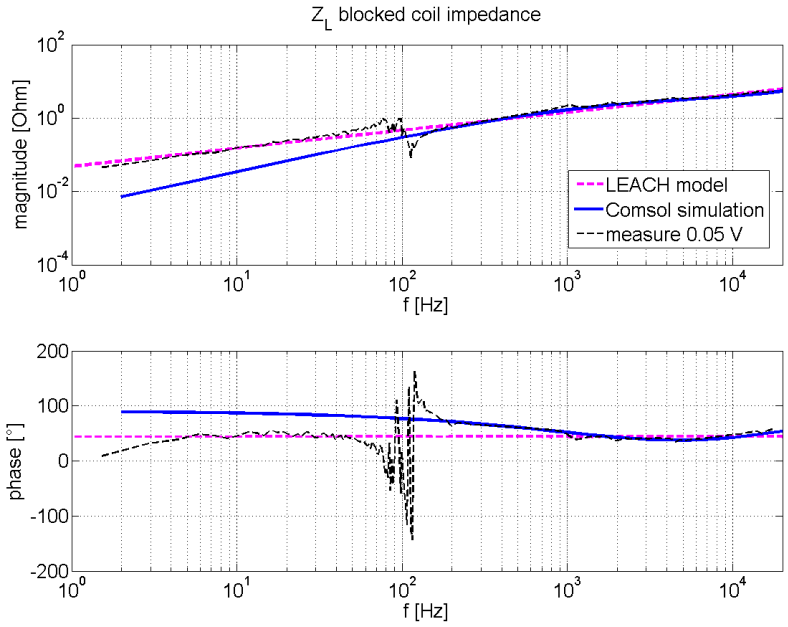

Figure 4.23: comparison of the results, measures up to $18kHz$

rest place, with a very strong not magnetic glue.
In that way it is possible to cut away all the electromechanical part of the impedance. Unluckily this is a destructive test and it was not possible to take that measure.

*DS*30.3

The result of simulation, compared with the measures, is shown in the Fig. 4.22 and 4.23:
the difference between the two pictures lays on the fact that the frequency intervals of the measures are different. As discussed in the chapter relative to the geometry, the device does not enjoy the property to be axial-symmetric. Now we can see the effect of the cuts on the Aluminium former that make it to behave either as a conductor nor as an insulator:

- on one hand the cuts prevent the former to create a loop that could link all the magnetic flux and allow the flow of the counteracting induced currents;
- on the other hand since the former is made by conductive material, the currents can flow and generate closed loops in the former thickness, then the result is a behaviour that is located at the middle way.

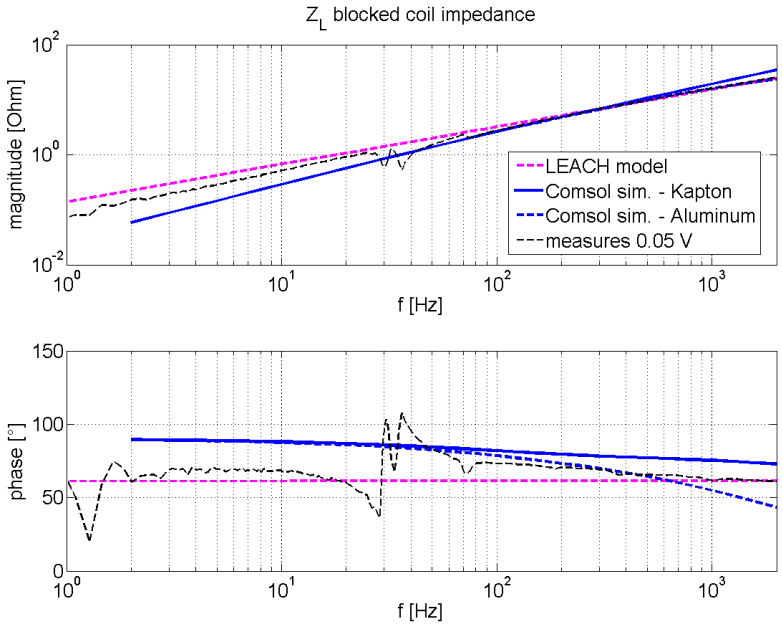

Figure 4.24: comparison of the results, measures up to $2kHz$

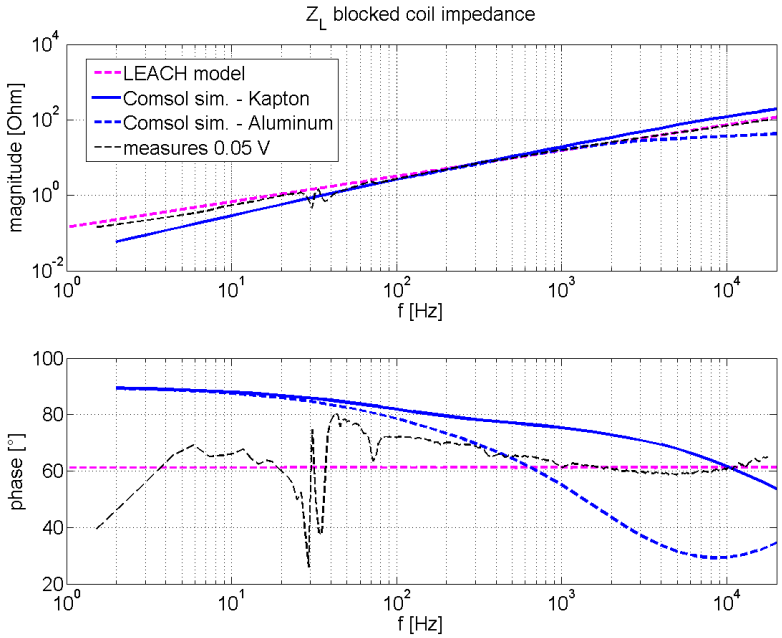

Figure 4.25: comparison of the results, measures up to $18kHz$

As an experiment, we tried to introduce a partially conductive material, called $pseudo - Aluminum$, that has the very same physical characteristics of

Aluminum, but a conductivity that is an order of magnitude lower.
If we choose a proper section of the frequency spectrum, the one where the woofers usually work (let's say $10 - 600$ $[Hz]$), we can see from the figure 4.26 that the configuration which fits better the measures is the one with the Kapton former:
so it will be the choice in all the next simulations.

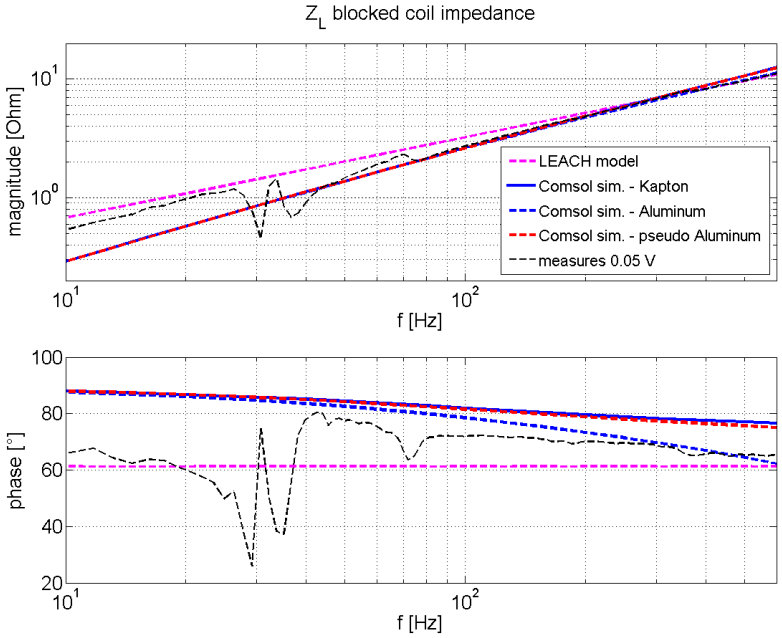

Figure 4.26: comparison of the results, measures up to $600Hz$

Chapter 5

Main non linear distortions in loudspeakers

5.1 introduction

When using the finite elements method, the main problem that is encountered is the need of taking in account a lot of behaviors that act inside of the loudspeaker with nonlinear characteristics.
Especially at higher signal amplitudes all loudspeakers behave more or less nonlinearly, generating signal components that do not exist in the input signal: there is a wide variety of nonlinear mechanisms occurring in loudspeaker systems, but we will take in account only the most relevant ones, neglecting those that can be assumed like a second order effects. Most of the dominant nonlinearities are caused by the transducer principle and are related directly to the geometry and the material properties of the motor, suspension, cone, and enclosure. Physical limits require a compromise, but some of the nonlinearities are also created intentionally to obtain a desired large-signal behavior (such as progressive stiffness).
Thus the design process yields transducers having regular nonlinearities.

5.1.1 Nonlinear suspension stiffness

Loudspeakers use a suspension system to center the coil in the gap and to generate a restoring force that moves the coil back to the rest position. Woofers usually have a suspension comprising a spider and a surround, as shown in Fig. 1, which allows movements in one direction only and suppresses rocking modes.

There is an almost linear relationship at low displacement, but at high displacement the suspension responds with more force than predicted by a linear spring. In response to a slow ac force the displacement generally follows with a hysteresis caused by losses in the material.

The restoring force $F = K_{ms}(x) \cdot x$ can be described by the product of the nonlinear stiffness $K_{ms}(x)$ and the coil displacement: since also the stiffness ins a function of the displacement, the expression of the force will contain a nonlinear dependence from the displacement, ant this will cause a nonlinear distortion of the input signal.

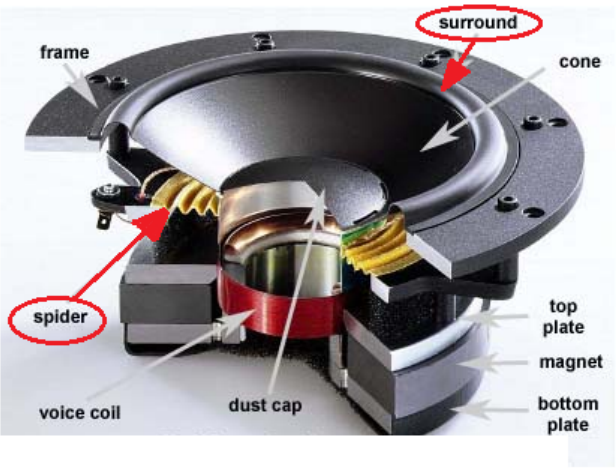

Figure 5.1: Sectional view of suspension system in conventional loudspeaker

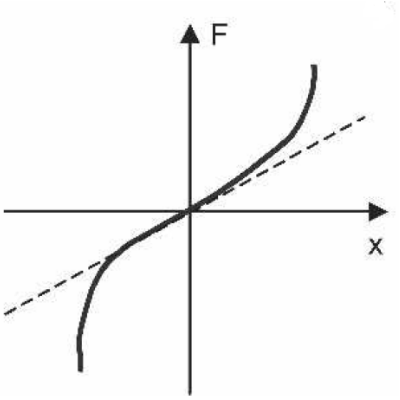

Figure 5.2: force deflection curve

Moreover the stiffness also varies with frequency due to the viscoelastic behavior of the suspension material: then the stiffness $K_{ms}(f)$ and compliance $C_{ms}(f) = 1/K_{ms}(f)$ are assumed to be frequency varying parameters to consider a dynamic property of the mechanical suspension. The mechanical system exposed to a sustained force will show varying displacement versus time (creep effect).
Due to the creep effect, stiffness of the suspension becomes smaller at low frequencies. The traditional low-frequency loudspeaker model needs to be extended to incorporate suspension creep by replacing the simple linear compliance by the dynamic transfer function:

$$C_{ms}(f) = C_{ms}(f_s)\left[1 - \lambda\, log_{10}\left(\frac{f}{f_s}\right)\right] \tag{5.1}$$

where C_{ms} is the linear compliance, f_s is the driver mechanical resonance

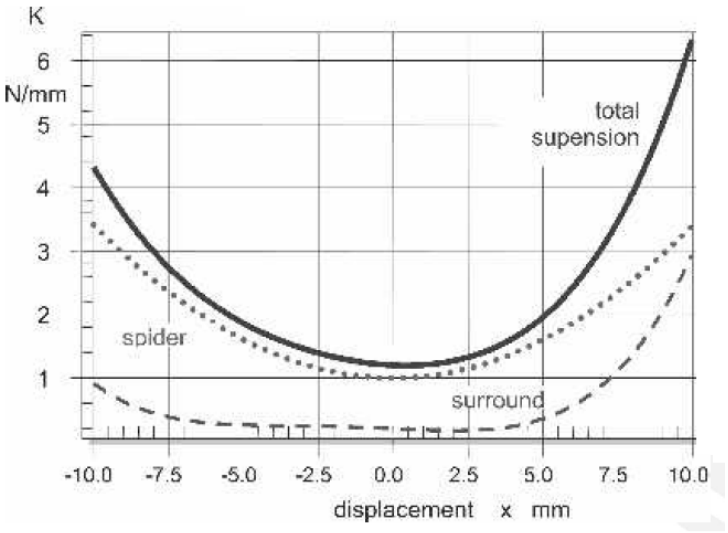

Figure 5.3: example of a mechanical stiffness characteristic

frequency and λ is a parameter that depends form materials and geometric characteristics of the spring.

5.1.2 Force factor

The force factor Bl(x) describes the coupling between the mechanical and electrical sides of the lumped parameter model of an electrodynamic transducer. This parameter is the integral of the flux density B versus the voice coil wire length l. the force factor $Bl(x)$ is not a constant but depends on the displacement x of the voice coil. Clearly, if the coil windings leave a gap, the force factor decreases since the flux density weakens. The nonlinear function is static (no frequency dependence) and can be represented as a nonlinear graph, table, or power series expansion. The shape of the $Bl(x)$ curve depends strongly on three factors:

- the geometry of the coil air gap configuration;
- the geometry of the coil itself;
- the magnet that has the duty of generating the B field.

There is an important distinction in the shape of the coil: indeed it could be sized with the same length of the air gap, or it could be over hanged (see Fig. 5.4). In the second case, as it can be seen in Fig. 5.5, the configuration is less sensible to the coil displacement, since the flux that hits the coil is the same for a longer displacement.

The force factor $Bl(x)$ is responsible of two nonlinear effects:

1. since it is the coupling factor between the electrical and the mechanical domain of the device, any variation of Bl(x) will influence the electrodynamic force $F = Bl(x) \cdot x$. This effect is also known as *parametric*

exitation of a resonating system. To see a relevant distortion, especially in the overhang configuration, it is needed a high level of displacement, the a very large input signal.

2. the second effect of the $Bl(x)$ is the fact that the back EMF generated by the movement of the coil in the permanent field now is displacement dependent. The back EMF is the result of the product between the force factor and the coil velocity,

$$E = Bl(x) \cdot \frac{dx}{dt}$$

then the mechanical damping, carried on the electrical side, it is no more linear due to the non ideality of the coupling factor.

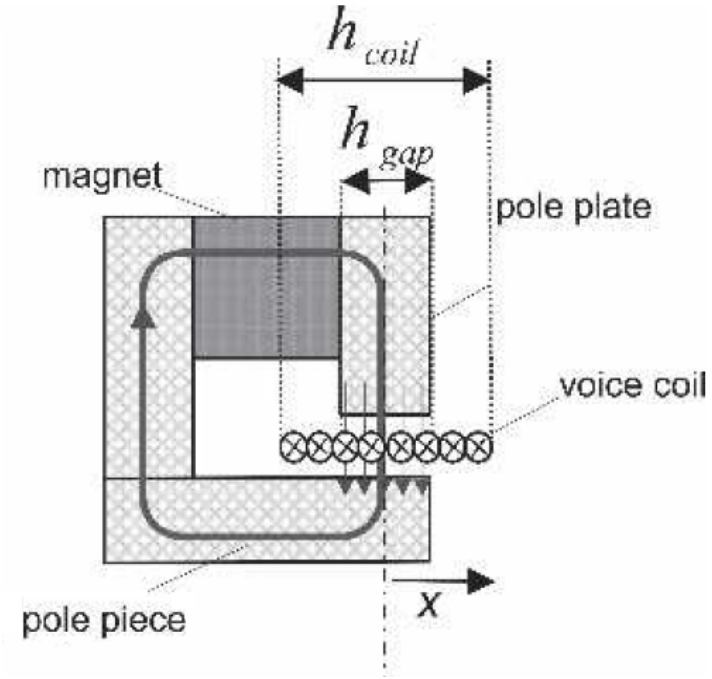

Figure 5.4: principle scheme of an overhang configuration

5.1.3 voice coil inductance

The global electrical input impedance depends on the position of the coil: indeed the electrical impedance is usually significantly higher for a negative displacement (coil in position) than a positive displacement (coil out position). This property can be explained easily if we take into account the displacement varying inductance:
the current in the voice coil produces a magnetic ac field penetrating the magnet, iron, and air, as shown in Fig. 5.6.
The magnetic flux depends on the position of the coil:

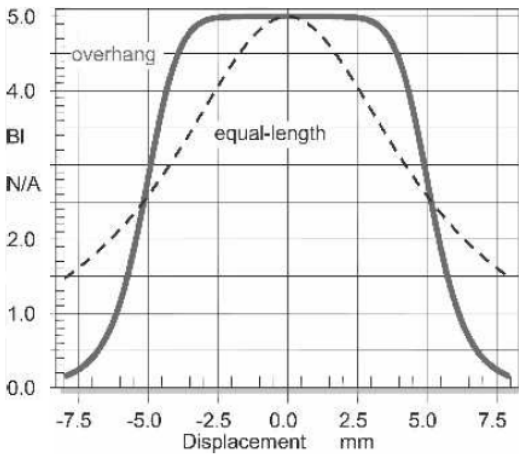

Figure 5.5: example of different configurations in coil length

if the coil is in free air above the gap, the inductance is much lower than when operating the coil below the gap where the surrounding material is steel, which decreases the magnetic resistance.

In addition to its dependence on displacement x the inductance also depends on the input current i. This is caused by the nonlinear relationship between magnetic field strength H and flux density $B = \mu(i)H$, as one can see in the figure 5.7. The working point with no current in the coil comes out from the magnetostatic situation of the magnetic circuit, without any external input except the one from the permanent magnet.
Due to the saturation of the magnetic material, there is a non symmetric behaviour:
indeed when the magneto-motive force get strengthened by the in coil flowing current, the surplus in the magnitude of the flux density is lesser than the reduction that take place when a negative current is circulating. This generates a time varying B field that generates as well a distorted back EMF and at last a distorted circulating current.
The effect of the varying permeability $\mu(i)$, which is very dependent on the specific magnetic material is also called *flux modulation*. The ac current also generates a hysteresis loop, which coincides with the losses in the iron material during one period of a sinusoidal current.

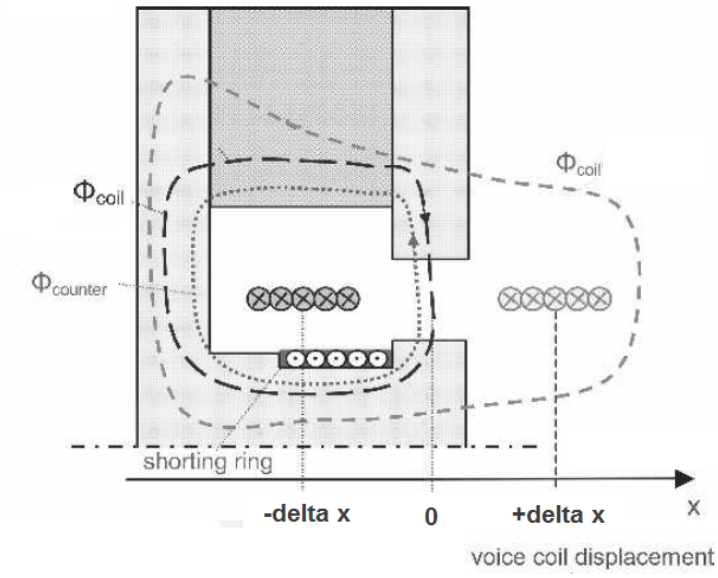

Figure 5.6: Motor structure of conventional driver using a shorting ring on the pole piece

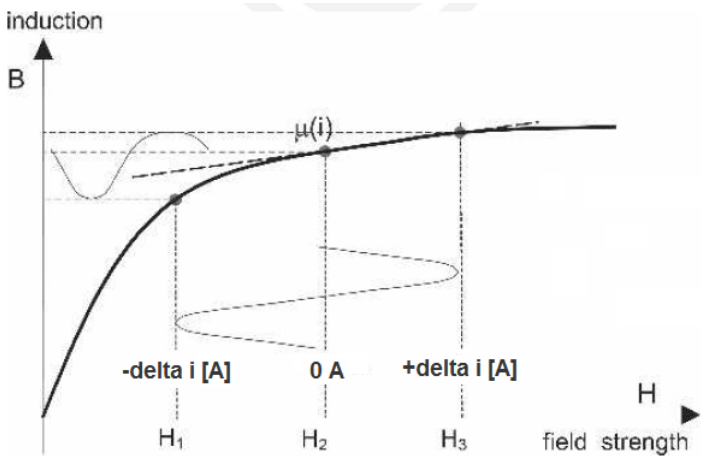

Figure 5.7: Flux density B versus magnetic field strength H of magnetic circuit, showing that permeability $\mu(i)$ depends on voice-coil

The time dependent flux density increases the impedance at higher frequencies and experimental evidences show that this increase cannot be explained by a simple ideal inductance. This difference from the expected behaviour can be explained if we take into account the inducted currents that flow in the conductive parts of the device and link with the coil ac magnetic field.

These Eddy's currents have the property to partially erase the flux density that comes from the coil, and ultimately they lower the inductance of the motor

winding. This property can be exploited in various ways, through the introduction of the *demodulation rings*:
this component acts basically like a short circuited secondary winding of a transformer; it can lower the input impedance at high frequencies and minimize the dependence of the inductance respect to the coil position.

Special models (Leach [3], Wright [4], cascaded LR network) are required to describe losses generated by eddy currents in the iron material and in the demodulation rings.
The discrete model using an inductance $L_e(x,i)$ in series with a second inductance $L_2(x,i)$ shunted by a resistor $R_2(x,i)$, as shown in figure 5.8, is a good candidate for capturing the nonlinear dependence on displacement and current.

In conclusion, the voice coil inductance has two main nonlinear effects:

1. the first effect of the displacement-varying inductance $Le(x)$ is the back-induced voltage in the electrical input circuit due to the time derivative of the magnetic flux and leads to the variation of the input impedance with coil displacement;

2. the second effect is an additional reluctance force $Fm(i,i_2,x)$, which drives the mechanical system directly. The reluctance force was the major driving force in the electromagnetic loudspeaker used 50 years ago. In today's electrodynamic transducers the reluctance force is an undesired rudiment that should be kept as low as possible.

If we make the hypothesis that the magnetic circuit is not saturated, then the flux-current relation is linear, i.e. $\varphi = Li$, and analytical expression for the reluctance force can be achieved. The energy stored in the flux density field is equal to

$$W_{mag} = \int_0^{\varphi_e} i_e \cdot d\varphi + \int_0^{\varphi_2} i_2 \cdot d\varphi$$

$$W_{mag} = \frac{1}{2}\left(i_e\varphi_e + i_2\varphi_2\right) = \frac{1}{2}\left(L_e i_e^2 + L_2 i_2^2\right) \tag{5.2}$$

Since as discussed before we saw that the inductance is function of the displacement and the current, $L = L(x,i)$, and given for known the fact that [16]

$$F = \left|\frac{\partial W_{mag}(i,x)}{\partial x}\right|_{i=cost} \tag{5.3}$$

we get the expression for the reluctance force acting on the motor coil, indeed substituting the expression 5.2 inside the equation 5.3 finally we get

$$F = \frac{1}{2}\left(\frac{\partial L_e(x)}{\partial x} i_e(t)^2 + \frac{\partial L_2(x)}{\partial x} i_2(t)^2\right) \tag{5.4}$$

Combining all the previous observations, we can draw an omni comprehensive equivalent circuit that takes care about all the nonlinear mechanisms discussed before.

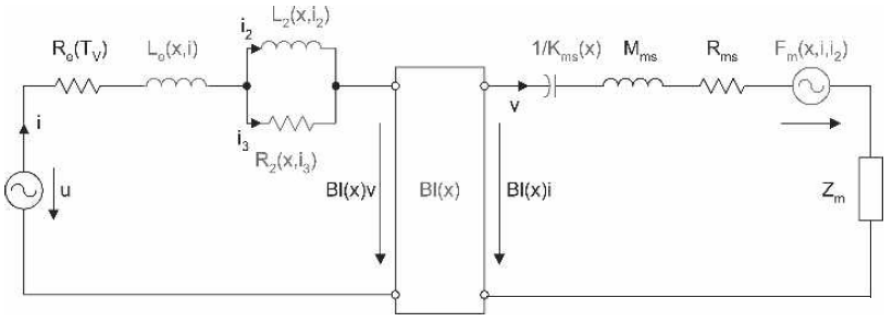

Figure 5.8: Loudspeaker equivalent circuit considering motor and suspension system

Chapter 6

The optimization problem

6.1 introduction

The main driving forces in today's industrial production are those that require the creation of new products that have to be cheap, especially concerning the design, and at the same time they have to show a very good quality, to compete in the market:
moreover under the need of cutting the expense, the stage of design, development and prototyping should be the shortest possible.
The engineering design comes out almost all the times like an iterative process that involves the succession of modeling, compromise, simulations, evaluations of results and decisions. If the results are not satisfactory as expected, new choices have to be taken regarding the parameters of the model, accordingly with the constraints, and a new synthesis process is repeated:
this goes on until the best solution is obtained by compared to some constraints, such as the cost of implementation or the nominal characteristics that are required to the device.

Then it is clear that the design is nothing else than an optimization process: to get best performances in the reduction of times and costs, this complex process can be automated through the coupling of the Finite Elements Method with an optimization algorithm. With today's computers, the computational power needed to generate complex multiphysics transient simulations is no more a problem, indeed every personal computer, with the right amount of patience provided by the owner, can deal with these kind of problems.
The challenge is the correct formalization of the optimization problem, because the algorithm has to be able to make the right decisions for ensuring the reaching of the best solution with the smallest amount of time.

6.2 Formalization of the problems

6.2.1 Single-objective optimization

Let us introduce some definitions:

- the vector $\bar{x} = [x_1, x_2, ..., x_n]^T$ the indipendent variables of the problem; linked with a physical problem, they can be imagined as the degrees of freedom of the design, like the geometry or the materials.
- the function $f(\bar{x}) : \Re^n \to \Re$ is called the *target function*, sometimes also *cost function*, and its minimization will be the purpose of the optimization algorithm;
- the vectors of constants $\bar{a} = [a_1, a_2, ..., a_n]^T$ and $\bar{b} = [b_1, b_2, ..., b_n]^T$ represent the bounds for the problem;in the most general approach they are coupled with the bound functions, i.e $\bar{f_b}(\bar{x}) = [f_b(x_1), f_b(x_2), ..., f_b(x_n)]^T$, but more frequently the vectors $\bar{a}$ and $\bar{b}$ define directly the allowed ranges for the indipendent variables;
- the imposition of bounds will generate a sub domain for the parameters, we can call it $\Omega \subseteq \Re^n$;
- the optimum vector, $\bar{x}_{opt}$ that is a set of parameters compatible with the constraints, for which it is always true the disequation
  $f(\bar{x}_{opt}) \leq f(\bar{x}) \ \ \forall\ \bar{x} \in \Omega$

$$\begin{cases} min\ f(\bar{x}) \\ \\ constraints\ \bar{a} \leq f_b(\bar{x}) \leq \bar{b} \end{cases} \tag{6.1}$$

6.2.2 Multi-objective optimization

The problem related to the multi-objective optimization can be described in a way that is closer to the mono-objective problem. In particular we are searching the vector $\bar{x} = [x_1, x_2, ..., x_n]^T \in \Omega \subseteq \Re^n$ that satisfies the n constraint (or bound) functions

$$\bar{a} \leq f_b(\bar{x}) \leq \bar{b} \tag{6.2}$$

and optimizes the *vector* of the objective functions

$$\bar{f}(\bar{x}) = [f_1(\bar{x}), f_2(\bar{x}), ..., f_k(\bar{x})] \in F \subseteq \Re^n \tag{6.3}$$

The vector of objective functions $\bar{f}(\bar{x})$ is a function that takes the values from Ω and elaborate them in F, that represents the space of the values allowed to be assumed by the objective functions. It is not very likely to find a solution $\bar{x^*}$ that represents at the same time the minimum of all the objective functions as it can be understood from the Fig. 6.1:

- the case *a* shows a very lucky case, that is not frequent in engineering problems, where it's easy to find in the solutions space a point that minimizes all the functions at the same time. This is not very common for the simple reason that in the applied problems, usually we ask the maximum performance at the lowest possible cost, so if such a solution existed, for any purpose there should be just one product in the market;

- it's more likely to find a domain shaped like the one flagged as case *b*. We can see that the optimum point $\left[f_1(x^{0(1)}), f_2(x^{0(2)})\right]$, called also *Utopia point*, does not belong to the solutions space F.

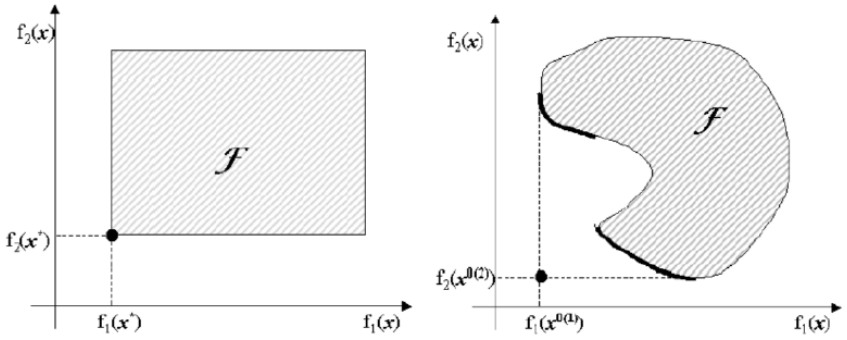

(a) Particular case of a One Point solution (b) Ideal point

Figure 6.1: two different cases related to the shape of F

Looking at the situation *b*, it not clear anymore which point represents the 'best' solution, so before going on we need a clear definition about what it is meant when we talk about the *best* solution of a multi-objective problem. The concept that plays as a basis for the definition we are going to introduce, was formulated for the first time by Francis Ysidro Edgeworth in 1881 and then it was well developed by the italian economist Vilfredo Pareto, in 1896. We can say that the vector $\bar{x}^* \in \Omega$ enjoys the *Pareto optimality* if and only if

$$\exists \bar{x} \in \Omega : \bar{f}_i(\bar{x}) \leq \bar{f}_i(\bar{x}^*) \quad i = 1, 2, ..., n \tag{6.4}$$

$$\bar{f}_i(\bar{x}) < \bar{f}_i(\bar{x}^*) \quad for\ at\ least\ one\ i \tag{6.5}$$

In other words,$\bar{x}^*$ belongs to the Pareto optimum if it is not possible to find another vector that can improve some objective functions without pushing away some others from the best point they already reached. Usually this definition does not represent just a point, so we talk about:

- *Pareto Set*, that is composed by all the vectors $\bar{x}^* \in \Omega$ that verify the relations 6.4 and 6.5;

- *Pareto front*, concerning all the solutions vectors $\bar{f}(\bar{x}^*) \in F$.

6.3 Choosing the algorithm

The Matlab suite includes also a tool called *Optimization toolbox*: in particular our attention was focused on an algorithm called *Patternsearch*. This belongs to a family of numerical optimization methods that do not require the gradient of the problem to be optimized. Hence PS can be used on functions that are not continuous or differentiable.
Such optimization methods are also known as direct-search, derivative-free, or black-box methods: they are precious since the computation of the gradient of functions whose value comes out from a finite element analysis it is affected by a non neglectable numerical error, especially if the gradient has a small value.

This is the reason why we decided also to try to implement some stochastic methods, that are commonly more robust that the deterministic ones,hence we focused on:

- the well known *Particle swarm optimizer*, called also PSO;
- the *Differential evolutionary algorithm*, that belong to the family of genetic optimizers.

The challenge was to understand if the stochastic methods were good enough in convergence, to be comparable with the performance of the deterministic method mentioned before.

All the results presented further are obtained considering for the three methods the same number of function evaluations during every call.

6.3.1 Benchmarck functions

The make a comparison between the optimizers, we needed to use them in a common test environment that was significant enough to generate results useful to make the proper choice. We decided to let the algorithms work over two different very well known benchmark functions, in particular:

- the *Six humps camel back*, a two dimension problem;
- the *Rosenbrock banana*,written for a ten dimensions domain.

Six humps camel back

This is the black beast for deterministic algorithms: it has four minima, two local and two global.
It is used to evaluate the robustness of the algorithms and the analytical expression is:

$$f(x,y) = (4 - 2.1x^2 + \frac{x^4}{3})x^2 + xy + (-4 + 4y^2)y^2 + 1.031285 \qquad (6.6)$$

and it shows two global minima, at coordinates

$$x_1 = 0.089842 \quad y_1 = -0.712656 \quad f(x_1, y_1) = 0$$

$$x_1 = -0.089842 \quad y_1 = 0.712656 \quad f(x_1, y_1) = 0$$

If one looks at the function shape from far away, she will appear like a valley, with apparently a big flat area in the middle.

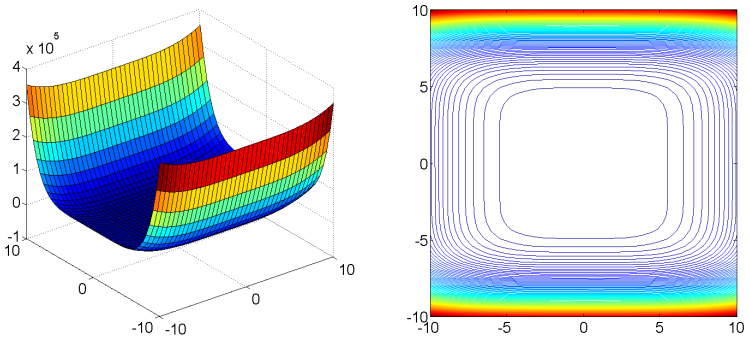

Figure 6.2: 3d view and contour plot of the six hump camel back function

But if we tighten the domain to a smaller range (see Fig. 6.3), we can see the particularity of this function and the reason for which it is used in the evaluation of the algorithms. The red dots represent the global minima, whilst the black arrows indicate the local minima: note that they work as traps for the deterministic algorithms, because they are stagnating points very near the global minima.

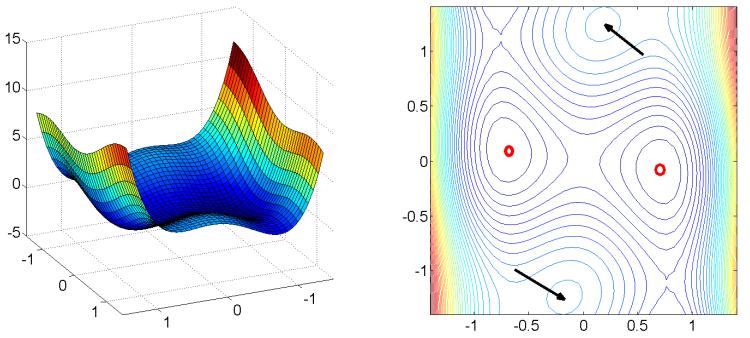

Figure 6.3: 3d view and contour plot of the six hump camel back function, with a detailed zoom on the minima area

Rosenbrock banana

This function is used to measure the ability of an algorithm to reach the convergence solution,and it is expressed by the formula:

$$f(x_1, x_2, ..., x_N) = \sum_{i=1}^{N-1} \left[(1 - x_i)^2 + 100(x_{i+1} - x_i^2)^2\right] \tag{6.7}$$

No matters the number of dimensions, it can be demonstrated that this function has evrey time just one global minimum:

$$(x_1, x_2, ..., x_N) = (1, 1, ...1) \quad f((x_1, x_2, ..., x_N)) = 0$$

The Fig. 6.4 shows the case of two dimensions.

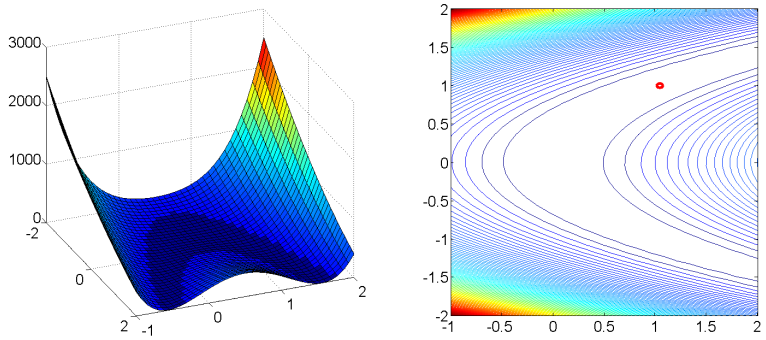

Figure 6.4: 3d view and contour plot of the Rosenbrock banana function

Using a logarithmic scale on the Z axis, on the function $\{f(x) + 1\}$, it is possible to see the narrow shape of the valley:
for every algorithm it is quite simple to slip until the lower part of the valley, but after it is quite complicated to move through the valley bottom, to reach the global minimum.

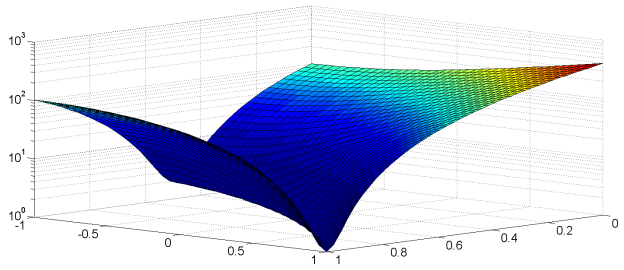

Figure 6.5: 3d view of the valley around the minimum point

The extension at ten dimensions is obviously mathematic, but the peculiarities seen before still exist.

6.3.2 Evaluation of performances

Robustness

We called the algorithms 10000 times, to work on the six humps camel back function; for each calling 1000 function evaluations were allowed to take place: in this way we can see if the methods find the true minima or if it stops in the trap local minima. This is our discriminating parameter:

it is sufficient to check the value given by the program at the last evaluation, if it's equal to 0.8, the method is stagnating in a local minimum, if it's zero it has converged. Defining a failure index and increasing it by an unit every time the algorithm does not reach the absolute minima, it is possible to compare the performances.

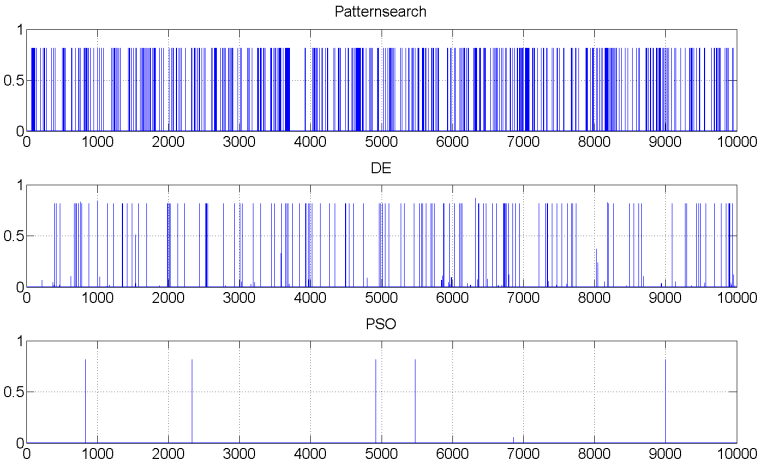

Figure 6.6: comparison between the three methods

Algorithm	callings	f eval.	Fail index
Patternsearch	10^4	10^3	4.36%
DE	10^4	10^3	1.24%
PSO	10^4	10^3	0.05%

Table 6.1: summary of comparison

The exploration tendency of the PSO comes out unquestionably:
the algorithm has almost the 100% of probability to find the best solution, then we can argue that it is the most robust. It is worth to know anyway that the PSO and the Patternsearch cannot be improved, the DE algorithm instead is just a self written base form with a lot of space for improvements. a lot of space for improvement

Convergence

We called the algorithms 1000 times, to work on the Rosenbrock banana function, extended for a 10 dimensions problem; for each calling 10000 function evaluations were allowed to take place:
we increased respect to before the number of evaluations, since we are dealing with a huge domain space, that requires a reasonable number of evaluations to be explored and to let the algorithms show their skills and peculiarities. For

first we worked on a relatively small domain, bounded in every dimension by the values $[-10; 10]$:

- Fig 6.7 shows the performance of the Patternsearch algorithm,that is the best value found for every calling. The continuous line is the mean value, that is drawn as well in the successive graph;
- Fig 6.8 compares the behaviour of all the three methods; moreover, to have an idea about the dispersion of solutions, we plotted as well the best and the worst case.

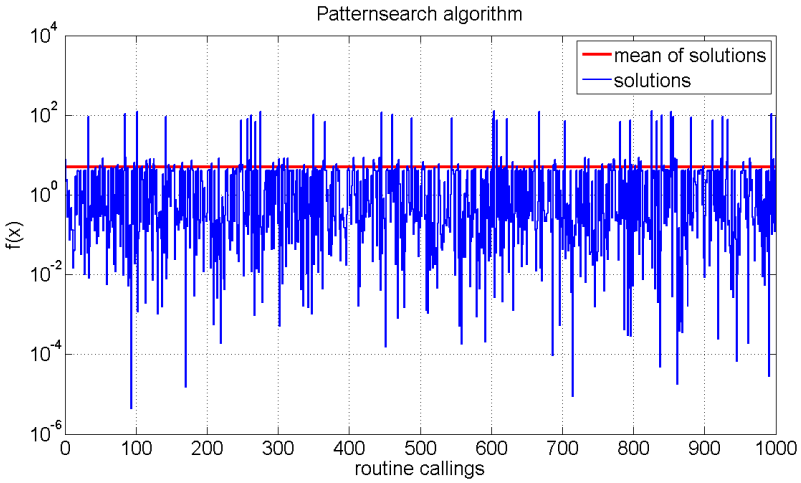

Figure 6.7: performance of Patternsearch

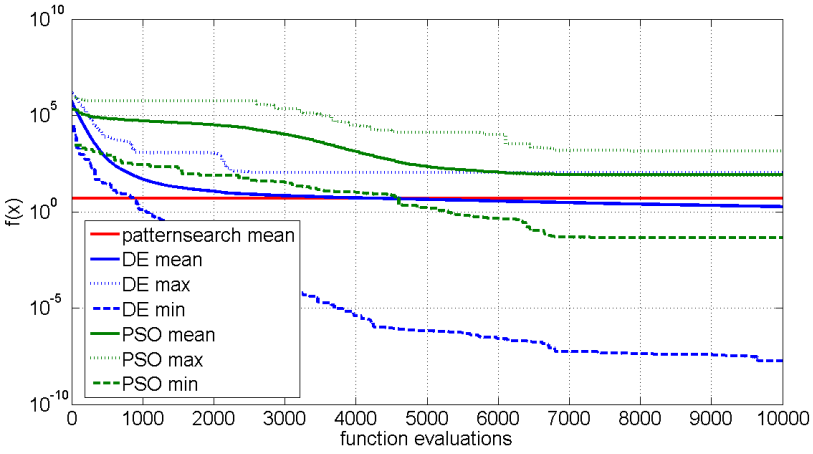

Figure 6.8: comparison among algorithms

It is trivial to see from Tab. 6.3 that the DE has the best behaviour under every point of view: it is by far better than the PSO, and comparable with the

Algorithm	callings	f eval.	Mean val.	Max val.	Min val.
Patternsearch	10^4	10^3	$4.93 \cdot 10^0$	$1.28 \cdot 10^2$	$4.30 \cdot 10^{-6}$
DE	10^4	10^3	$1.81 \cdot 10^0$	$1.07 \cdot 10^2$	$1.76 \cdot 10^{-8}$
PSO	10^4	10^3	$7.96 \cdot 10^1$	$1.36 \cdot 10^3$	$4.41 \cdot 10^{-2}$

Table 6.2: summary of comparison, domain $[-10; 10]$ $\forall$ dim

Patternsearch. Ten we enlarged the bounds to the values $[-10^3; 10^3]$, in every dimension: this was made to see the ability of the routines to find their path also in a very extended environment.

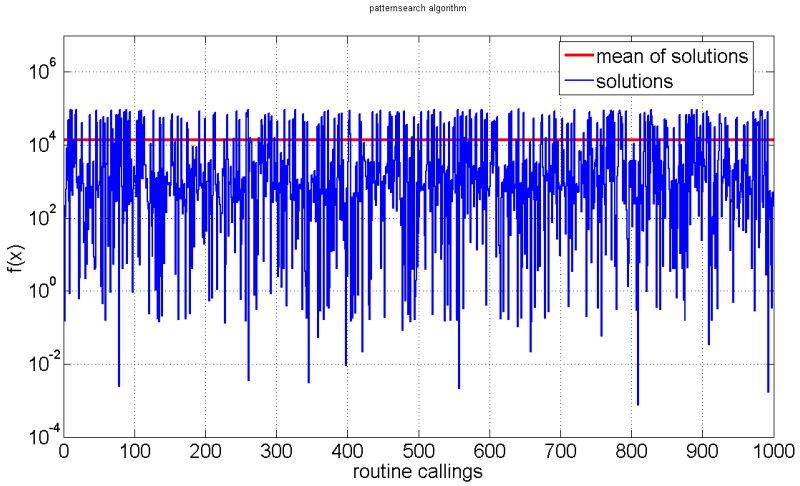

Figure 6.9: performance of Patternsearch

Algorithm	callings	f eval.	Mean val.	Max val.	Min val.
Patternsearch	10^4	10^3	$1.36 \cdot 10^4$	$9.41 \cdot 10^4$	$7.56 \cdot 10^{-4}$
DE	10^4	10^3	$9.18 \cdot 10^1$	$1.84 \cdot 10^3$	$7.56 \cdot 10^{-5}$
PSO	10^4	10^3	$8.26 \cdot 10^5$	$1.26 \cdot 10^7$	$1.44 \cdot 10^2$

Table 6.3: summary of comparison, domain $[-10^3; 10^3]$ $\forall$ dim

After having analysed the Tab. 6.3, we decided once for all that even if the DE algorithm is not the most robust, we want manage with his failure rate since the reward is a very good convergence, better by far respect the one showed by the competitors.

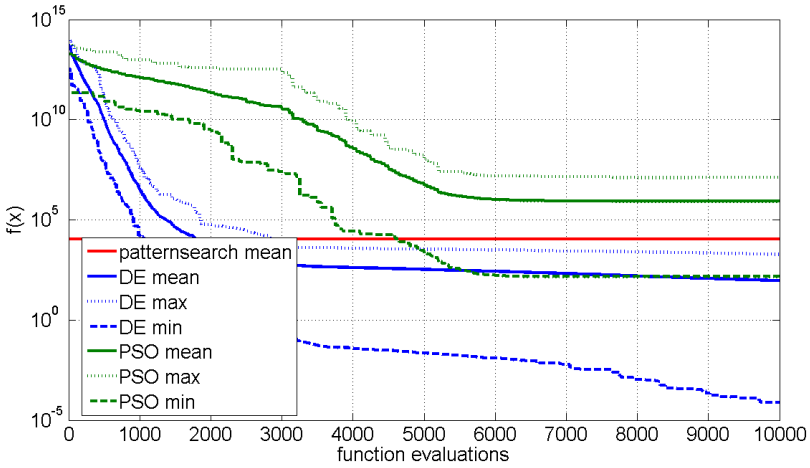

Figure 6.10: comparison among algorithms

Further DE improvements

To get better results, we implemented an improved technique for the genetic algorithm, known as aysinchronus or aggressive approach. Basically instead of generating all the sons concurrently, every time a son is generated, it fights immediately with his father, and if he wins, he will take immediately the place of his father, concurring in the generation of all the other sons:
the motto indeed is *use good solutions now!*.

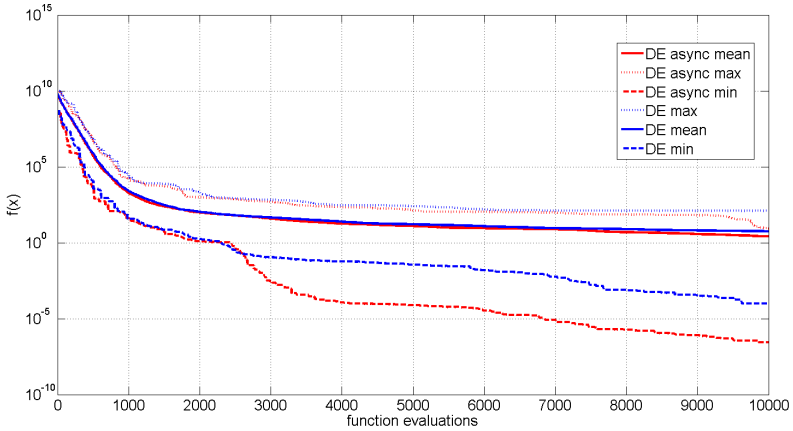

Figure 6.11: comparison between different DE versions

As one can see from the table 6.4, there is a general improvement concerning the band where all convergence paths lie: indeed all the band related to the asynchronous method is shifted down. Anyway, the mean behaviour is almost the same, and the improvement is less effective than expected:
this can be explained with the fact that the high number of dimensions of the

Algorithm	callings	f eval.	Mean val.	Max val.	Min val.
DE	10^4	10^3	$5.66 \cdot 10^0$	$1.23 \cdot 10^2$	$9.86 \cdot 10^{-5}$
DE async	10^4	10^3	$2.61 \cdot 10^0$	$8.49 \cdot 10^0$	$2.79 \cdot 10^{-7}$

Table 6.4: summary of comparison, domain $[-10^2; 10^2] \; \forall$ dim

domain erase almost all the benefits gained from using immediately the good solutions. The algorithm has to search in a very wide space, and the number of iterations used for the comparison is not high enough to show any appreciable difference in the mean curves.
We think that since our target is to compute a maximum 5000 evaluations, the complexity of the asynchronous improvement is not justified, and for the next simulations we will use the basic version of the DE algorithm.

Chapter 7

Main results

7.1 introduction

The main goal of the project is to create a software that can choose and evaluate the effectiveness of the introduction of demodulation rings in a loudspeaker. It is almost impossible to create an equivalent analogical model, for the following reasons:

- the magnetic circuit is saturated, and the iron cross section area is not constant, so it is almost impossible to evaluate analitically the magnetostatic solution and the working point of the magnet;
- the magneto quasistatic problem involves the presence of Eddy currents, that are another source of non linearity in the model, due to the skin depth;
- we cannot ignore the coil movement, then we have to introduce in our problem formulation also the dependency from space;
- considering the iron conductive parts(centre pole, top pole,base pole),one demodulation ring and the coil fed by a time dependent voltage source, the equivalent circuit seen from the terminals of the coil is fairly complex;we are dealing with a of transformer, with one primary coil and four secondary windings, all connected in parallel.
  Moreover we cannot use the classical three-windings-trasnformer theory, because since there is not a common magnetic circuit that acts like a nucleus for all the windings, we cannot assume that the four self inductances have the same mutual indictance quote. So it's impossible to achieve a useful and flexible analogical model.

7.2 General description

Since we cannot count on any kind of analytical model, we have relied on finite elements method:
then what we have done is to couple Comsol program to an optimization algorithm written in Matlab, through a live link tool given with Comsol suite. Fig. 7.1 gives a wider overview over the connections we realized.

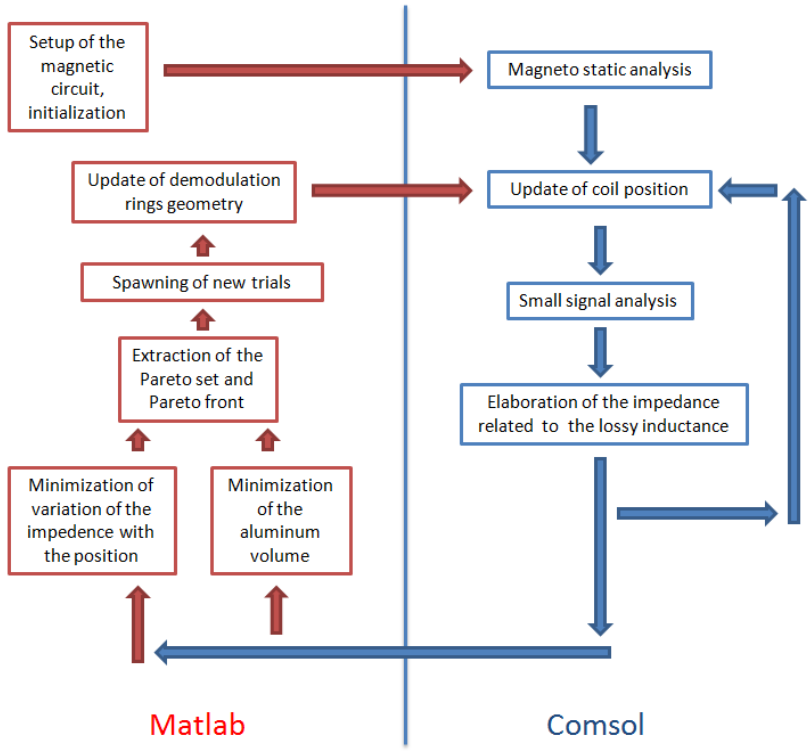

Figure 7.1: logical scheme about how the algorithm works

7.3 Experiments

For the sake of simplicity we will use the following definitions:

- with *ring 1* we refer to the ring located inside the air cap and attached to the centre pole;
- with *ring 2* we mean the one located inside the air cap and attached to the magnet;
- with *ring 3* we refer to the one located over the centre pole.

We worked both on the SV 165 and the $SSF - 082$,the following ones are the experiments we settled up fot the optimizator.

1. a fast optimization on $SSF-082$ with the ring 1 (100 function evaluations - 3 d.o.f.);

2. a fast optimization on $SSF-082$ with the ring 2 (100 function evaluations - 3 d.o.f.);

3. a very fast optimization on $SSF-082$ with the ring 3 (50 function evaluations - 3 d.o.f.);

4. a deep optimization on $SSF-082$ with the rings 1 and 3 (300 function evaluations - 6 d.o.f.);

5. a deep optimization on $SSF-082$ with the rings 1,2 and 3 (600 function evaluations - 9 d.o.f.);

6. a deep optimization on SV 165 with the copper cap and the ring 2 (200 function evaluations - 3 d.o.f.);

7. a deep optimization on SV 165 with the copper cap and the rings 2 and 3 (300 function evaluations - 6 d.o.f.);

8. a deep optimization on SV 165 without the copper cap but with just the rings 2 and 3 (200 function evaluations - 6 d.o.f.).

It is worth noting that not all the possible combinations have been considered,indeed some observations made on purpose can be very helpful in reducing the number of different prototypes:

- the ring 1 is expected to work better than the ring 2; the Fig. 7.2 shows the distribution of the equipotential lines of the magnetic vector potential, that are tangent to the magnetic flux density field.
  As one can see, there is a non neglectible part of lines that don't flow across all over the magnetic circuit, but jump directly through the inner air gap, that acts like a shortcut;these lines are linking just the ring located near the centre pole, so they cannot be neautralized by the induced currents on the ring 2, because it cannot see them.

- the ring 3 when it is used just alone, doesn't provide an increasing in the performance of the device, but on the contrary it contributes to enhance the variation of the coil impedence with the position.
  We made some simulations in comsol to verify it, keeping the external border of the ring aligned with the centre pole profile and changing just width and height: the results are shown in Fig. 7.3. We can see for every curve that the variation between the value at the rest position an the maximum offset is increasing with the volume of Aluminum.

- it is useless to simulate a combination of rings 1 and 2, indeed due to their position, they will act almost in the same way, except the fact that we are expecting a worse behaviour from the ring 2.

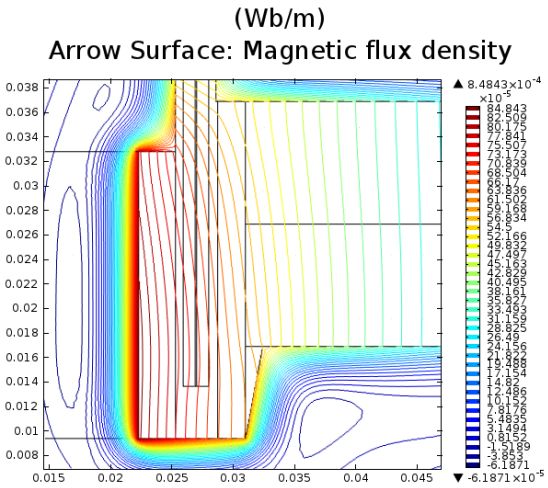

Figure 7.2: distribution of the magnetic vector potential generated by the voice coil current in the $SSF - 082$ geometry

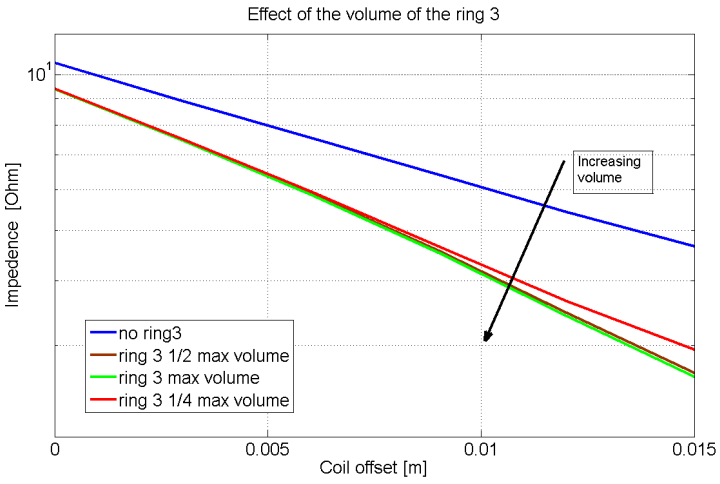

Figure 7.3: comparison between different solutions with just the ring 3

7.4 $SSF - 082$ optimizied

7.4.1 $SSF - 082$ with ring 1

In Fig. 7.4 it is shown the Pareto front obtained after 100 evaluations:
it is interesting to see that non a huge amount of aluminum is used, even better we can obtain a huge reduction in the impedence variation at a small material price.

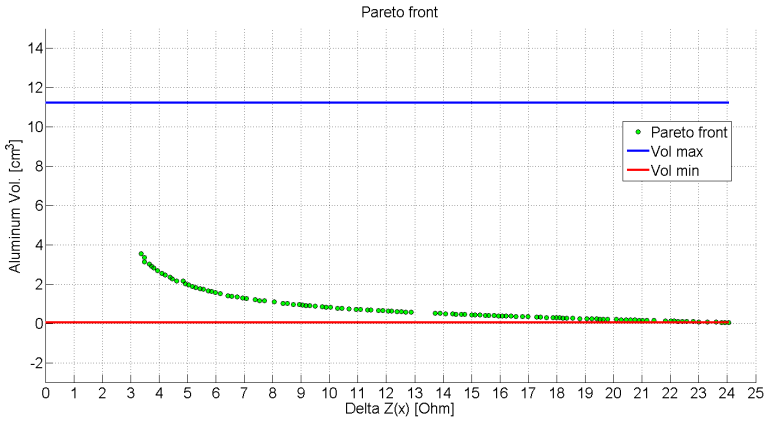

Figure 7.4: $SSF - 082$ with ring 1

7.4.2 $SSF - 082$ with ring 2

In Fig. 7.5 it is shown the Pareto front obtained after 100 evaluations:
it is still valid the observation made for the previous front, indeed the two rings have a very similar position and act mostly alike.

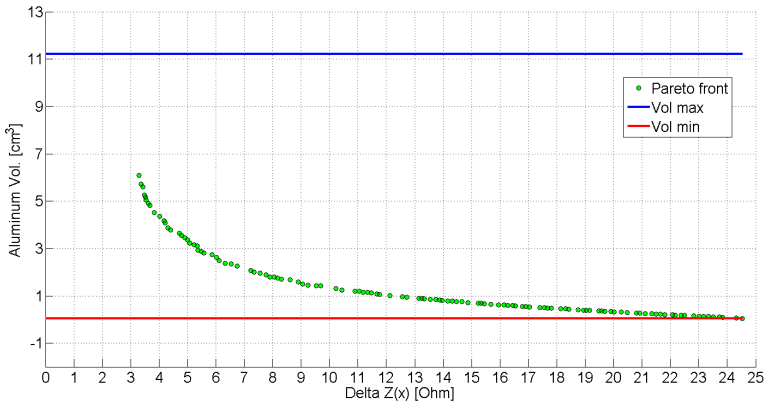

Figure 7.5: $SSF - 082$ with ring 2

7.4.3 $SSF - 082$ with ring 3

In Fig. 7.6 it is shown the Pareto front obtained after 50 evaluations:
the front collapses in one point that is dominating all the possible solutions. It is worth noting that the solution founded requires the minimum allowed quantity of aluminim, this means that the optimizator is trying to remove the ring 3, accordingly with the obsevation made before.
Due to the result, it was no necessary to make fore iteration, gaining in this way some time to dedicate for other elaborations.

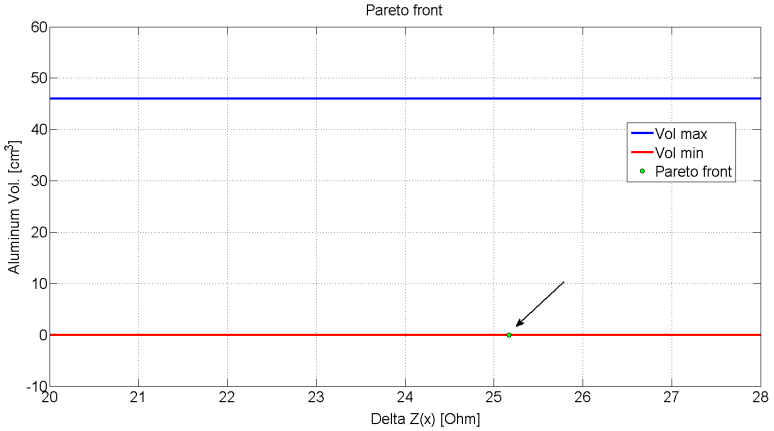

Figure 7.6: $SSF - 082$ with ring 3

7.4.4 $SSF - 082$, comparison between the solutions with ring 1 and ring 2

Making a comparison between the fronts relative to the rings 1 and 2 allow us to magnify the fact that the ring 1 works better, since it is linked with a higher amount of flux lines, as seen in the previous observation. Note that it possible to obtain the same performances with the half amount of material volume!

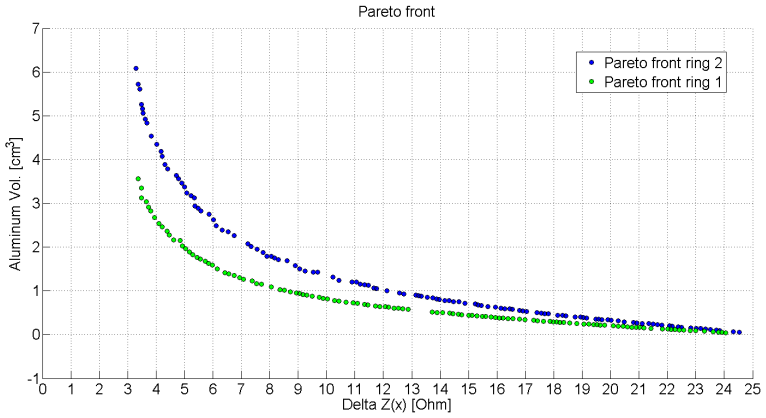

Figure 7.7: $SSF-082$,comparison between the solutions with ring 1 and ring 2

7.4.5 $SSF-082$ with rings 1 and 3

In Fig. 7.8 it is shown the Pareto front obtained after 300 evaluations:
once again, there is no need to a huge amount of material to get good performances.

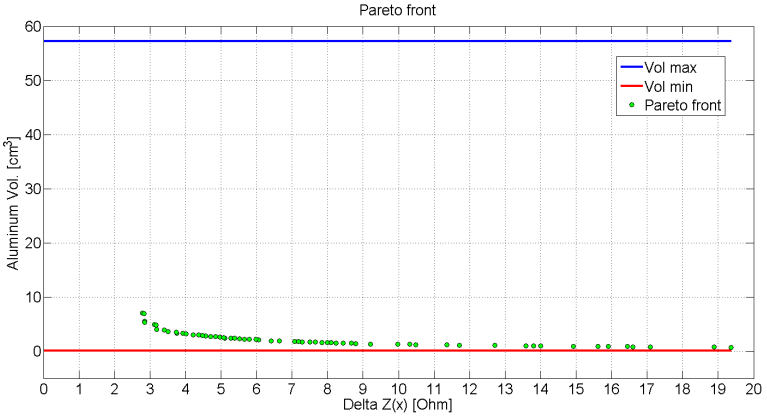

Figure 7.8: jhjhkfdgsgs

7.4.6 $SSF-082$ with rings 1, 2 and 3

In Fig. 7.9 it is shown the Pareto front obtained after 600 evaluations:
this was the toughest problem, due tho the amount of degrees of freedom.

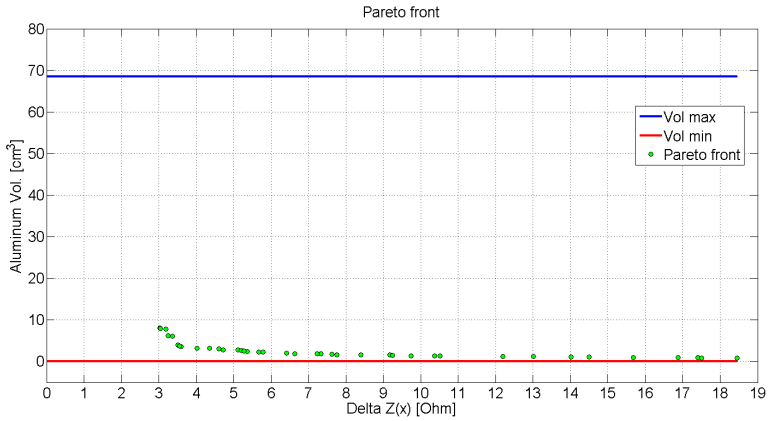

Figure 7.9: jhjhkfdgsgs

7.4.7 $SSF - 082$, comparison of all solutions

this is the most important result, since from the Fig. 7.10 it is possible for a company to make a decision about what are the best solutions that are going to be chosen and produced.
The black line on the right represents the value of the impedence variation without any ring, it represent the upper limit.
Let's see how it is almost useless to use the ring 2, alono or in combination with the other rings:
the best performances are obtained with the ose of ring 1 and 3 simultaneously, while the best ratio *perferomance/volume* belongs to the solution with just the ring 1 (see Fig. 7.11)

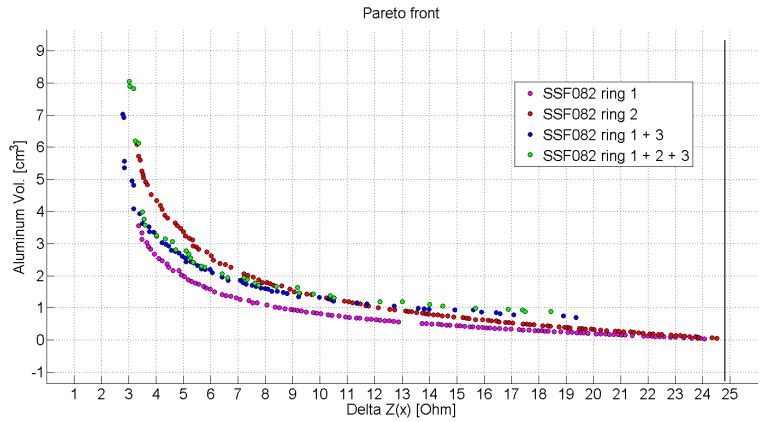

Figure 7.10: comparison among all solutions

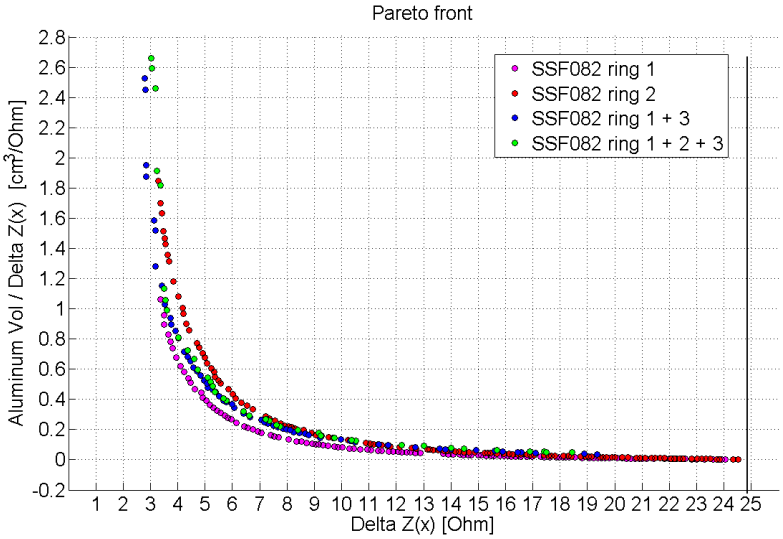

Figure 7.11: comparison among all solutions

7.5 $SSF-082$ Choice of the prototypes

Accordingly with the company, we decided to choice the solutions that minimize the variation of the impedence, despite the amount of aluminum required:
this was suggested by the fact that the device will be sold like a prfessional loudspeaker, so in the high market level, where the cost is not the primary driver that influences the coustomer's choice.
In Tab. 7.1 we reported the details concerning the position and the sizes of the rings in the chosen models.

Models	*ring* 1	*ring* 2	*rings* $1+3$	*rings* $1+2+3$
$r1\ w$	$3.00 \cdot 10^{-3}$		$3.00 \cdot 10^{-3}$	$2.34 \cdot 10^{-3}$
$r1\ h$	$7.95 \cdot 10^{-3}$		$3.00 \cdot 10^{-3}$	$5.13 \cdot 10^{-3}$
$r1\ z$	$22.00 \cdot 10^{-3}$		$23.39 \cdot 10^{-3}$	$11.89 \cdot 10^{-3}$
$r2\ w$		$1,25 \cdot 10^{-3}$		$0.71 \cdot 10^{-3}$
$r2\ h$		$25.54 \cdot 10^{-3}$		$26.77 \cdot 10^{-3}$
$r2\ z$		$10.91 \cdot 10^{-3}$		$9.9 \cdot 10^{-3}$
$r3\ w$			$5.50 \cdot 10^{-3}$	$7.98 \cdot 10^{-3}$
$r3\ h$			$3.86 \cdot 10^{-3}$	$4.02 \cdot 10^{-3}$
$r3\ r$			$18.33 \cdot 10^{-3}$	$8.80 \cdot 10^{-3}$

Table 7.1: Main features of the voice coils

7.5.1 Geometries

$SSF - 082 - ring\ 1$ **geometry**

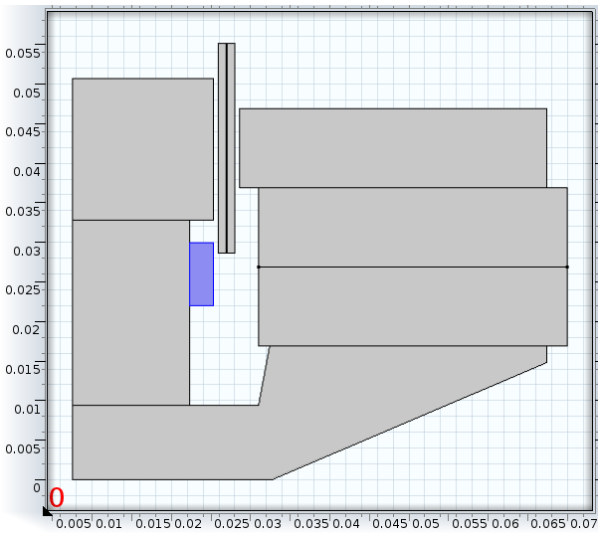

Figure 7.12: $SSF082$ geometry with ring1

$SSF - 082 - ring\ 2$ **geometry**

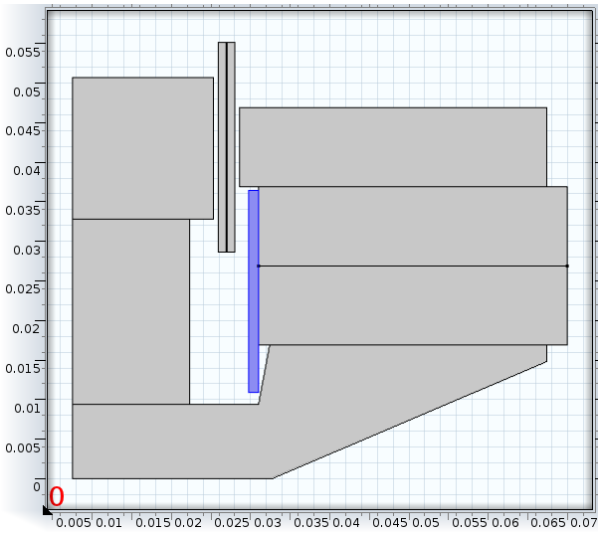

Figure 7.13: $SSF082$ geometry with ring2

$SSF - 082 - rings\ 1 + 3$ **geometry**

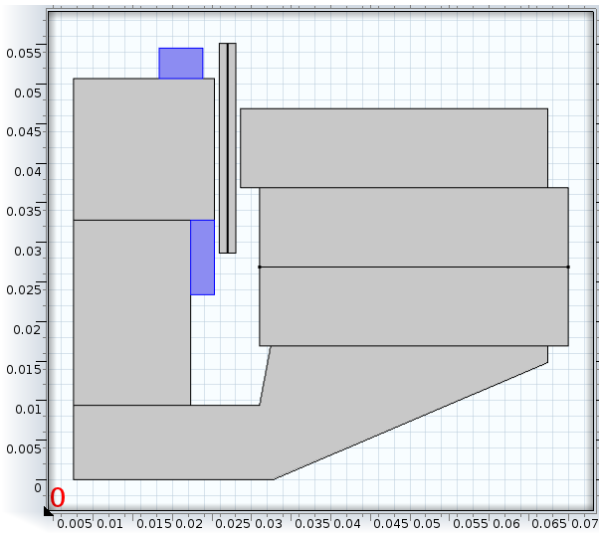

Figure 7.14: $SSF082$ geometry with ring1+3

$SSF - 082 - rings\ 1 + 2 + 3$ **geometry**

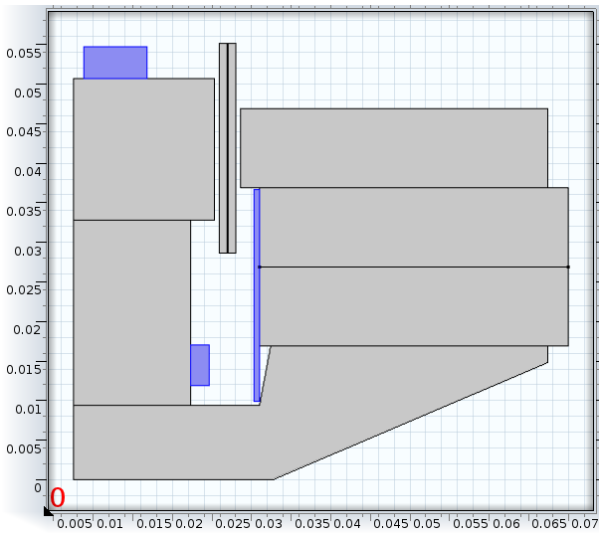

Figure 7.15: $SSF082$ geometry with ring1+2+3

7.5.2 Characterisation of the impedence

The following section represents the effective impedence seen from the coil teminals,fonction of the coil offset, less than the R_{DC} resistance. To obtain it it is necessary to extract form the finite elements method the value of the module and the phase of the golbal impedence, and then separate it in a resistive and inductive part:
toghether they represent an equivalent model of the lossy inductance, funtion of the offset and the frequency.
to get a meaningfu resut, we chose three diffrent frequencies, on the bottom, the middle and the top part of the frequency range where the device has to work.

Effective resistance

The shape of the curve can be justified easily:

- when the coil is immersed, she links whith her flux both the aluminum ring and the iron, so the circulation of the Eddy currents is easy and the losses are high;
- when the coil is in the rest position, she links with her flux for main just the iron, that has a conductivity lower than the aluminum; we can see that the losses are going down, since the Eddy currents are reduced;
- when the coil reaches the upper point of the excursion, she links just the aluminum ring (if it is present), but in any case the magnetic coupling is very weak, since the material surrounding the coil is almost air; then the inducted currents are the lowest possible.

We can see also the effect of the frequency, that make the family of curves translate towards higher values:
this phoenomenon is related to the fact that the magnetic materials tend to expel the variable flux from their inner part, allowing the induced currents to flow trough a smaller and smaller cross section, increasing then the equivalent resistance.

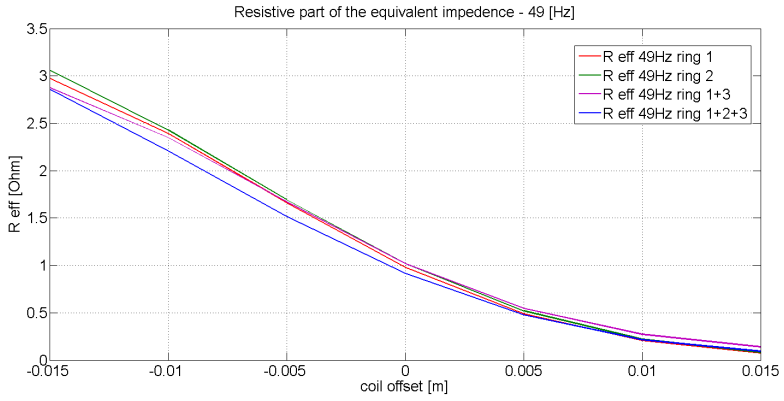

Figure 7.16: effective resitance

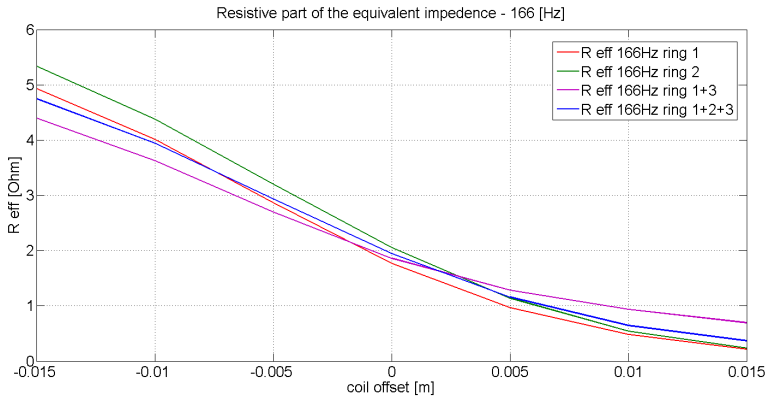

Figure 7.17: effective resitance

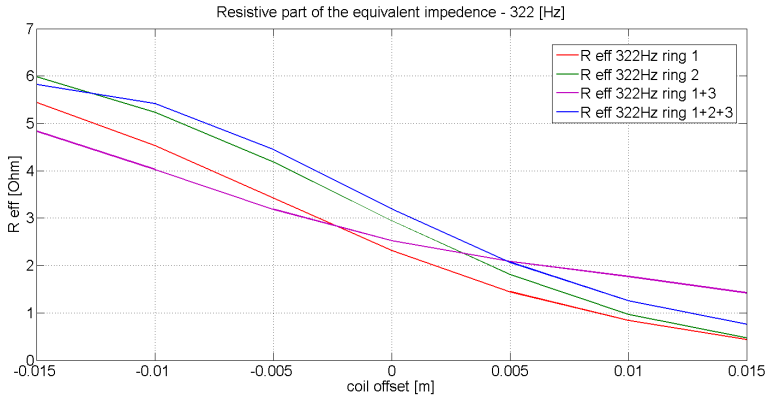

Figure 7.18: effective resitance

Effective inductance

We can see that the curves are charaterized by a bell shape:

- when the coil is dipped inside the magnetic complex, there's the action of ring 1 or 2 that helps to keep the inductance value low;
- when the coil reaches the outer point of her excursion, there is just air, so the inductance is naturally decreased;
- when the coil crosses through the rest point, she couples herself stronger with the mangetic circuit, so the inductance is increased.

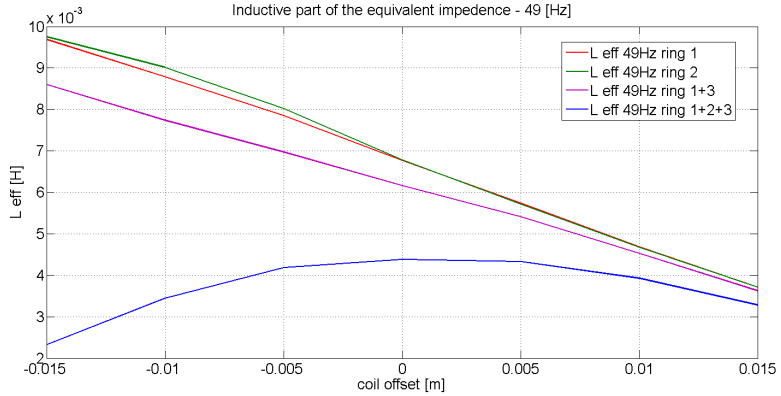

Figure 7.19: effective inductance

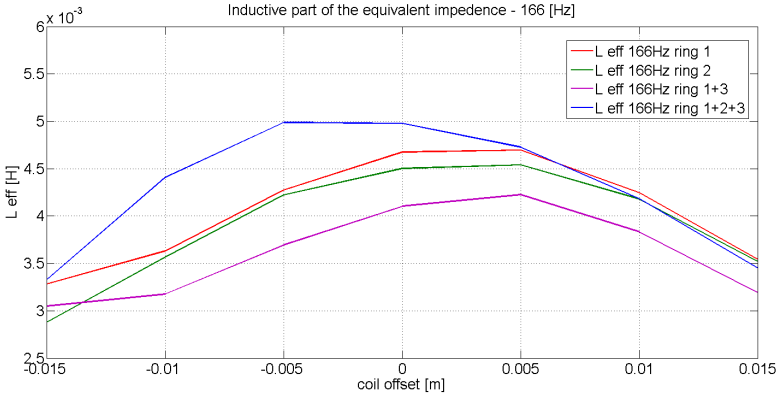

Figure 7.20: effective inductance

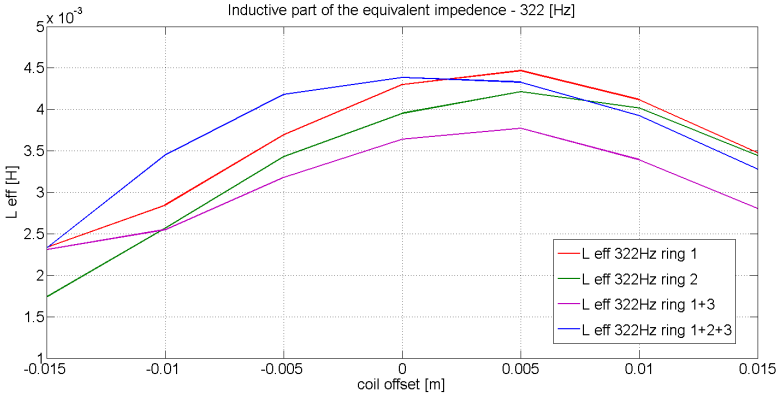

Figure 7.21: effective inductance

7.6 *SV* 165 optimizied

7.6.1 *SV* 165 with ring 2.png

In Fig. 7.22 it is shown the Pareto front obtained after 200 evaluations:
it is interesting to see that non a huge amount of aluminum is used, even better

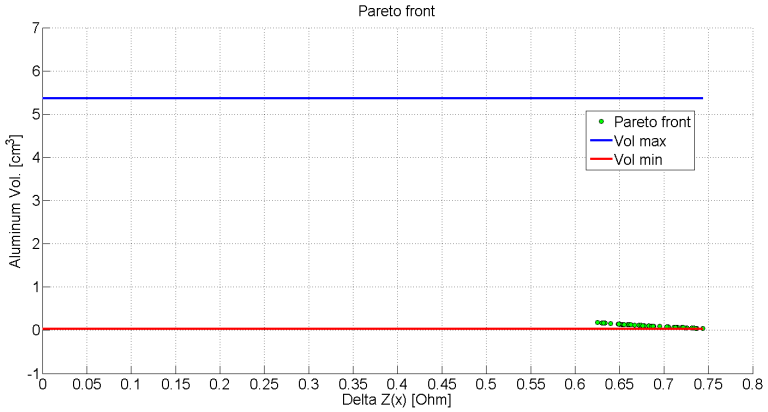

Figure 7.22: *SV* 165 with ring 2

we can obtain a huge reduction in the impedence variation at a small material price.

7.6.2 *SV* 165 with rings 2 ad 3

In Fig. 7.23 it is shown the Pareto front obtained after 300 evaluations:
basically what we can find is that the ring 3 tends to provide worse performances, indeed the optimizator tries to minimize the amount of aluminum used for the rings. Note that in practice it exist only one solution, that is dominating all the other possibilities.

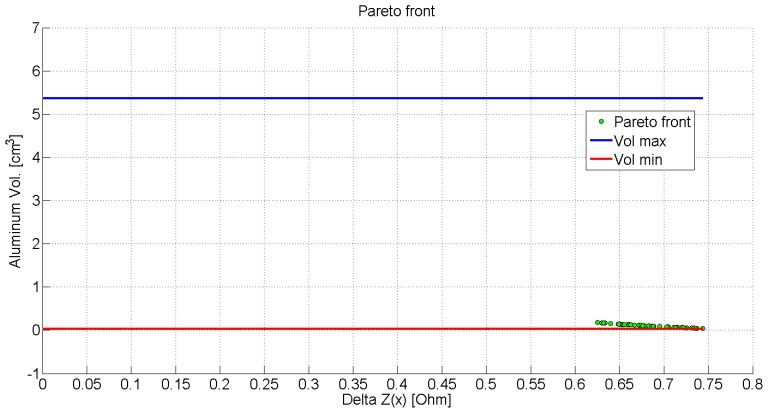

Figure 7.23: *SV* 165 with rings 2 and 3

7.6.3 *SV* 165 with rings 2 ad 3, no copper cap

In Fig. 7.24 it is shown the Pareto front obtained after 200 evaluations:
we removed the copper cap, and provided an optimization with just considering the two aluminum rings. Once again, there is no the need of a big amount of

aluminum to get the minimum variation of the impedence with the coil movement.

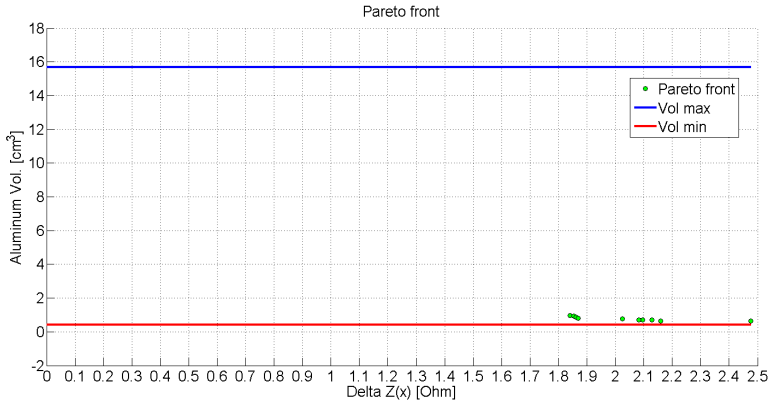

Figure 7.24: *SV* 165 with rings 2 and 3, no copper cap

7.6.4 *SV* 165 , comparison of all solutions

this is the most important result, since from the Fig. 7.25 it is possible for a company to make a decision about what are the best solutions that are going to be chosen and produced.
The vertical lines represent the value of the impedance variation without any ring, it represent the upper limit:
more precisely, the red and blue ones are related to the device with only the copper cap, while the green one refers to the device without also the copper cap.
Let's see how it is almost useless to use the ring 3 alone: the best performances in reducing the variation of the impedance are obtained with the use of ring 2 coupled with the copper cap, or combining the ring 2 with the ring 3in the device without the copper cap.
The best ratio *performance/volume* belongs to the solution with just the ring 2 (see Fig. 7.11)

Figure 7.25: comparison among all solutions

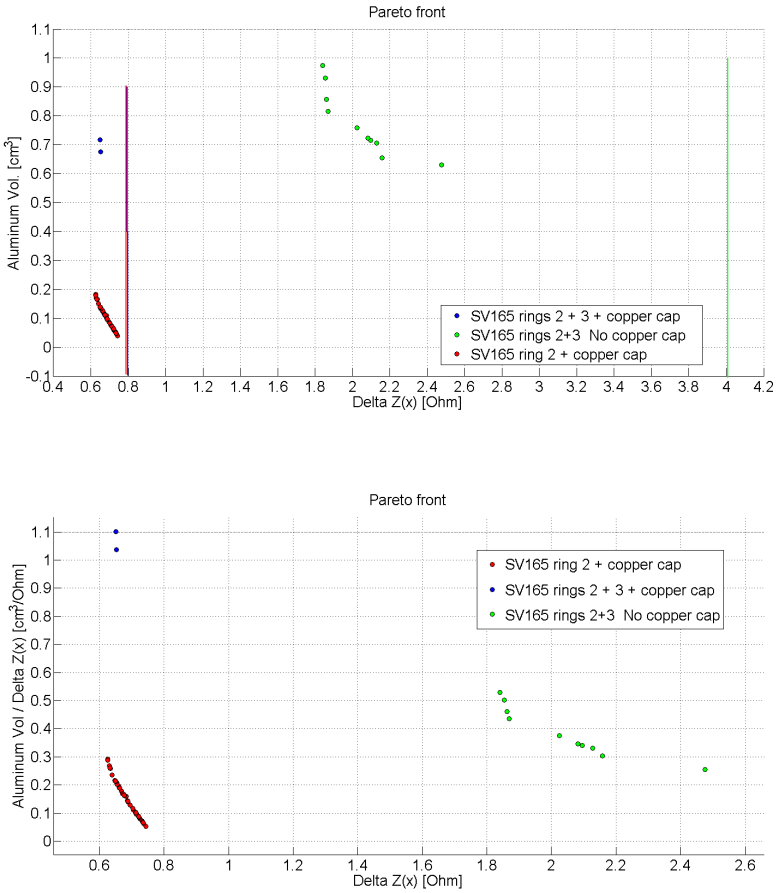

Figure 7.26: comparison among all solutions

7.7 $SSF - 082$ Choice of the prototypes

Accordingly with the company, we decided to choice the solutions that minimize the variation of the impedance, despite the amount of aluminum required:
this was suggested by the fact that the device will be sold like a prfessional loudspeaker, so in the high market level, where the cost is not the primary driver that influences the coustomer's choice.
Off course we neglected the solution with just the ring 3, because it has been shown that this way of design is completely dominated by the solution with rings 2 and 3. In Tab. 7.2 we reported the details concerning the position and the sizes of the rings in the chosen models.

Models	*ring* 2	*ring* $2 + 3$*nocppercup*
$r2\ w$	$0.57 \cdot 10^{-3}$	$0,52 \cdot 10^{-3}$
$r2\ h$	$2.31 \cdot 10^{-3}$	$5.30 \cdot 10^{-3}$
$r2\ z$	$18.44 \cdot 10^{-3}$	$21.60 \cdot 10^{-3}$
$r3\ w$		$3.48 \cdot 10^{-3}$
$r3\ h$		$3.73 \cdot 10^{-3}$
$r3\ r$		$5.50 \cdot 10^{-3}$

Table 7.2: Main features of the voice coils

7.7.1 Geometries

SV $165 -$ *ring* 2 **geometry**

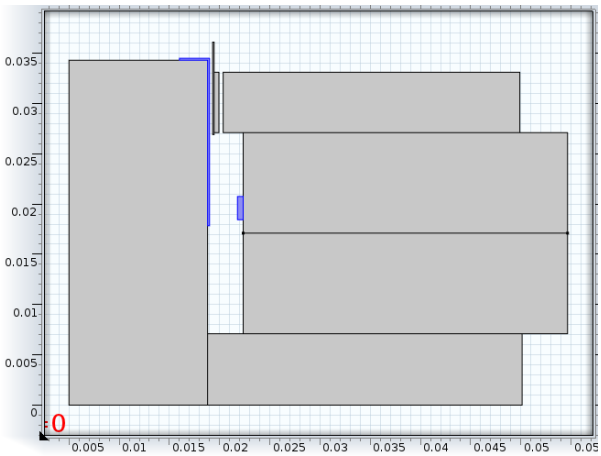

Figure 7.27: *SV* 165 geometry with ring2

SV $165 -$ *rings* $2 + 3$ **geometry**

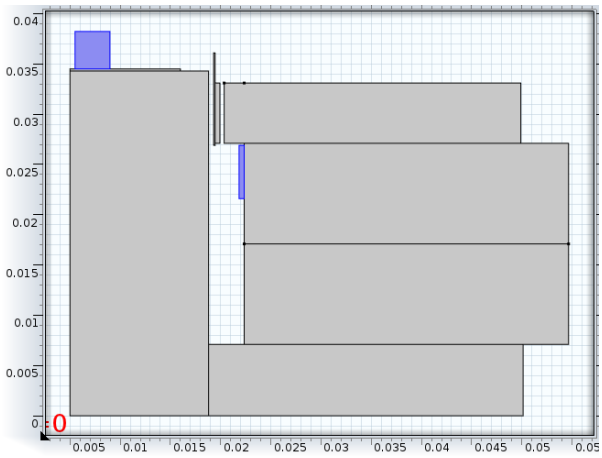

Figure 7.28: SV 165 geometry with rings 2 and 3, no copper cap

7.7.2 Characterisation of the impedence

The following section represents the effective impedence seen from the coil teminals,fonction of the coil offset, less than the R_{DC} resistance. To obtain it we followed the very same way explained it the previous equivalent section, relative to the $SSF - 082$.
To get a meaningfu resut, we chose three diffrent frequencies, on the bottom, the middle and the top part of the frequency range where the device has to work.

Effective resistance

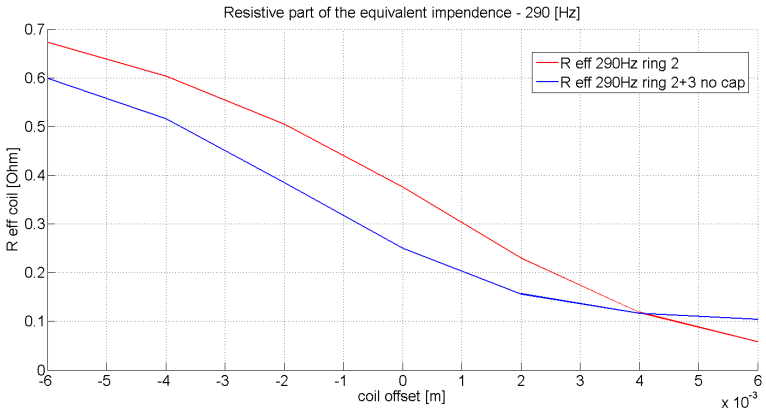

Figure 7.29: effective resitance

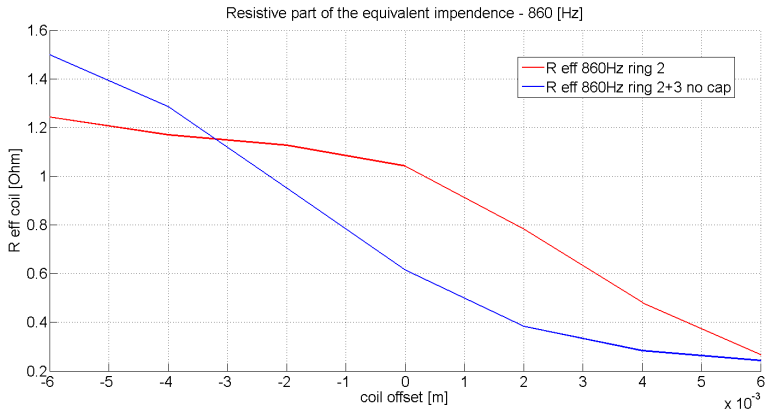

Figure 7.30: effective resitance

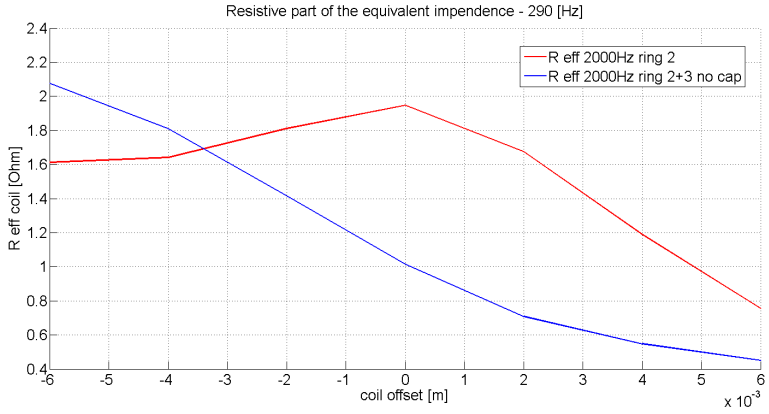

Figure 7.31: effective resitance

Effective inductance

We can see that the curves are charaterized by a bell shape:

- when the coil is dipped inside the magnetic complex, there's the action of ring 1 or 2 that helps to keep the inductance value low;
- when the coil reaches the outer point of her excursion, there is just air, so the inductance is naturally decreased;
- when the coil crosses through the rest point, she couples herself stronger with the mangetic circuit, so the inductance is increased.

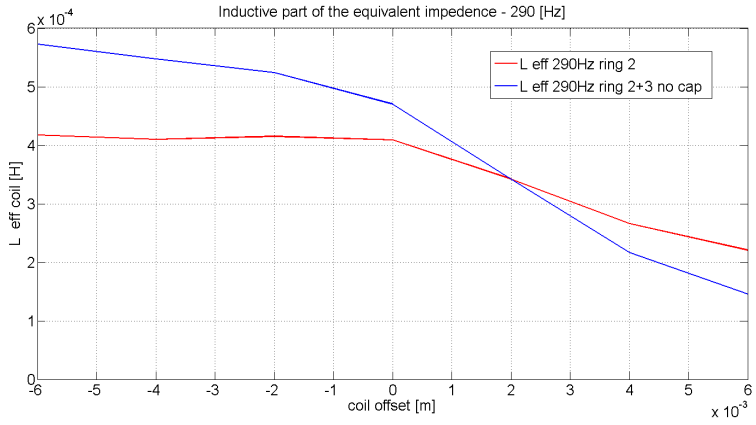

Figure 7.32: effective inductance

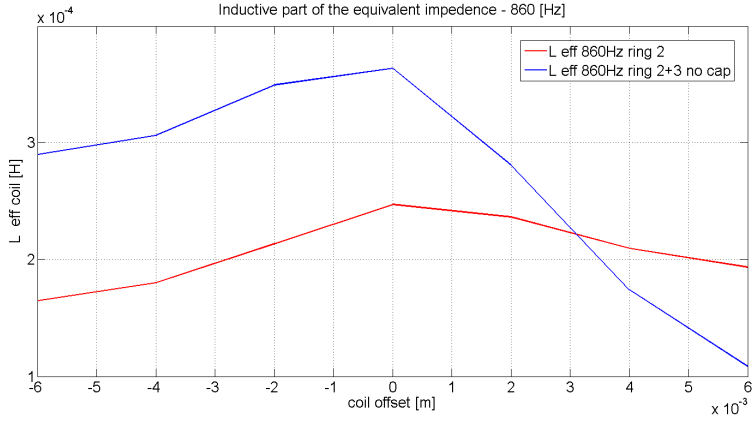

Figure 7.33: effective inductance

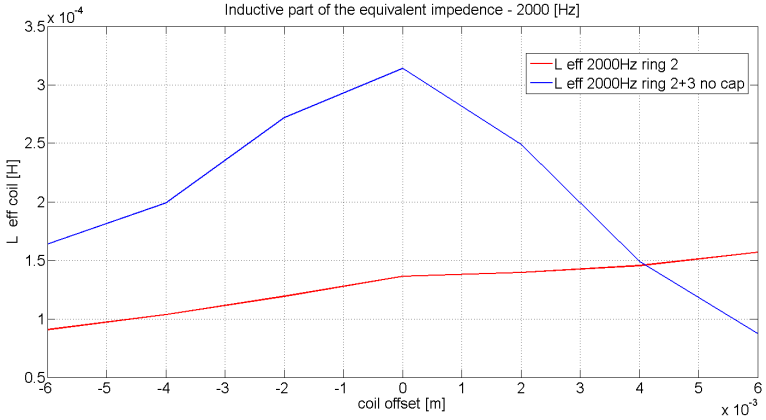

Figure 7.34: effective inductance

7.8 further developments

We worked just on the shape, the number and the position of the demodulation rings:
off course this is just the beginning, indeed there are a lot of possibilities that have still to be explored.
Once the optimization algorithm is written and the geometry loaded, the fantasy has no more boundd, we can work for example on:

- the type of material used for the rings;
- the possibility of combining different materials in sandwiches structures, to obtain different behaviors with the frequency increasing;
- we can consider geometries that are more complex than just rectangular sections;
- we can combine also the design of the voice coil in the optimization project, since the lossy impedance depends directly from the shape, position and number of turns of the coil;
- we can consider also the possibility to add also the design of the magnetic circuit in the optimization process.

Unfortunately the time useful for the development of the thesis is coming to an end:
but before closing the work we want to show a couple of examples of the way to follow, conscious that the research is very far to be finished.

7.8.1 $SSF - 082$ with ring 1-new trials

We made two different optimizations, using the very same geometry for the magnetic circuit:

- one trial was made with a copper ring, instead of using aluminum;
- the second trial was made considering a coil that has half of the height respect to the reference design.

The Fig. 7.35 shows the comparison among the new trials and the old result explained before.

As one can see, we can't disregard the optimization of the demodulation rings from the shape of the coil, indeed as we can see, making the coil shorter give a benefit to the constancy of the voice coil impedance respect to the offset.
Moreover, we can assert that the choice of materials is critical:
it is worth to remark that nothing has changed, except the composition of the ring, that is made now by copper.A great improvement was obtained, all the curve is indeed translated towards the utopia point:
the Pareto front of the copper ring is actually dominating all the previous solutions.

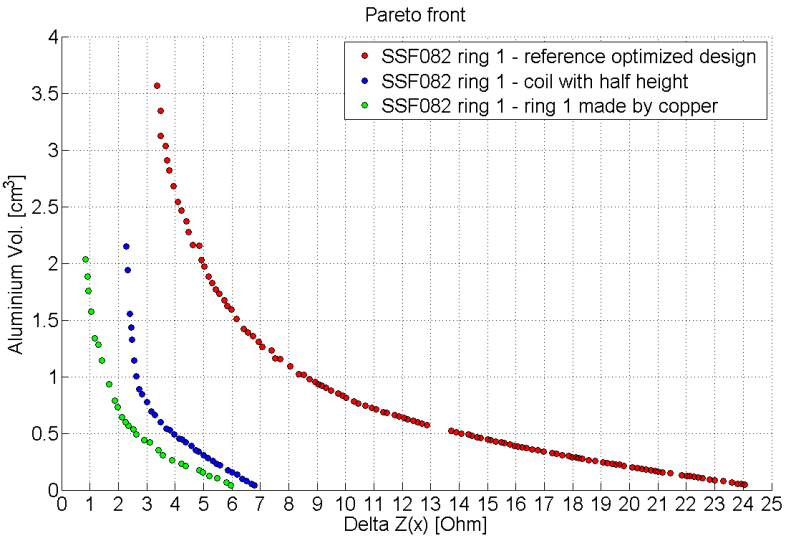

Figure 7.35: Comparison among new trials

Chapter 8

Measurements on prototypes

8.0.2 introduction

This section is dedicated to show the improvements and the benefits derived from the introduction of th demodulation rings in the models SV 165 midrange and $SSF-082$ subwoofer: unluckily at the time of the writing, the subwoofer has just realized in China and since the measurement system is in Italy, there's no time to wait the arrival of prototypes. The measures has been produced using the LSI module of the Klippel Distortion Analyzer, concerning:

- the variation of the force factor with the coil offset, $Bl(x)$;
- the variation of the inductance with the motor coil offset, $L(x), i = 0$;
- the variation of the inductance with the motor coil current, $L(i)$;
- the THD related to the fundamental harmonic wave, for all the frequency spectrum.

8.0.3 SV 165 midrange

SV 165 with copper cap and ring 2

The following figures show the parameters described in the introduction.

Looking at the measures, it is really hard to quantify the size of the improvements, and this can be explained easily:
the model SV 165 is already a finished product, designed and thought to work very well. It is really hard to modify a finished product, since the degrees of freedom are not enough to allow the optimizer to find really better solutions. The reason because we decided to work on it anyway it was because it was possible to get the measures in time to included them in the thesis,since the pieces of the device were already in stocks.

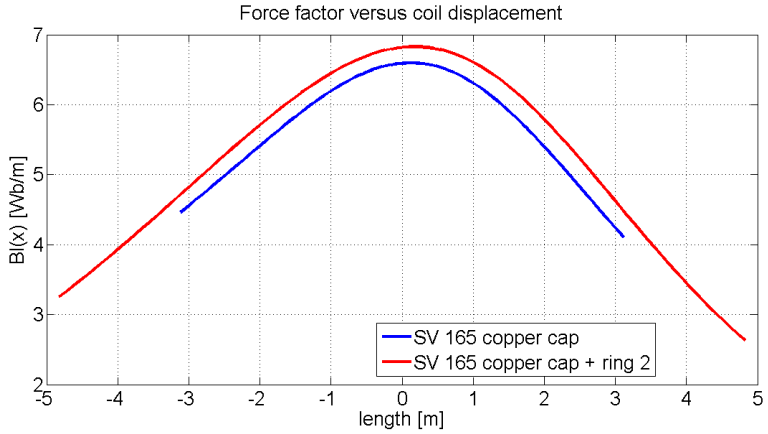

Figure 8.1: Bl(x), *SV* 165

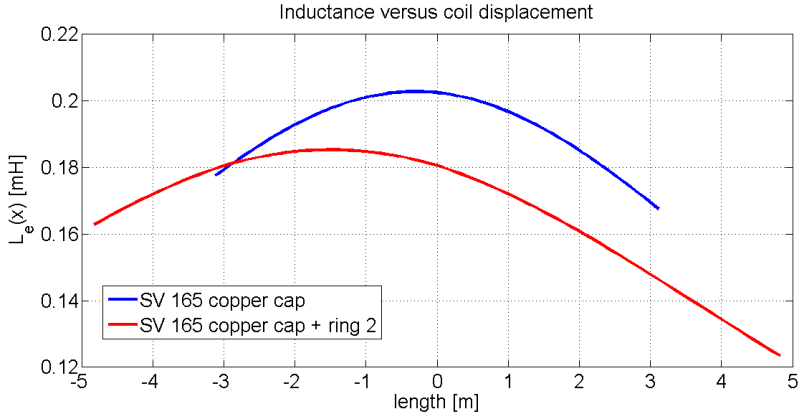

Figure 8.2: L(x),*SV* 165

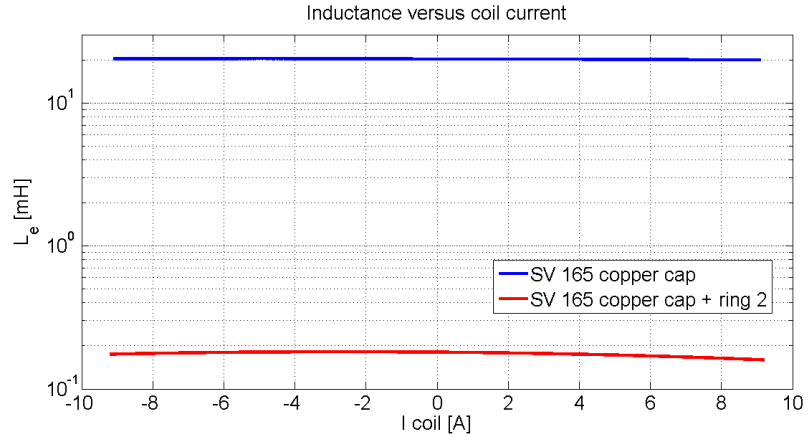

Figure 8.3: L(i),*SV* 165

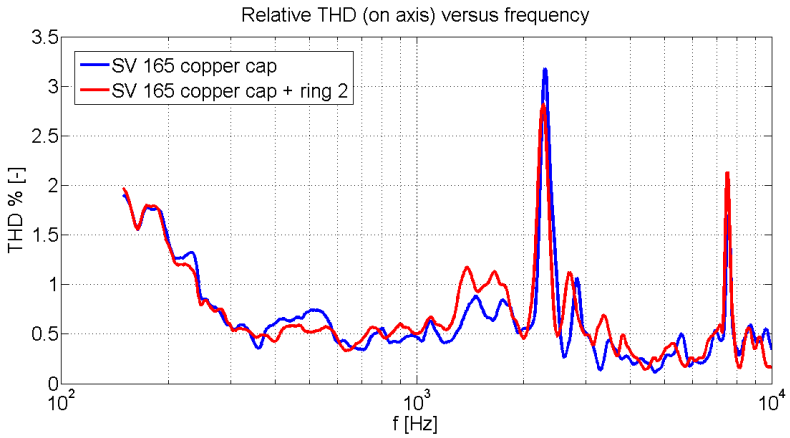

Figure 8.4: Total Harmonic Distortion, *SV* 165

SV 165 **without copper cap, with rings 2 and 3**

The following figures show the parameters described in the introduction.

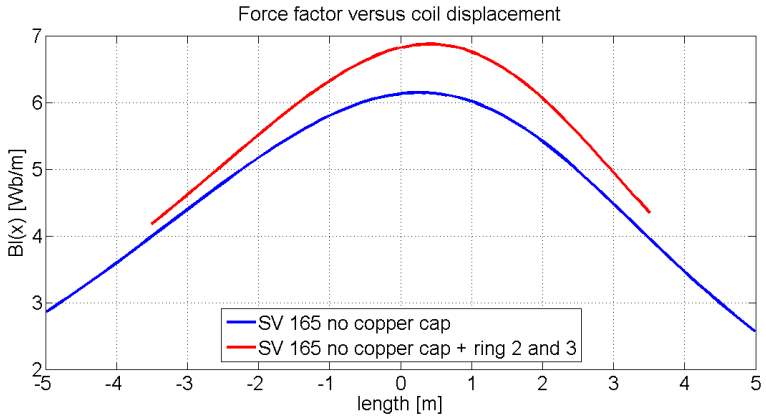

Figure 8.5: Bl(x), *SV* 165

We can observe a general improvement in the shapes of the parameters: the variation is smoother, and also the symmetry in enhanced. except for the very low frequencies, we observe a general reduction in the THD almost all over the spectrum.

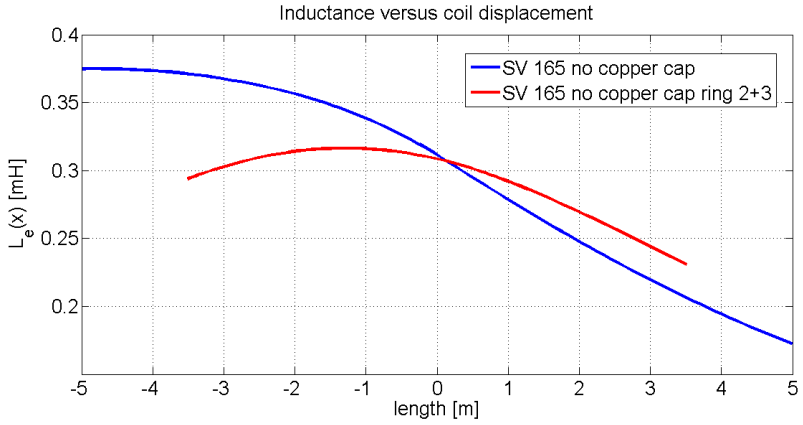

Figure 8.6: L(x), *SV* 165

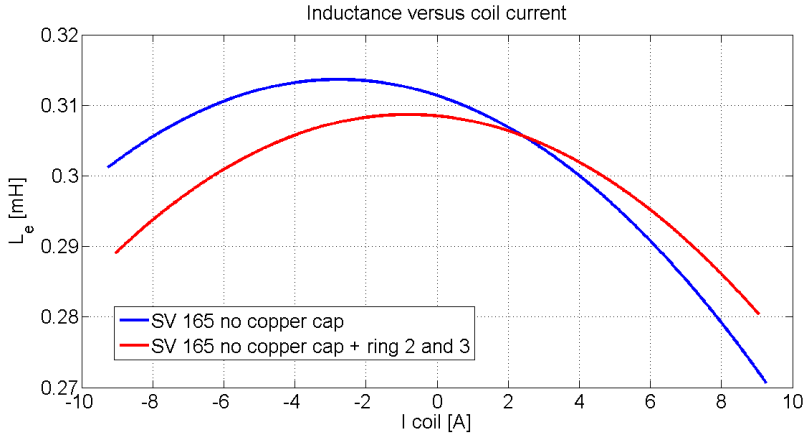

Figure 8.7: L(i), *SV* 165

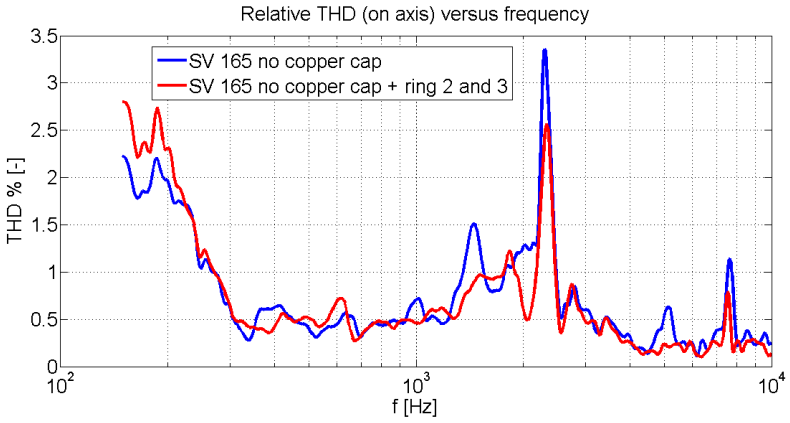

Figure 8.8: Total Harmonic Distortion, *SV* 165

Bibliography

[1] Irina A. Aldoshina, Alexander Voishvillo, and Victor Mazin. "Modeling of Flux Modulation Distortion in Moving-Coil Loudspeakers by the Finite-Element Method". In: vol. Preprint 3996, AES Convention 98. February 1995.

[2] Fabio Blasizzo. "A New Thermal Model for Loudspeakers". In: *J. Audio Eng. Soc.* 42.1/2 (2004).

[3] John Borwick. *Loudspeaker and Headphone Handbook*. Third edition. Linacre House, Jordan Hill, Oxford: Butterworth-Heinemann, 2001.

[4] Gilbert Briggs. *Loudspeakers*. Fourth Edition. England: Wharfedale Wireless Works Ltd, 1955.

[5] Marco Carlisi, Mario Di Cola, and Andrea Manzini. "An alternative approach to minimize Inductance and related Distortions in Loudspeakers". In: 2005. Chap. Convention Paper 6421.

[6] Antonio Delladio. *Aeroelectrical optimization design of a small horizontal axis wind turbine*. 2012.

[7] Vance Dickason. *The Loudspeaker Design Cookbook*. Seventh edition. Peterborough, New Hampshire: Audio Amateur Press, 2006.

[8] Mark Dodd. *Application of the finite element method to model the nonlinear voice coil motion produced by a loudspeaker magnet assembly*. Tech. rep.

[9] Mark Dodd. "The Transient Magnetic Behaviour of Loudspeaker Motors". In: vol. Preprint 5410, AES Convention 111. December 2001.

[10] Mark Dodd, Wolfgang Klippel, and Jack Oclee-Brown. "Voice Coil Impedance as a Function of Frequency and Displacement". In: 2004.

[11] Michael Hedges and Yiu Lam. "Accuracy of Fully Coupled Loudspeaker Simulation Using COMSOL". In: 2009.

[12] Wolfgang Klippel. *Measurement of Large-Signal Parameters of Electrodynamic Transducer*. Tech. rep.

[13] Wolfgang Klippel. *Nonlinear Modeling of the Heat Transfer in Loudspeakers*. Tech. rep.

[14] John Eargle M. *Loudspeaker handbook*. 1st ed. New York: Chapman Hall, c1997, 1997.

[15] W. Leach Marshall. "Loudspeaker Voice-Coil Inductance Losses: Circuit Models, Parameter Estimation, and Effect on Frequency Response". In: *J. Audio Eng. Soc.* 50.6 (2002).

[16] Giovanni Martinelli and Augusto Morini. *Lezioni di teoria unificata delle macchine elettriche rotanti*. Padova: SGE, 1992.

[17] *MatWeb - Online Materials Information Resource*.

[18] *Material size of round wires*.

[19] Victor Y. Mazin. "Modeling of Magnetic Hysteresis and its Influence on Harmonic Distortion in Electrodynamic Loudspeakers". In: vol. Preprint 4865, AES Convention 106. 1999.

[20] Steve Mowry and Thailand Phuket. *Nonlinear Quasi-dynamic DC and AC FEM for Electro-dynamic Audio Transducer Motor Assembly Simulation*. Tech. rep.

[21] Philip Newell and Keith Holland. *Loudspeakers for music recording nd reproduction*. First edition. Linacre House, Jordan Hill, Oxford: Elsevier, 2007.

[22] C. W. Rice and E. W. Kellogg. *Notes on the Development of a New Type of Hornless Loudspeaker*. 1925.

[23] Chester W. Rice and Edward W. Kellogg. "Notes on the Development of a New Type of Hornless Loudspeaker". In: Transactions of the American Institute of Electrical Engineers 44 (1925), pp. 461–475.

[24] steve Morwy. "Inductance et al. â A Closer Look at AC, Part 1". In: *Voice coil, the periodical for the loudspeaker society* (2006).

[25] Knud Thorborg and Andrew Unruh D. "Electrical Equivalent Circuit Model for Dynamic Moving-Coil Transducers Incorporating a Semi-Inductor". In: *J. Audio Eng. Soc* 58.9 (2008).

[26] Knud Thorborg, Andrew Unruh D, and Christopher Struck J. "An Improved Electrical Equivalent Circuit Model for Dynamic Moving Coil Transducers". In: 2007.

[27] John Vanderkooy. "A Model of LoudspeakerDriver Impedance IncorporatingEddyCurrents in the PoleStructure". In: *J. Audio Eng. Soc.* 37.3 (1989).

[28] Alexander Voishvillo and Victor Mazin. "Finite-Element Method of Modeling of Eddy Currents and Their Influence on Nonlinear Distortion in Electrodynamic Loudspeakers". In: Preprint 4085, AES Convention 99 (October 1995).

[29] Alexander Voishvillo and Victor Mazin. "Finite-Element Method of Modeling of Eddy Currents and Their Influence on Nonlinear Distortion in Electrodynamic Loudspeakers". In: vol. Preprint 4085, AES Convention 99. October 1995.

[30] J. R. Wright. "An Empirical Model for LoudspeakerMotor Impedance". In: *J. Audio Eng. Soc.* 38.10 (1990).

[31] Elettromedia s.r.l. *DS30 data sheet*.

[32] Elettromedia s.r.l. *SV 165 - data sheet*.